Effect of exposure on the erodibility of intertidal mudflats

A thesis

submitted in partial fulfilment

of the requirements for the degree

of

Doctor of Philosophy in Earth Science

at

The University of Waikato

by

HIEU MANH NGUYEN

THE UNIVERSITY OF
WAIKATO
Te Whare Wānanga o Waikato

2021

ABSTRACT

Sediments on intertidal flats are exposed during low tides. Under the effect of exposure, the water content of sediments decreases because of the evaporation process, which alters the erosive behaviour of cohesive sediments, and therefore changes the patterns of erosion/accretion on intertidal flats. Consequently, exposure indirectly affects the intertidal morphology. An understanding of how exposure alters the erodibility of sediment on intertidal flats is critical to predicting the resilience of intertidal zones into the future during which sea-level rise is believed to exacerbate erosion in low-lying areas.

Sediments were collected from an intertidal mudflat in the Firth of Thames, New Zealand in different seasons from 2017 to 2019 for laboratory experiments. Two experiments (Exp. 1 and Exp. 2) were set up in order to explore the effect of exposure including air temperature and exposure duration on erodibility of cohesive sediments. The EROMES device was used to measure the erosion potential of sediment (erosion threshold, τ_{cr} N m^{-2} and erosion rate, *ER* g m^{-2} s^{-1}). Exp. 1 investigated erodibility of sediments exposed to a wide range of temperatures (controlled at 0, 8, 25 and 40°C) for 6 h. Meanwhile, Exp. 2 was designed to examine the effect of exposure duration on erodibility. In this experiment, a systematically-changed exposure duration (6 h, 1, 4 and 10 d) was used to mimic a wide range of exposure that might happen on an intertidal flat during a year (set to mimic the Firth of Thames field site). Experimental results indicated that erosion resistance of sediments significantly increased (increased τ_{cr}, and decreased ER) corresponding to decreased water content after exposure. The higher the air temperature and the longer the exposure duration, the more stable the sediments were. For instance, the water content of exposed sediments decreased by 1.01 to 1.78 times, a rate which was a function of increasing temperature. The τ_{cr} of exposed experiments was 1.2 to 2.2 times higher, whereas *ER* decreased 1.2 to 6.2 times. After 10 d, exposure increased τ_{cr} by 1.7 to 4.4 times and decreased *ER* by 11.6 to 21.5 times compared with 6 h of exposure.

Semi-empirical models fitted datasets from Exp.1 and Exp. 2 were used to predict the variations of τ_{cr} and ER as functions of air temperature, T (°C) and exposure

duration, D (h). These semi-empirical models were used to extend a Delft3D numerical model to test the effect of exposure on intertidal mudflat profiles and development of tidal channel networks. Model results indicated that exposure enhanced the more flat-topped shape of intertidal mudflats. Higher air temperature resulted in stronger effects on bed level change. For example, for the case of 40°C, bed level built up by 0.039m after one year of model time. Regarding the development of channel networks on intertidal mudflats, the exposure effect tended to create denser and deeper channel networks compared to model runs without the exposure effect. Our findings, therefore, contribute to the prediction of the intertidal morphology development, which will help to understanding the resilience of tidal flats and salt marshes in future under the effect of sea-level rise and global warming.

ACKNOWLEDGEMENTS

I am very thankful to Prof. Karin Bryan for giving me the opportunity to do my PhD under her supervision. Thank you for your enthusiasm, encouragement, patience, and inspiration. To be your student is one of the luckiest events in my life. I would like to truly thank Prof. Conrad Pilditch, my second supervisor for his critical comments and very interesting discussions for all my papers. I also would like to thank Dr. Vicki Moon a member of my PhD supervision panel with her important comments for my first paper.

Fortunately, there were so many people that accompanied me through this long journey. I am grateful to my wife, Hoa Nguyen who always encourages me and for being with me although we had to separate for two years during her Master study in Australia. My parents, Don Nguyen and Quy Tran with their unconditional love and support of all my decisions. I thank my wife's parents, Quyet Nguyen and Le Duong for their encouragement and help to look after of my son when I was not able to be with him. My son, Kent, is the greatest motivation for me. I would like to thank all my relatives back to Vietnam for their understanding and encouragement.

I am grateful for University of Waikato Doctoral Scholarship, the Tipping Points project in the Dynamic Seas programme of the New Zealand Sustainable Seas National Science Challenge and the INTERCOAST programme between University of Waikato and Bremen University for providing scholarship and funding for my conference attendance in Germany and New Zealand that allowed me to undertake my research.

I acknowledge the invaluable assistance in the field in the Firth of Thames, which would not have been possible without Hieu Dao, Benjamin Stewart, John Montgomery and Pradeep Sign. Also thanks to Dean Sandwell, Rebecca Gibson, Lynne Parker, Annette Rodgers and Warrick Powrie, Erik Horstman, and Rebecca Gallagher in assisting with laboratory work.

I especially thank Assoc. Prof. Zeng Zhou at Hohai University for helpful comments for my first paper and to be a co-author for my third and fourth papers. My special thanks to Benjamin Stewart and Amin Rahdarian for their immense support and discussion in using of Delft3D for my thesis.

Finally, I would like to thank Mariana Cussioli, Benjamin Stewart, Bérengère Dejeans, Victor Godoi, Peter De Ruiter, Hemanth Bharadwaj, John Montgomery, Ben Norris, Amin Rahdarian (my friends/colleagues in the same office) for interesting talks during our lunches and tea breaks.

TABLE OF CONTENTS

LIST OF TABLES

LIST OF FIGURES

Chapter 1

General Introduction

Intertidal mudflats and saltmarshes comprise a transition zone between marine and terrestrial systems, and because they are so productive, play significant roles in the well-being of humans and other species. However, they are also the most vulnerable ecosystem on Earth (Foster et al., 2013; Kirwan and Megonigal, 2013). Coastal zones throughout the world are being threatened by many factors such as sea-level rise, tidal inundation, sediment supply, and agricultural use (Spanger-Siegfried et al., 2014; Xie et al., 2018). Intertidal flats are exposed during low tides and submerged at high tides, and the duration of exposure is dependent on the relative difference between bed and tide levels. The alteration between wet and drained states may affect the sediment water content, and so the erosion properties of intertidal sediments. In addition, long duration exposure might result in drought and changes in porewater chemistry and salinity which cause marsh dieback (Hughes et al., 2012).

Climate change and sea level rise (SLR) are believed to threaten intertidal coastal habitats (Spanger-Siegfried et al., 2014), and effects on habitat connectivity and ease of landward migration are likely important for the long-term viability of coastal habitats in the face of SLR (Kirwan et al., 2016a). Furthermore, coastal habitats are "squeezing" in response to SLR, where they are unable to migrate landward due to, for example, coastal development (Doody, 2013). Recently, one of the priorities of coastal conservation is to identifying existing and potential new approaches to relieve coastal squeeze and facilitate coastal habitat migration in response to SLR (Fitzsimons et al., 2015). Therefore, understanding the evolution of coastal morphology is critical to planning how we might adapt to SLR. This thesis aims to explore a new approach to understand erosive behaviour of intertidal mudflats and how it changes after exposure to air. The hypothesis is that evaporation during exposure causes a change in water content which controls the

erodibility. Scaling up laboratory results to understanding how the coastal morphology might change is then done by incorporating laboratory-derived empirical functions into numerical models.

1.1 Background

Water content of soil is defined as ratio of amount of water per unit mass of solid particles (*W*, %). Any changes in water content of cohesive sediment will lead to changes in plastic behaviour of the sediment. The relationship between water content and behaviour of cohesive sediment can be described by the Atterberg limits. Water content has been widely recognised as a key factor controlling the erosive behaviour of cohesive sediments, as it directly influences mechanical properties of clays (e.g. Amos et al., 2004; Bale et al., 2007; Van Ledden et al., 2004; Winterwerp and Van Kesteren, 2004). Specifically, any changes in water content alters the plastic properties of cohesive sediments (Grim, 1962; Winterwerp and Van Kesteren, 2004). The water content at which sediments change from a solid to a plastic state, and from a plastic to a liquid state are called the plastic and liquid limits (or Atterberg Limits), respectively (Grim, 1962). The limits are specific to each sediment type and depend on properties such as grain size, organic content (OC) and clay minerals of the sediment (Grim, 1962).

The water content of intertidal sediments can decrease during exposure due to evaporation and/or draining and increase during submersion by infiltration of water molecules within pores of the substrate (Yong and Warkentin, 1966). The frequency and duration of exposure depend on the tide and bed level, and intertidal flats are expected to have longer exposure duration during neap tides (at elevations above the neap tidal range). Bale et al. (2007) have indicated that cohesive sediments with Liquid Index (LI) > 1 are easily entrained meanwhile sediments with LI < 1 are more resistant to erosion. As presented in Figure 1.1, PL and PI are constant attributes of a sediment on an intertidal flat, while the actual water content (*W*) of sediment is controlled by exposure via evaporation. Consequently, LI is regulated by exposure, which in turn controls erosion

properties of cohesive sediments. Therefore, an understanding of how water content change will significantly contribute to predicting the erodibility of sediments.

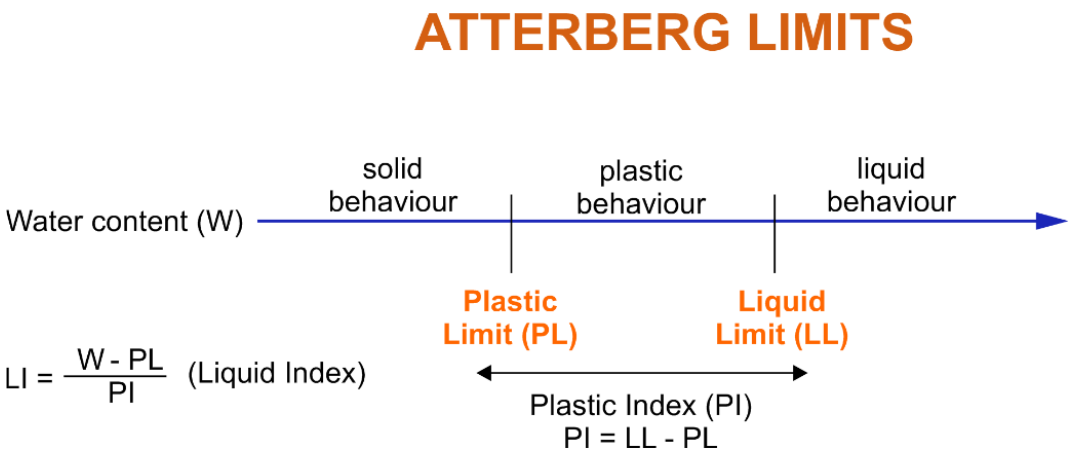

Figure 1.1 Atterberg limits showing plastic limit (PL) and liquid limit (LL) are measures of water content that reflect behaviour of cohesive soils change from solid to plastic and plastic to liquid, respectively. Plastic index is the degree of difference between the liquid and plastic limit.

Biological and physical factors interact to influence erosion properties of sediment (Black et al., 2002; Grabowski et al., 2011). For example, the growth of biofilms on intertidal mudflats stabilises the sediment against erosion (e.g. Black et al., 2002; Chen et al., 2017; Friend et al., 2003). The presence of biofilm creates smoother surfaces which reduces drag force on the surfaces (Paterson, 1989), and biofilm growth within pores is believed to increase binding between particles, making sediment more resistant to erosion (Underwood and Paterson, 2003). Chlorophyll-a has been widely used in previous studies as a proxy for biofilm biomass which is seasonally variable, dependent on weather conditions during exposure and nutrient availability (Davoult et al., 2009; Migné et al., 2004; Staats et al., 2001; Tolhurst et al., 2006a). In addition, the growth of biofilm within pore spaces might reduce evaporation which in turn affects water content of sediment (Lianfang et al., 2009; Vandevivere and Baveye, 1992; Volk et al., 2016). In this research, the

effect of *Chl-a* content (representative of seasonal biofilm growth on intertidal mudflats) on erodibility of sediment will be explored in Chapters 2 and 3.

Previous studies have shown that exposure strengthens cohesive sediments against erosion (Fagherazzi et al., 2017; Tolhurst et al., 2006a; Widdows et al., 1998), and the stabilised effect is not lost in subsequent subaerial period (Fagherazzi et al., 2017). During low tides intertidal mudflats are emerged, and exposure will cause evaporation and decrease the water content of surficial sediments. The significant relationship between water content and erodibility of cohesive sediments has been widely recognised in the literature, and any changes in the water content will alter its plastic behaviour and erosion properties (Jacobs et al. 2011; Van Ledden et al. 2004; Winterwerp et al. 2018; Winterwerp and Van Kesteren 2004; Zhou et al. 2016a). Chapter 2 of this thesis will systematically explore the effect of a wide range of air temperature on erosion resistance of cohesive sediments.

Exposure duration of intertidal zones is dependent on water level and bed elevation, and in some cases exposure can last for weeks (e.g. during neap tidal conditions). Han and Zhou (2013) and Kobayashi and Miyagawa (1992) showed that evaporation only occurs on the surface layer of sediments where they are directly affected by current flows during submergence. Dingman (1994) introduced a model predicting evaporation rate of water from exposed sediments that is affected by many meteorological factors such as air temperature, solar radiation, relative humidity of the atmosphere and wind speed. The stabilizing effect of exposure on cohesive sediment on intertidal flats has been investigated in previous studies (Fagherazzi et al., 2017; Tolhurst et al., 2006a; Widdows et al., 1998); however, these studies were only based on short-term exposure designed to replicate the average time exposed at mean sea level on an intertidal mudflat with a diurnal un-distorted tide (e.g. 7 h in Widdows et al. (1998)). Chapter 3 of this thesis sought to address this limitation in the previous studies.

Exposure affects the erodibility of sediment on intertidal mudflats, which in turn alters the evolution of intertidal morphology. The shape of the intertidal profile is critical in determining how a coastal landscape will function (both ecologically and in terms of eco-defence). Process that modify the type of profile that develops are whether waves or tidal forcing dominate, the sources of sediment, the grain size of the sediment supply, and elevation of the flat relative to the mean sea level. Ultimately, these effects work together to shape intertidal profiles, and they can range from the extremes of concave or convex (Bearman et al., 2010). Tidal currents enhance convexity whereas waves favour concavity (Friedrichs et al., 1996; Pritchard and Hogg, 2003; Zhou et al., 2015). Sandier tidal flats, in turn, tend to be associated with wave-dominated areas, and muddier flats are more common in tide-dominated areas (Yang et al., 2008; Zhou et al., 2015). Moreover, elevated tidal range enhance more convex upward intertidal profiles (Friedrichs, 2011; Kirby, 2000). Erosional flats tend to be more concave upward, meanwhile accretionary tidal flats are observed to become more convex upward (Dyer, 1998; Kirby, 2000; Le Hir et al., 2000; Mehta, 2002; Van Rijn, 1998). Recent numerical modelling exercises have focused on reproducing these subtle variations in the profile of intertidal flats. Nevertheless, one of the effects that has not been well considered yet in profile models is the effect of atmospheric exposure on the properties of cohesive intertidal sediments. In Chapter 4 of this thesis, I applied empirical models (developed in Chapters 2 and 3) in a numerical coastal model to explore the effect of exposure on intertidal mudflat profile evolution.

Tidal channels and their branched networks will characterise intertidal zone landscapes (Vandenbruwaene et al., 2013). Tidal channel networks are vital to the evolution of intertidal zones, providing main paths for exchanging of water, nutrients, sediments and biota between lands and oceans (Fagherazzi et al., 1999; Zedler and Kercher, 2005; Zhou et al., 2014). Many factors are believed to affect the channel network formation and evolution such as vegetation, tidal prism, initial perturbation or anthropogenic reclamation and de-reclamation (e.g. Belliard et al., 2015; Chen et al., 2020; Kearney and Fagherazzi, 2016; Temmerman

et al., 2012; Vandenbruwaene et al., 2013). Simulation models have been used extensively to explore medium and long-term evolution of tidal channel networks (e.g. Belliard et al., 2015; D'Alpaos et al., 2005; Dastgheib et al., 2008; Lanzoni and D'Alpaos, 2015; Van Oyen et al., 2014). These models solve the coupled equations describing hydrodynamics, sediment transport, biological activities and morphological change, covering various spatial and temporal scales. Also, a wide range of environments such as salt marshes, intertidal flat and mangrove have been modelled in previous studies (Belliard et al., 2015; van Maanen et al., 2015; Zhang et al., 2016). However, to our knowledge, there is no study undertaken to understanding the effect of exposure on the development of intertidal channel systems. Chapter 5 will focus on investigating the effect of exposure on development of channel networks on intertidal mudflats.

1.2 Thesis objectives

In summary, this thesis explores the effect of ambient temperature and exposure duration on erosion properties of cohesive sediments on intertidal mudflats. In addition, this research aims to model the effect of these factors on intertidal mudflat profile and channel networks development in cohesive coastal environments. To constrain the study, experiments and modelling were designed around a case-study in the Firth of Thames, New Zealand. To address the thesis objectives, the following research questions were answered:

1. How does ambient air temperature affect erodibility of exposed sediment on intertidal mudflats?

2. How does exposure duration affect erodibility of sediment on intertidal mudflat? This question is dived into two sub-questions:

- What is the effect of the length of exposure on erodibility?

- How does erodibility change after subsequent flooding cycles (recovery after re-wetting)?

3. How does exposure affect the morphological development of the intertidal mudflat profile?

4. How does exposure affect the development of intertidal drainage channel networks?

1.3 Thesis structure

These objectives are dealt with using datasets from two experiments on cohesive sediment collected from an intertidal mudflat in the Firth of Thames, New Zealand. General research questions are divided into four scientific articles in Chapters 2, 3, 4 and 5, respectively. Each chapter consists of a completed article including abstract, introduction, methods, results, discussion and conclusions. Each article answered one big research question and can stand alone; however, they are strongly connected and systematically address the overarching theme of the study. In Chapter 6, general conclusions of the thesis, limitations of the current study and future research topics are discussed.

The first scientific article (Chapter 2), titled *Influence of ambient temperature on erosion properties of exposed cohesive sediment from an intertidal mudflat Nguyen et al., 2019)*, has been published in *Geo-Marine Letters*. This chapter systematically explored relationship between ambient temperature and erosion properties (erosion threshold, τ_{cr} *N* m^{-2} and erosion rate*, ER g* m^{-2} s^{-1}) of exposed sediments. Here I examined the effect of ambient temperature ranges that would occur between day and night time, between seasons and over longer (e.g. global-warming) time scales, by measuring the change in erodibility in natural intertidal sediments exposed to different temperatures.

The second scientific article (Chapter 3), titled *The effect of long-term aerial exposure on intertidal mudflat erodibility (Nguyen et al., 2020)*, has been published in *Earth Surface Processes and Landforms*. This Chapter systematically explored the effect of exposure on variation in erosion properties (erosion threshold, τ_{cr} *N*

m^{-2} and erosion rate, *ER* g m^{-2} s^{-1}) of cohesive sediments during much longer-term (after 6 h, 1, 4 and 10 d) exposure.

The third scientific article (Chapter 4), titled *Modelling the effect of aerial temperature and exposure period on intertidal mudflat profiles (Nguyen et al., In Prep.).* This Chapter integrated models fitted in datasets gained from Chapters 2 and 3 into a numerical coastal profile modelling. The hypothesis is that erodibility of sediments caused by exposure (including exposure temperature - *T*, ° C and duration - *D*, h) as well as *Chl-a* content (a proxy of biofilm biomass) can change the way in which coastal profiles evolve. The effects of exposure along with *Chl-a* content, initial sediment bed composition (percentage of mud and sand) and spring and neap tidal cycles (effects current velocity and exposure period) on intertidal flat profile were investigated using the modifications to the bed transport sub-routines of Delft3D.

The fourth scientific article (Chapter 5), titled *Modelling the effect of temperature and exposure on intertidal channel networks in cohesive coastal environments (Nguyen et al., In Prep.)*. This Chapter also integrated semi-empirical models fitted to datasets collected from experiments presented in Chapters 2 and 3 into Delft3D hydrodynamic-sediment transport model to explore the influence of exposure on the formation and development of channel patterns on an intertidal mudflat. This article addressed the hypothesis that differential exposure rates on topography with random elevation perturbations may play a role in the development of channel patterns in cohesive environments.

Chapter 2

Influence of ambient temperature on erosion properties of exposed cohesive sediment from an intertidal mudflat

Nguyen, H.M., Bryan, K.R., Pilditch, C.A. and Moon, V.G., (2019). Influence of ambient temperature on erosion properties of exposed cohesive sediment from an intertidal mudflat. Geo-Marine Letters: 1-11. https://doi.org/10.1007/s00367-019-00579-x.

Contribution of authors

Chapter 2 presents the article entitled “Influence of ambient temperature on erosion properties of exposed cohesive sediment from an intertidal mudflat”, published in 2019 in the Geo-Marine Letters.

Sediment samples using for laboratory experiments were obtained during fieldwork in the Firth of Thames, New Zealand, which I designed and executed as part of my PhD research. I also designed and conducted laboratory experiments, processed and analyzed all the data, produced figures and wrote the manuscript. My co-authors assisted with planning field- and lab-works, edited drafts and advised on directions.

Abstract

Intertidal flats regularly emerge and submerge in accordance with changes to the water level occurring over tidal cycles. The alteration between wet and drained states may affect the sediment water content, and so the erosion properties of intertidal sediments. This study examined the influence of ambient temperature on the erodibility of exposed cohesive sediment from an intertidal mudflat in the Firth of Thames, New Zealand in Dec 2017 and Mar 2018. The EROMES device was used to measure the erosion potential of sediment (erosion threshold, τ_{cr} N m^{-2} and erosion rate, *ER* g m^{-2} s^{-1}). Samples were drained and exposed to temperatures of 0, 8, 25 and 40°C, chosen to mimic natural exposed conditions, while submerged samples simulated natural flooded conditions. Results showed that the cohesive sediment became more resistant to erosion when exposed to air compared to submerged samples as a consequence of decreased water content. The water content of exposed sediments decreased by 1.01 – 1.78 times, a rate which was a function of increasing temperature. The τ_{cr} of exposed experiments was 1.2 to 2.2 times higher, whereas *ER* decreased 1.2 to 6.2 times. Both the Dec 2017 and Mar 2018 sampling dates showed a similar pattern of increasing resistance to erosion (higher τ_{cr} and lower *ER*), which corresponded to depleted water content of the exposed sediment at higher temperatures.

Keywords: sediment stability, erosion potential, erosion rate, erosion threshold, intertidal zones, The Firth of Thames

2.1 Introduction

Soft sediments comprise extensive ecosystems on Earth that provide habitats and food for many species such as fish and birds (Snelgrove, 1999). Intertidal areas also create habitats for fringing vegetation like salt marshes and mangrove forests that inhabit tidal margins of low-energy coasts and estuaries (Sterling and Hurley, 2008). If the intertidal sedimentation rate is lower than the rate of sea level rise, increasingly frequent coastal flooding will either cause the vegetation zone to shrink, or force shoreward migration if the available space exists (McCarthy, 2001). In contrast, although reducing flooding risk, higher sedimentation rates of finer particles can have negative impacts on habitats in the long term (Andersen et al., 2007; Hewitt et al., 2003; Thrush et al., 2003). For example, fine sediment inputs are considered as ecological stressors on tidal flats, reducing e.g. pore-water flushing and shellfish filtration capacity, which subsequently alters the habitats (Bartzke et al., 2013; 2017; Thrush et al., 2003). Hence, understanding processes controlling erosion and deposition of sediment in intertidal zones will contribute to predicting the long term stability and morphodynamic equilibrium of coastal and estuarine ecosystems (Zhou et al., 2017).

Although the impact of hydrodynamic conditions on erosion and transport of sediment has been a focus of many previous studies, erosion properties of cohesive sediments have been more challenging to quantify because of the confounding effects of cohesion (e.g. Daly et al., 2011; Grabowski et al., 2011; Hunt et al., 2015; Zhang and Yu, 2017; Zhou et al., 2015). Erodibility is defined as a movement tendency of sediment, which can be represented by the erosion threshold T_{cr} N m^{-2}) and erosion rate (ER g m^{-2} s^{-1}) (Andersen, 2001; Harris, et al. 2016). In general, the erodibility of sediment is governed by a combination of the physical and geochemical properties of the sediment itself, the environment where the sediment is deposited and biological processes. These factors are all dynamically linked, and their net impact on erodibility depends on their interactions (Grabowski et al., 2011).

Mudflats are exposed during low tides, and evaporation may decrease the water content of the surface layer. At the beginning, evaporation occurs at the sediment surface and depletes the water content of this layer. During this stage, the evaporation zone shifts downward, and a dry surface layer is formed (Han and Zhou, 2013). In a study on evaporation of cohesive sediment, the thickness of the dry surface layer was shown to depend on hydraulic properties of the sediment and the exposure duration, varying from 0 to 2 cm (Kobayashi and Miyagawa, 1992). Water content has been proven to have a strong relationship with erodibility, and any variation in the water content of a cohesive sediment will lead to changes in its plastic behaviour that alters the erosion properties (Jacobs et al., 2011; Van Ledden et al. 2004; Winterwerp et al. 2018; Winterwerp and Van Kesteren 2004; Zhou et al. 2016a). A freshly deposited mud with high water content behaves as viscous flow in response to shear stress and so is easily entrained while a drier mud exhibits plastic behaviour and will be more resistant to erosion (Amaryan, 1993; Gillott, 2012; Winterwerp and Van Kesteren, 2004). However, this generalisation is not always the case in natural sediments. For instance, a previous study (Amos et al., 2003) documented a lacustrine sediment that had a notably high erosion threshold (0.5 N m^{-2}) despite a high water content (wet bulk density is less than 1100 kg m^{-3}). A field study compared the erosion potential of exposed and submerged mud, and showed a remarkable decrease in *ER* (hundred times lower) and increase in τ_{cr} (more than 3 times higher) of mud exposed to air for 7 h (Widdows et al., 1998). The bed shear strength of sediment increased due to evaporation when mudflats emerged, with this strengthening effect remaining during the subsequent flooded periods (Amos et al., 1988; Fagherazzi et al., 2017).

The evaporation rate of sediment is influenced by many atmospheric factors (e.g. solar radiation, relative humidity, ambient temperature and wind speed), and sediment properties such as permeability and porosity (Dingman, 1994; Davarzani et al., 2014). Here we focus for the first time on the influence of ambient temperature on water content and so the erodibility of exposed sediments. In

addition, temporal variation in erodibility can relate to changes in sediment properties and biofilm abundance. Biofilms, generally consisting of photosynthesizing microorganisms and their extracellular polymeric substances (EPS), have been widely reported in the literature as an important factor stabilizing sediments. For instance, adhesion of sediment can be increased by biofilms, which reduces resuspension and causes the surface sediment to be more stable than the underlying layers (Austen et al., 1999; Friend et al., 2003; Paterson and Black, 2000). Chlorophyll-a (*Chl-a*; a proxy for biofilm biomass) on mudflats varies widely between months, and so the effect of biofilms on sediment stability is likely to vary seasonally (Migné et al., 2004; Murphy et al., 2009). Despite knowing that water content affects erosion properties and that temperature is a principal factor controlling water content through evaporation on mudflats, there has been no study that systematically explores the relationship between ambient temperature and erodibility of exposed sediments. Here we sought to examine the effect of ambient temperature ranges that would occur between day and night time, between seasons and over longer (e.g. global-warming) time scales, by measuring the change in erodibility in natural intertidal sediments exposed to different temperatures. To measure seasonal changes, sediment properties including *Chl-a* as a proxy for variability in biofilm biomass were considered by collecting samples in early summer (Dec 2017) and early autumn (Mar 2018).

2.2 Methods

2.2.1 Sediment collection and preparation

Sediment samples were collected at a single study site on the upper part of the intertidal mudflat in the Firth of Thames, New Zealand (37° 8'31.61"S, 175°32'10.81"E) at low tide on 5 December 2017 and 19 March 2018, when ambient temperatures were 14°C and 25°C, respectively. The Firth of Thames, located in the Waikato region, is a mesotidal estuary of ~800 km^2 (Swales et al., 2015). Tides in the Firth are characterised as semi-diurnal with spring and neap tidal ranges of 2.8 and 2.0 m, respectively (Swales et al., 2019). The Firth annually

receives ~190,000 tonnes of sediment from two rivers (Piako and Waihou), which has caused a rapid accretion of the mudflat (cm y^{-1}) (Swales et al., 2015). Tidal current speeds on the mudflat are reported to be less than 0.2 m s^{-1} (Swales et al., 2015). The mangrove forest colonised an approximate of 800 m wide band on the intertidal flat from 1 to 1.89 m above mean sea level (Montgomery et al., 2018). In the area, mean precipitation is ~1211 mm y^{-1} (Swales et al., 2015), and mean daily minimum air temperature of 0 - 8°C in winter and mean daily maximum air temperature of 20 - 25°C in summer (Chappell, 2014). Sediments deposited in the Firth are smectite clay-rich muds (Swales et al., 2019). On the upper parts of the intertidal flat, sediments have a dry bulk density in a range of 0.38 – 0.57 g cm^{-3}, organic matter content of 6.4 – 13 % and grain density of 2.65 g cm^{-3} (mean value of deposited sediments over the 6 years period from 2007 to 2013 (Swales et al., 2019). Note, however, that these properties are likely to vary to an unknown degree in both space and time.

Twenty surficial sediment samples (depth 0 - 5 mm) were collected on each sampling date and subdivided for analysis of grain size distribution, organic content (OC) and *Chl-a*. The sediment sub-samples used for *Chl-a* analysis were kept in the dark and frozen at -20°C, all other sub-samples (for grain size and OC) were kept at 4°C prior to analysis. Grain size distribution was determined using a laser particle analyser (model Malvern Mastersizer 2000), and samples were pre-treated with 10% H_2O_2 to remove organics and 5% calgon solution to separate soil particles (Day, 1965). OC was estimated as the weight loss on ignition (450°C) for 4 h (Matthiessen et al., 2005) and *Chl-a* (µg g^{-1} dry weight sediment) was determined by the fluorometric method after extraction with acetone (Arar and Collins, 1997).

Twenty Perspex sediment cores (10 cm diameter, 10 cm sediment depth) were also collected on each sampling date and sealed for laboratory erosion experiments. Prior to sealing, the cores were slowly filled with 10 cm column of artificial seawater with a salinity of 28). This salinity is consistent with unpublished

measurements made by the co-authors offshore from the site in April 2016 (28-30; Seabird CTD) in 2-5 m water depth at high tide. Submersing the sediment kept the sediment surface more stable during transport, and the effect of the 10 cm water column on the consolidation of samples is small and negligible (Fiot and Gratiot, 2006). A siphon was used to minimise disturbance of the sediment surface during filling and bubble-wrap was carefully placed on the sediment surface before the filling, then removed on finishing. The submerged cores were then transported back to the laboratory and kept in a dark cool room at 16°C to reduce metabolism; thus the sediment conserved the natural condition of the sampling time before draining prior to treatments (Harris et al., 2016). Unfortunately, some cores were discarded due to (1) being disturbed during transport and (2) the presence of crabs that led to significant sediment disturbance during erosion runs, leaving 14 cores from the Dec 2017 and 15 cores in the Mar 2018 campaigns. Along with the cores for erosion measurements, 15 cores (10 cm diameter, 10 cm depth) on each sampling date were also collected. Those samples were sealed and stored at 4°C for water content analysis.

When sediment samples arrived at the laboratory, three submerged cores were kept undrained and run immediately for erosion measurements. In the case of the exposed trials, the water above the cores was gently drained using a siphon until approximately a couple of millimetres remained above the sediment surface. Because the sediment surface was soft, unconsolidated and prone to disturbance, we retained a few mm of water on the surface then used tissue paper repeatedly placed along the inside edge of the core wall at the meniscus surface to wick the last of the water away. We tested this draining technique on three cores and the measured water content varied by less than 3%.

Sediment cores for exposed trials were treated with a wide range of ambient temperatures including 0°C, 8°C, 25°C and 40°C in which the upper limit of 40°C and the lower limit of 0°C were incorporated to encompass the extremes occurring at our field site. Emersion length varies, depending on tide levels and

bed elevations on the mudflat relative to mean sea level. A six-hour duration was applied to the treatments, which is the average time exposed at mean sea level on an intertidal mudflat with a diurnal un-distorted tide.

Cores were placed in a controlled temperature room at the treatment temperatures for 6 h before the erosion measurements. Logging thermometers were deployed to make sure that temperatures inside the room were consistent, and the monitoring data showed that temperatures varied by less than 3%. All the experiments and erosion measurements were done within two days after collection from the mudflat. To avoid bias between the treated cores due to variations in the time taken to do erosion measurements (cores could not be run simultaneously), the treatment order of cores for erosion measurements was randomly chosen. Trials were replicated with three cores for the submersion experiment and three cores for each of the exposure temperatures, for both the Dec 2017 and Mar 2018 sampling dates.

The second set of 15 cores (10 cm diameter, 10 cm depth; 3 cores per treatment) collected for water content measurements on each sampling date were treated in the same way as erosion cores with submerged and exposed conditions prior to water content analysis. A bias between these cores and erosion cores (which were transported submerged) might be present because sediment cores for water content analysis were stored in drained states. Therefore, they were filled with 10 cm water above the sediment surface for 6 h (equivalent to the submerged duration of erosion cores during transport) to minimise the bias. After exposure treatments, 5 mm deep sediment samples were extracted from the core surfaces and tested for relative water content. Relative water content was calculated as a percentage between the mass of water and mass of dry substances in the samples, and the mass of water is determined by the amount of water lost after drying samples in an oven at 105°C for 24 h (Cambell and Mulla, 1990). The water content is assumed to be the same as the water content of corresponding erosion cores treated with the same conditions.

2.2.2 Erosion measurements

The measurements of erosion potential were carried out using the EROMES device (Andersen, 2001; Andersen et al., 2010; Andersen and Pejrup, 2002; Austen et al., 1999; Friend et al., 2003; Harris et al., 2016; Schünemann and Kühl, 1991) (Figure 2.1A). The EROMES system includes the Perspex tubes that were used to collect sediment cores, a propeller to generate bed shear stress, a baffle to prevent cyclical flow and an optical backscatter sensor (OBS) to record the concentration of sediment in suspension every second (Schünemann et al., 1991). A standard operating procedure for the EROMES is described in Andersen (2001) and Harris et al. (2016). Once the tube was filled up with 20 cm of artificial seawater (salinity of 28, temperature 18 - 20°C), the propeller, baffle and OBS were positioned 3 cm, 1.5 cm and 6.5 cm above the sediment surface respectively. A filling step lasted for about 2 minutes (we did not try to replicate the time scale of tides in our experiments). Bed shear stress was increased from 0.1 to 2.0 N m^{-2}, in increments (steps) of 0.1 N m^{-2}, each with a duration of 2 min. During each EROMES run, 5 water samples were extracted from the water column to calibrate the OBS, at steps encompassing the range of bed shear stresses, and filtered using glass microfiber filter papers (GF/C, Whatman brand). At least 100 ml of water sample was collected, and the amount was immediately replenished with the same amount of artificial seawater.

Suspended sediment concentration (SSC, g L^{-1}) was calculated by dividing the dry weight of sediment (where pre-weighed filter papers were dried at 105°C for 10 h) by the water sample volume. Calibration relationships to convert OBS readings (mA) to sediment concentrations were computed separately for each core (r^2 ranged from 0.94 to 0.99). T_{cr} (N m^{-2}) is the bed shear stress which caused a nominal erosion rate of 0.1 g m^{-2} s^{-1} and *ER* (g m^{-2} s^{-1}) is defined as an erosion rate of sediment at a given nominal bed shear stress of 0.5 N m^{-2} (Andersen, 2001; Andersen et al., 2005; Harris et al., 2016). A mean value of SSC corresponding to each incremental step of bed shear stress (T_b, N m^{-2}) was calculated by averaging

all values of SSC recorded over the 2-min duration of each step. Using a time series of mean SSC values at each step of bed shear stress, erosion rate (E, g m^{-2} s^{-1}) corresponding to the step was calculated. Then an exponential curve ($E = a \times e^{b\mathrm{T}_b}$) that fitted E against T_b was used to derive measures of the erosion potential (T_{cr} and ER) (Harris et al., 2016).

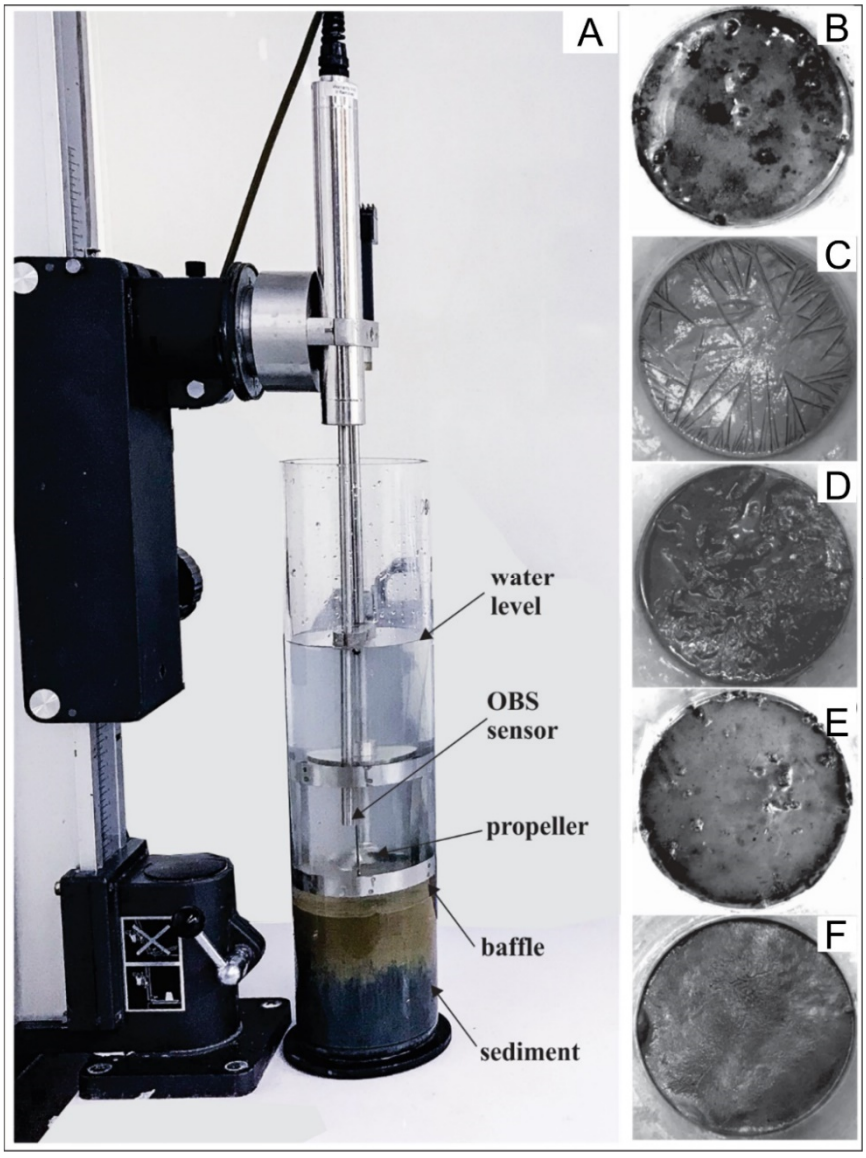

Figure 2.1 A) Setup of the EROMES device. The EROMES core surface immediately after B) draining from the submersion state (i.e. underwater for 6 h during transport to laboratory) and after 6 h exposure at 0 °C (C), 8 °C (D), 25 °C (E) and 40 °C (F). The water content of surficial layer visibly changed with exposure to higher temperatures (compare (D – F)), whereas the surface of the core treated at 0 °C frozen.

2.2.3 Statistical analysis

Statistical analyses were conducted to test whether differences occurred between seasons, between exposed and submerged samples, and between treatment temperatures for unfrozen, exposed cores. A one-way ANOVA was used to assess whether significant differences in sediment properties existed between the Dec 2017 and Mar 2018 sampling dates (n = 20 on each date). To see whether emersion influenced erosion potential, we compared submerged with exposed experiments using a two-way ANOVA that examined interactive effects of two independent fixed factors; temporal variation (between Dec 2017 and Mar 2018) and ambient temperature (treatments) on the τ_{cr} and *ER* variables (n = 3 in each treatment). When the interaction term was significant, Tukey's HSD (Honestly Significant Difference) post-hoc tests were used to establish whether differences between submerged and exposed treatments existed within sampling dates (n = 3 in each treatment). The one-way ANOVA was also used to test for significant differences between water content, erosion potential of two sampling dates within each temperature and to test for trends in erosion potential within exposed, unfrozen treatments with treated temperatures from 8°C to 40°C (n = 3 in each treatment). The relationship between erosion measures and temperature and water content were also examined using regression analysis, and the best fit function was chosen based on significance level and r^2. If a significant linear relationship existed, a test for homogeneity of slopes compared the two regression lines to assess the effect magnitude of the independent factors on τ_{cr} and *ER* between the two sampling dates (n = 3 in each treatment). The 0°C experiment was excluded from this analysis because a frozen water layer covered the sediment surface after the treatments, and the sediment erosion characteristics were clearly different from the higher-temperature treatments. We used the Statistica 13© package to do the statistical analyses. In this study, a statistical test is significant if the probability (p-value) was less than 0.05.

2.3 Results

2.3.1 Sediment properties

Mean grain size (D_{50}, µm) for Dec 2017 samples was significantly smaller than that of the sediments collected in Mar 2018, ($p < 0.001$). As a consequence, the mud (grain size < 63 µm) content for samples from the Dec 2017 was higher than that for the Mar 2018 sediments ($p < 0.05$). There was also a significant increase in *Chl-a* content in Mar 2018 (which was 2.4 times higher than that in Dec 2017; $p < 0.001$) (Table 2.1).

Table 2.1 Summary of sediment properties

	Dec 2017	Mar 2018
D_{50} (µm)	6.37 ± 1.05	8.90 ± 0.99
Clay (%)	37.77 ±4.13	26.30 ± 2.80
Silt (%)	55.25 ± 5.28	63.41±3.77
Sand (%)	6.95 ± 2.76	10.25 ± 3.10
Chl-a (µg g^{-1})	9.18 ± 2.72	21.64 ± 5.79
OC (%)	9.76 ± 0.28	10.10 ± 3.21

Data are presented as means ± one standard deviation (n = 20)

2.3.2 Effect of the exposure on erodibility of intertidal sediments

Comparison between exposed and submerged treatments showed that τ_{cr} increased 1.2 to 2.2 times, and *ER* decreased 1.1 to 6.5 times. There was a significant difference between τ_{cr} from submerged and exposed experiments ($p < 0.001$). Submerged samples always had the lowest τ_{cr}, and exposed 40°C samples had highest τ_{cr} (Figure 2.2A). τ_{cr} of 0°C treatments was higher than the 8°C and lower than the 25°C treatments, which was replicated in both sampling dates. The statistical analysis indicated that there was a significant difference between the 40°C and the submerged treatments ($p < 0.05$) in Mar 2018, but there were no differences between the submerged and the rest of the treatments in Dec 2017. *ER* patterns were similar for both sampling dates (Figure 2.2B). The 40°C treatments had the lowest *ER* while submerged treatments showed the highest

ER, followed by samples of 8°C, 0°C and 25°C, respectively. Sediment collected in Mar 2018 had an extremely low *ER,* which fluctuated between replicates; therefore, no significant differences were detected between submerged and exposed treatments. In contrast, *ER* of the Dec 2017 sediments were high, and *ER* of the submerged treatment was significantly higher than in the 25°C and 40°C exposure treatments ($p < 0.001$), and the 0°C ($p < 0.05$) treatment. The 8°C treatments were easily eroded and were not different from the submerged samples (one-way ANOVA, $p = 0.29$).

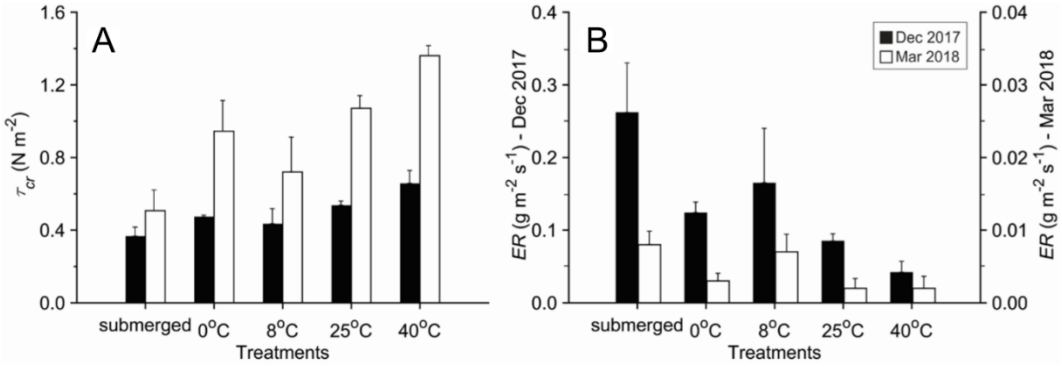

Figure 2.2 A) Mean erosion threshold (T_{cr}) and B) erosion rate (*ER*) as a function of treatment and sampling date. Error bars correspond to one standard error.

2.3.3 Temperature sensitivity in exposed sediments

In general, a significant relationship between water content and exposure temperature was found for both sampling dates (quadratic polynomial fit, $p < 0.001$). Relative water content of sediment cores decreased when exposure temperature increased, with water content of the Dec 2017 sediments decreasing from 314% (submerge state) to 176% (at 40°C exposure) and by a similar amount in Mar 2018 (from 308% to 165%; Figure 2.3). The one-way ANOVA indicated significant differences in water content between different temperatures within the same date ($p < 0.001$) but no significant differences in water content between the dates ($p > 0.05$).

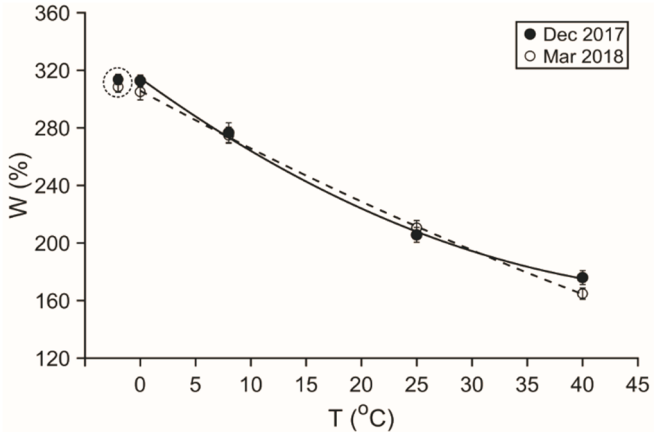

Figure 2.3 Relationship between relative water content (*W, %*) and ambient temperature (*T*, °C). Data points circled by the dashed line represent the water content at drained state from the submersion. Quadratic polynomials have been fitted to the remaining data points ($r^2 > 0.94, p < 0.001$). Error bars correspond to ± one standard error.

Increasing ambient temperature decreased water content of the sediments, and so increased the stability of exposed sediments (Figure 2.4). As the consequence of lower water content of the sediments exposed to a higher temperature, a significant increasing trend of T_{cr} was detected in the unfrozen, exposed samples (linear fit, p <0.05 for both dates) (Figure 2.4A). Although there was an outlier value of T_{cr} in the 8°C treatment from Mar 2018 (which we do not know the cause of), the relationship was still significant. A significantly decreasing trend (logarithmic fit, p < 0.05) in *ER* as a function of temperature was detected in the non-frozen exposed treatments from the Dec 2017 sediments. A negative relationship was found between relative water content and T_{cr} (linear fit, p < 0.05) for both sampling dates while *ER* was positively correlated to relative water content (quadratic polynomial fit, p < 0.05) (Figure 2.4B and 2.4D). *ER* in Mar 2018 did not show a significant trend; the *ER* of treatments was very small and variable (0.002 - 0.008 g m^{-2} s^{-1}) (Figure 2.4C). Similarly, there was no statistically significant relationship between relative water content and *ER* in Mar 2018 (p = 0.08) (Figure 2.4D).

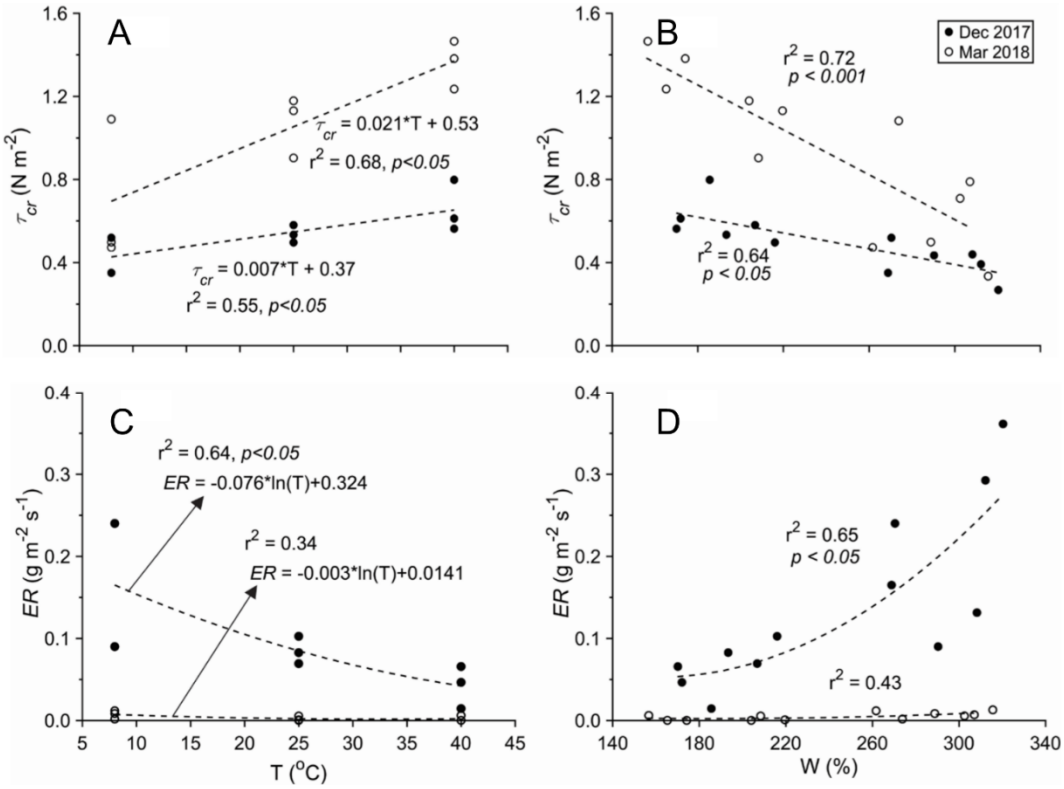

Figure 2.4 Change in (A) erosion threshold (T_{cr}) and (C) erosion rate (*ER*) with ambient temperature (T) and change in (B) T_{cr} and (D) *ER* with relative water content (*W*). *p* values are not presented for non-significant regressions.

2.3.4 Seasonal differences

The statistical tests for homogeneity of slopes showed a significant difference between the two regression lines of T_{cr} and temperature ($p < 0.05$), with the Mar 2018 having higher slopes (Figure 2.4A) indicating that increasing temperature had a greater effect in Mar 2018 compared to the Dec 2017. Erosion measurements in Dec 2017 and Mar 2018 were compared to test for temporal variation in T_{cr} and *ER* (Figure 2.2). Overall, the Mar 2018 sediments showed higher T_{cr} and much lower *ER,* and so were more stable than the Dec 2017 samples. There was a significant difference in T_{cr} between the 40°C Dec 2017 and the 40°C Mar 2018 treatments ($p < 0.05$). *ER* were significantly different between submerged treatments ($p < 0.001$) and between 8°C ($p < 0.05$) treatments of the Dec 2017 and the Mar 2018 sediments.

2.4 Discussion

Our results showed, with the exception of the 0°C treatment, that the higher the temperatures to which the sediments were exposed, the lower their water content, which leads to more stabilized sediments (higher τ_{cr} and lower *ER*). Increasing water content (150 - 350%, comparable to our study of 165 - 315%) is often linearly correlated with a decrease in cohesive sediment stability; however, over wider ranges (30 - 1200%), the relationship may be non-linear (Amaryan, 1993). At high water content, the water layer absorbed by clay particles is thicker, which forces particles apart, reducing inter-particle interaction. This process might weaken the bond between particles and destroy any network structure inside the mud (Yong and Warkentin, 1966). Conversely, drying of cohesive sediments is accompanied by shrinkage that brings particles to close together, which tends to strengthen attractive forces between them (Yong and Warkentin, 1966). Water content decrease induces consolidation and increases bulk density, which has also been shown to increase the stability of muddy sediments (Winterwerp and Van Kesteren, 2004; Grabowski et al., 2011). Note that the shrinkage limit for a smectite clay sediment is in the water content range of 45 – 62% (Yong and Warkentin, 1966), which is much lower than the lowest water content of our sediment (~165%). τ_{cr} and *ER* within treatments were quite variable, making it difficult to detect changes between some treatments with confidence; in future more replication is required. Our observation that the erosion properties of the upper few millimetres of sediment on intertidal mudflats can be highly variable was consistent with Houwing (1999).

The Dec 2017 sediments were finer than the Mar 2018 sediments, which should cause a lower evaporation rate because the porosity of fresh cohesive sediment increases when the mean grain size increases and so creates more pore space for free water movement between particles, and subsequently higher permeability (Urumovic´, 2016). Moreover, the higher clay content leads to lower permeability of the Dec 2017 sediments, which in turn lowers evaporation rate during exposure

(Winterwerp and Van Kesteren, 2004). Nevertheless, there were no statistically-significant differences in water content when two sampling dates were compared within a treatment. It might be that the higher level of biofilm embedded on the surface of the Mar 2018 sediments led to a reduction in hydraulic conductivity as found by Volk et al. (2016) and a lower evaporation rate during exposure. A negative correlation between organic matter and hydraulic conductivity has also been reported (Nemes et al., 2005) and therefore, the higher organic content observed in Mar 2018 might also contribute to a reduction of hydraulic conductivity.

Sediments from Mar 2018 were significantly more stable than those from Dec 2017, which may be explained by the difference in sediment properties (Table 2.1). In particular, the *Chl-a* in the Mar 2018 samples was much higher than that in the Dec 2017 samples. Previous studies have documented that high *Chl-a* content is positively related to τ_{cr}, and negatively related to *ER* (Andersen, 2001; Austen et al., 1999; Sutherland et al., 1998). Biofilms have been observed to make a smoother sediment surface that reduces frictional drag at the surface, and adhesion of sediment also increases with biofilms where they physically bind sediment grains (Paterson, 1989).

Freezing caused an effect on erosion potential because of ice formation on the sediment surface. For the 0°C experiment, τ_{cr} was lower than that of 25°C and higher than the 8°C treatments, while *ER* was higher than that of 25°C and lower than that of 8°C for both sampling dates (Figure 2.2A and 2.2B). In terms of water content, we would expect the 0°C and 8°C experiments to be similar because evaporation is low at low temperatures (Dingman, 1994). However, after treating at 0°C for 6 h, a thin layer of ice occurred at the sediment surface and the layer needed to melt to allow the erosion of sediment in sub-layers (Figure 2.1C). Hence, those samples were more stable during the initial increments of bed shear stress, which led to lower erodibility compared to the 8°C treatment. Previous studies have shown that freezing and ice formation increase aggregate stability under the

impact of water flow by bringing near surface sediment particles into contact with each other (Czurda et al., 1995; Dagesse, 2013; Lehrsch et al., 1993). Moreover, increasing salinity of surface seawater from 18 to 35 would decrease the freezing point of the seawater by about 1°C (Fujino et al., 1974). Therefore, the effect of salinity variation on the freezing point of seawater should be considered in future work concerning the stability of intertidal sediments.

A study on the impact of water content, bulk density and yield stress on erosion threshold of cohesive sediments with various median grain sizes ranging between 6 - 72 µm was conducted by Zhang and Yu (2017). Cohesion (or inter-particle interaction) of cohesive sediments is directly related to the yield stress. Their study presented results in a modified Shields diagram showing critical Shields parameter ($\theta_{cr} = \tau_{cr} /(\rho_s - \rho)gD_{50}$), where ρ_s is the grain density of sediments, ρ is density of water, g is gravitational acceleration) as a function of dimensionless sediment size parameter ($D^* = D_{50}[g(\rho_s - \rho)/(\rho\upsilon^2)]^{1/3}$, where $\upsilon = 9.68\times10^{-7}$ m^2 s^{-1} at 20°C, is the kinematic viscosity), which allowed comparison with previous studies on cohesive sediment. The range of erosion thresholds that we measured was consistent with previously published results (Xu et al., 2015; Zhang and Yu, 2017) (Figure 2.5).

The difference in θ_{cr} was caused by different bulk densities, whereas the variation was attributed to yield stress (or cohesion) differences in Xu et al. (2015) and Zhang and Yu (2017), respectively. In our experiments, the water content causes the variation of θ_{cr}, and changes in water content might in turn lead to changes in consolidation state and bulk density of sediments (which we did not measure). θ_{cr} at similar D^* of our study were higher than that in Zhang and Yu (2017). It is because the criterion to define the incipient motion of sediments (3.2×10^{-6} to 7.4×10^{-6} kg m^{-2} s^{-1}) used in their study was lower than our criterion (10^{-4} kg m^{-2} s^{-1}). Another reason is that deliberately disturbed sediments were used in their study to compare θ_{cr} of the same sediment with different yield stress. The disturbance of muddy sediments reduces yield stress and lowers erosion threshold of the

sediments (Zhang and Yu 2017). In contrast, our cores are composed of natural and less disturbed mud, and so should have higher yield stress compared to the disturbed ones. In the conventional sense of the Shields diagram, higher θ_{cr} is expected for finer sediments; our result, however, displayed lower θ_{cr} for the Dec 2017 mud (D_{50} = 6.37 µm) that are finer than the Mar 2018 mud (D_{50} = 8.9 µm). In addition, *Chl-a* has been proved to significantly increase erosion threshold of sediments, which is consistent with the higher θ_{cr} for the Mar 2018 sediments.

Although many studies have been conducted to understand factors that affect the erosion potential of cohesive deposits, a better model to predict erosion quantities is still not available (Grabowski et al., 2011; Zhang and Yu, 2017). Cohesive sediment transport models apply a range of different formulas to simulate erosion processes. Among various equations, the Partheniades's formulation developed in 1965 has been widely applied in numerical transport models of cohesive sediment (e.g. Borsje et al., 2008; Franz et al., 2014; Zhou et al., 2016b):

$$E = ER \times (\frac{\tau_b}{\tau_{cr}} - 1)$$

Applications of the formulation to the erosion of cohesive sediment in intertidal areas can be seen in previous studies, where in general these erosion parameters and critical bed shear stresses for erosion were set to constant values during tide cycles (Borsje et al., 2008; Franz et al., 2014; Zhou et al., 2016b). For examples, *ER* and T_{cr} were set to 5×10^{-2} and 10^{-1} g m^{-2} s^{-1}; 0.2 and 0.4 N m^{-2} in Borsje et al. (2008) and Zhou et al. (2016b), respectively. Changes in erosion properties of the sediment in intertidal areas due to an emersion have been ignored in these models. By comparing *E* calculated from *ER* and T_{cr} using the submerged treatment results and *E* from *ER* and T_{cr} using the results of the exposed treatment including the influence of temperature (i.e. using the regression equations), *E* could decrease by 1.3 - 14.3 times depending on the exposure temperatures (which control how much water evaporated from the sediments). Therefore, future

modelling efforts should consider the strengthening effect of ambient temperature on the erosion resistance.

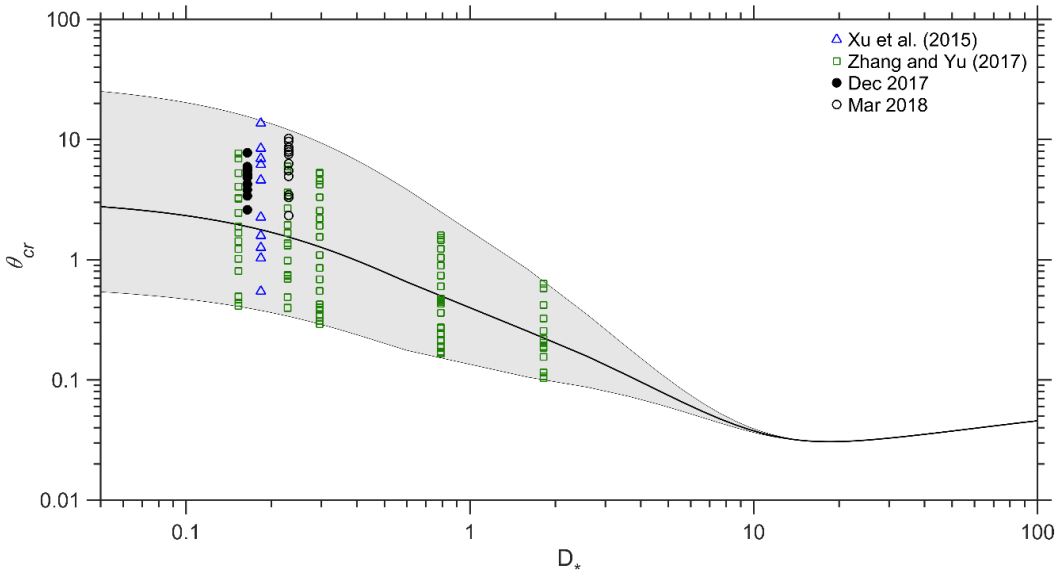

Figure 2.5 A modified Shields diagram comparing results with previously published data relating the critical Shields parameter (θ_{cr}) to the dimensionless grain size parameter (D^*). The shaded area shows variable ranges of θ_{cr} (after Zhang and Yu, 2017).

The global mean temperature has been predicted to be higher in the coming years than it has been in the last century. Between 2081 - 2100, it has been projected to increase 1, 1.8, 2.2 and 3.7°C compared to the 1986 - 2005 reference period in climate change scenarios RCP2.6, RCP4.5, RCP6.0 and RCP8.5, respectively (Collins et al., 2013). Our regression equations (Figure 2.4A and 2.4C) showed that even the lowest scenario RCP2.6 will cause an τ_{cr} increase of 1.1 (±0.01, error corresponds to ± one standard error) - 1.7 (±0.01) % and *ER* decrease of 2.4 (±0.03) - 10.2 (±0.70) % for an increase in temperature at each extreme of the range 8 - 40°C. The temperature increase associated with the highest scenario RCP8.5 has the strongest effect on erodibility of cohesive sediment, where τ_{cr} increases by 4.0 (±0.02) - 6.1 (±0.10) %, and *ER* declines by 8.9 (±0.13) - 37.7 (±2.43) %. These changes to the erodibility of sediment mean that intertidal mudflats will be more

stable, and may be more likely to retain sediment and increase elevation relative to rising sea levels. As suggested in Kirwan et al. (2016a), more research about the influence of climatic forces on erosion or accretion of seaward edge of coastal marshes are needed to improve predictions of marsh adaptability to sea level rise.

This study has considered seasonal changes in erodibility of sediments by collecting data in early summer and early autumn; however our measurements may not represent the range of natural variation because many sediment properties such as *Chl-a* might change widely during winter and summer (Migné et al., 2004; Murphy et al., 2009). Sediments were only from one site, the Firth of Thames, which limits the ability to generalise the findings. Higher water content directly changes plasticity of cohesive sediment and reduces erosion resistance (Winterwerp and van Kesteren, 2004) so therefore, it is essential to include plastic and liquid limits of sediments in any future study. Although preliminary observations suggest that the strengthening effect remained during subsequent flooding, we do not yet have the evidence to generalise this statement. At some point, the sediments must return to their original less-consolidated condition because relatively unconsolidated sediments were collected from an intertidal region which is regularly exposed and re-flooded. We are planning a new suite of experiments to address this question.

2.5 Conclusions

A higher ambient temperature during exposure results in lower relative water content of surface sediment that tends to result in more stabilized sediments in the subsequent flood periods. The increase in τ_{cr} (by 1.2 to 2.2 times) and decrease in *ER* (by 1.2 to 6.2 times) corresponding to elevated exposed temperatures were triggered by a 1.01 – 1.78 times decrease in relative water content. *Chl-a* significantly stabilised sediments even when they have larger median grain sizes that are expected to have lower critical shear stress in a traditional mean of the Shields diagram. Freezing temperatures caused a thin layer of ice to form on the sediments, which delayed the onset of erosion, and so decreased erodibility.

Our findings on erosion properties of sediment indicated that substantial changes can occur during tidal cycles because of varying exposure conditions, which may ultimately contribute to changing the intertidal morphology as temperature changes over the coming years. In terms of ambient exposure temperature, erosion resistance of cohesive intertidal sediments emerged during low tides is expected to be strengthened as a consequence of global warming.

Chapter 3

The effect of long-term aerial exposure on intertidal mudflat erodibility

Nguyen, H. M., Bryan, K. R., & Pilditch, C. A. (2020). The effect of long-term aerial exposure on intertidal mudflat erodibility. Earth Surface Processes and Landforms, 45(14), 3623-3638.

Contribution of authors

Chapter 3 presents the article entitled “The effect of long-term aerial exposure on intertidal mudflat erodibility”, published in 2020 in the Earth Surface Process and Landforms.

Sediment samples using for laboratory experiments were obtained during fieldwork in the Firth of Thames, New Zealand, which I designed and executed as part of my PhD research. I also designed and conducted laboratory experiments, processed and analyzed all the data, produced figures and wrote the manuscript. My co-authors assisted with planning field- and lab-work, data analysis, statistical methods, edited drafts and advised on directions.

Abstract

Intertidal zones by definition are exposed to air at low tide, and the exposure duration can be weeks (e.g. during neap tides) depending on water level and bed elevation. Here we investigated the effect of varying exposure duration (6 h – 10 d) on intertidal mudflat erosion (measured using the EROMES device), where the effects of water content and biofilm biomass (using chlorophyll-*a* content as a proxy, *Chl-a* μg g^{-1}) were taken into account. Sediments were collected between spring-summer (in Oct 2018, Jan 2019 and Feb 2019) from an intertidal site in the Firth of Thames, New Zealand. Longer exposure duration resulted in more stable sediments (higher erosion threshold (T_{cr}; N m^{-2}) and lower erosion rate (*ER*; g m^{-2} s^{-1})). After 10 d, exposure increased T_{cr} by 1.7-4.4 times and decreased *ER* 11.6 – 21.5 times compared with 6 h of exposure. *Chl-a* and water content changed with exposure duration and were significantly correlated with changes in T_{cr} and *ER*. The stability of sediments after two re-submersion periods following exposure was also examined and showed that the stabilising effect of exposure persisted even though water content had increased to non-exposure levels. Re-submersion was associated with an increase in *Chl-a* content, which likely counteracted the destabilising influence of increased water content. A site-specific model, which included the interplay between evaporation and biofilm biomass, was developed to predict water content as a function of exposure duration. The modelled water content ($W_{Mod.}$) explained 98 % of the observed variation in water content ($W_{Obs.}$). These results highlight how exposure period can cause subtle changes to erosion regimes of sediments. An understanding of these effects (for example in sediment transport modelling) is critical to predicting the resilience of intertidal zones into the future when sea-level rise is believed to exacerbate erosion in low-lying areas.

Keywords: sediment stability, low-lying areas, erosion rate, erosion threshold, intertidal zones, long-term exposure, the Firth of Thames

3.1 Introduction

Intertidal ecosystems, including sand/mud flats, salt marshes, and mangroves are some of the most productive and yet among the most vulnerable ecosystems on Earth (Kirwan and Megonigal, 2013). Coastal zones throughout the world are being threatened by many factors such as sea-level rise, insufficient sediment supply, and conversion into agricultural lands (Xie et al., 2018). As sea level rises, the ability of these ecosystems to trap sediments and increase their elevation will determine their long-term stability. Sediment retention depends on the balance between erosion and accretion, along with the consolidation of sediments after deposition (Gilman et al., 2008). Moreover, intertidal ecosystems can be dynamically connected; for example, short-term sediment dynamics on intertidal flats might determine long-term cyclic behaviour of marshes (Bouma et al., 2016). A key parameter governing sediment dynamics is the bed resistance to the erosive forces generated by waves and currents.

Water content has been widely recognised as a key factor controlling the erosive behaviour of cohesive sediments, as it directly influences mechanical properties of clays (e.g. Amos et al., 2004; Bale et al., 2007; Van Ledden et al., 2004; Winterwerp and Van Kesteren, 2004). Specifically, any changes in water content alter the plastic properties of cohesive sediments (Grim, 1962; Winterwerp and Van Kesteren, 2004). The water content at which sediments change from a solid to a plastic state, and from a plastic to a liquid state are called the plastic and liquid limits, respectively (Grim, 1962). The limits are specific to each sediment type and depend on properties such as grain size, organic content (OC) and clay minerals of the sediment (Grim, 1962). The water content of intertidal sediments can decrease during exposure due to evaporation and/or draining and increase during submersion by infiltration of water molecules via burrows and within pores of the substrate (Yong and Warkentin, 1966). The frequency and duration of exposure depend on the tide and bed level, and intertidal flats are expected to have longer exposure duration during neap tides (at elevations above the neap tidal range).

Evaporation only occurs on the surface layer of sediments during the exposure, which reduces the water content of the surficial layer (0 – 2 cm depth depending on the hydraulic properties of sediments and duration of exposure) (Han and Zhou, 2013; Kobayashi and Miyagawa, 1992). The evaporation of water from exposed sediments is affected by many meteorological factors such as air temperature, solar radiation, relative humidity of the atmosphere and wind speed (Dingman, 1994). Also, the evaporation rate is affected by the pre-existing water content as sediment with lower water content have a lower rate and vice versa (Brutsaert, 2014; Hang et al., 2016; Teuling et al., 2006).

In addition to water content, other physical and biological factors interact to influence sediment erodibility (Black et al., 2002; Grabowski et al., 2011). For instance, the growth of biofilms is believed to decrease the effective porosity by clogging pore spaces between particles, which in turn reduces the hydraulic conductivity of sediments (Lianfang et al., 2009; Vandevivere and Baveye, 1992; Volk et al., 2016). As a consequence of the growth of biofilms, the evaporation that occurs during exposure might decrease and affect water content. Previous studies have found that biofilms often colonise intertidal mudflats, and stabilise sediments against erosion (e.g. Black et al., 2002; Chen et al., 2017; Friend et al., 2003). The presence of biofilms within pores in sediments enhances inter-particle attraction by physically bonding them together (Underwood and Paterson, 2003), while biofilms embedded on the sediment surface make it smoother which reduces drag force imposed on the bed surface (Paterson, 1989). Biofilms generally consist of microphytobenthos and their extracellular polymeric substances (EPS), and microphytobenthos growth is dependent on air temperature, light, and nutrient availability (Davoult et al., 2009; Migné et al., 2004). Seasonal changes in sediment properties strongly affecting sediment erodibility (Black et al., 2002; Nguyen et al., 2019; Widdows et al., 2000) are largely driven by temporal variation of chlorophyll-a (*Chl-a* μg g^{-1}; a proxy for biofilm biomass) over seasonal and shorter time scales (Migné et al., 2004; Nguyen et al., 2019; Staats et al., 2001; Tolhurst et al., 2006a). Microphytobenthos uptake water

for metabolic functions (which change seasonally). In nature, EPS exist as highly hydrated molecules (approx. 99% water) (Decho, 1990) thus playing an important role in water retention by preserving an extremely hydrated microenvironment around biofilm organisms that contributes to desiccation tolerance (Flemming, 2016). The uptake of water by biofilms during growth may enhance the stabilisation of intertidal sediments. Conversely, biofilms cover the surface, which may prevent evaporation during exposure.

Exposure has been shown to stabilise exposed cohesive sediments (Fagherazzi et al., 2017; Nguyen et al., 2019; Tolhurst et al., 2006a; Widdows et al., 1998), with the strengthening effect remaining in subsequent flooding cycles (Fagherazzi et al., 2017). However, these studies only investigated the erodibility after short-term exposure, the average time exposed at mean sea level on an intertidal mudflat with a diurnal un-distorted tide (e.g. 6 h in Nguyen et al. (2019), and 7 h in Widdows et al. (1998)). Here we sought to systematically explore the effect of exposure on variation in erosion properties (erosion threshold, τ_{cr} N m^{-2} and erosion rate, *ER* g m^{-2} s^{-1}) of cohesive sediments during much longer-term (after 6 h, 1, 4 and 10 d) exposure, such as occur on the high parts of the intertidal flat during neap tides. We also aimed to explore how long the strengthening effect of exposure persisted over subsequent flooding cycles (as shown in Fagherazzi et al., 2017) and the role of microphytobenthos in stabilisation. Our results indicate the importance of water content in controlling erosion. We then used our measurements and existing formulations for evaporation rate (e.g. Fagherazzi et al., 2017), to develop a new model to predict water content of sediments during exposure, which ultimately could be incorporated into coastal sediment transport models. We also provided an understanding of the effect of biofilm growth on evaporation rate, by replicating our experiments over two seasons (springtime, Oct 2018 and summertime, Jan/Feb 2019) in which biofilm growth rates were different.

3.2 Study site

Muddy sediments were collected from a single representative site (lat -37.141840°, long 175.537054°) on the upper part of an intertidal mudflat in the Firth of Thames, a meso-tidal estuary of ~800 km^2 in the Waikato region, New Zealand (Figure 3.1A and 3.1B) (Swales et al., 2015).

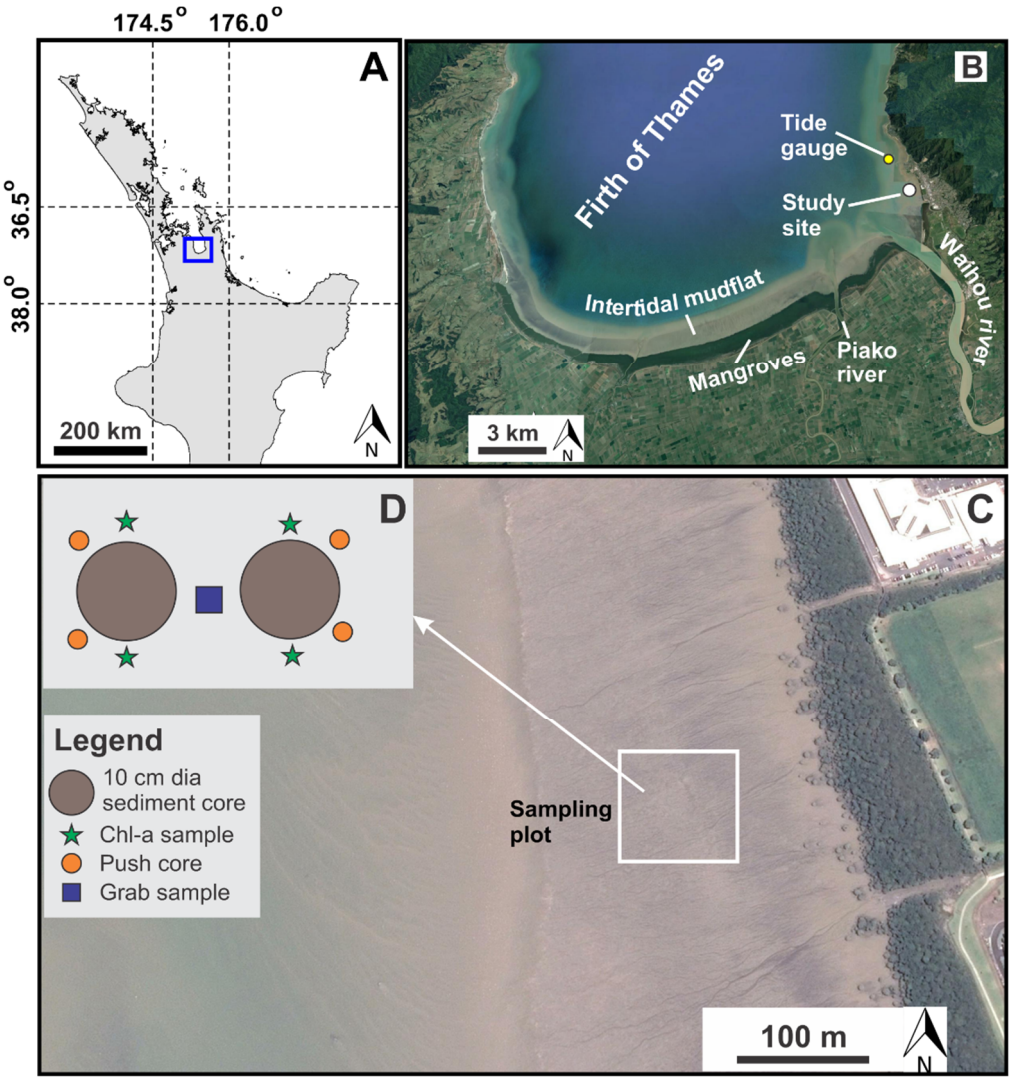

Figure 3.1 A) Location of the Firth of Thames in North Island, New Zealand (blue box). B) Location of the study site. C) A sampling plot on the upper intertidal flat. D) A sampling event associated with each EROMES core in the sampling plot (24 – 30 sampling events for each date). See text for further details. (Image courtesy of Google Earth, Imagery Date, 18 Oct 2018).

The intertidal sediments mainly consisted of fine particles of 55 – 63% silt, 26 – 38% clay and 7 – 10% very fine sand, mean grain size (D_{50}) of 6.4 – 8.9 µm (Nguyen et al., 2019), grain density of 2.65 g cm^{-3}, dry bulk density of 0.38 – 0.57 g cm^{-3} and organic content (OC) of 6.4 – 13% (Nguyen et al., 2019; Swales et al., 2019, also summarised in Roskoden et al., 2019), typical of many mudflats globally (e.g. Bale et al., 2007; Zhang and Yu, 2017). Tides in the Firth are semidiurnal with a spring tidal range of 2.8 m and a neap tidal range of 2.0 m (Swales et al., 2019). The region has relatively cold winters and hot summers with mean minimum and maximum air temperatures of 0 – 8° C and 20 – 25° C, respectively (Chappell, 2014).

A year of tide level data (Aug 2017 - Sep 2018) was used to estimate the frequency and duration of submersion and exposure events for different bed elevations on the intertidal flat to inform experimental treatments (Figure 3.2). The data were acquired from a tide gauge (Figure 3.1B) located in Kuranui Bay in the Firth of Thames, lat -37.127297°, long 175.520795°, about 1.8 km from the sampling site (provided by the National Institute of Water and Atmospheric Research – NIWA. The datum for bed elevation and tide level is mean sea level (MSL). The exposure duration was always less than 12 h for the lower parts of the intertidal mudflat (elevations < 1.0 m), while longer exposure durations occurred on the upper parts due to spring and neap tide variations (Figure 3.2B). For instance, at a bed elevation of 1.6 m, there were 236 events of 6-12 h exposure, 23 events lasting between 12 - 120 h and 20 events of greater than 120 h over a year. In contrast, submersion at an elevation of 1.6 m was less frequent (< 265 events annually). The submerged duration for the upper parts was mostly 0 – 3 h, and a submersion duration of greater than 4 h was the most common for the lower parts (Figure 3.2C).

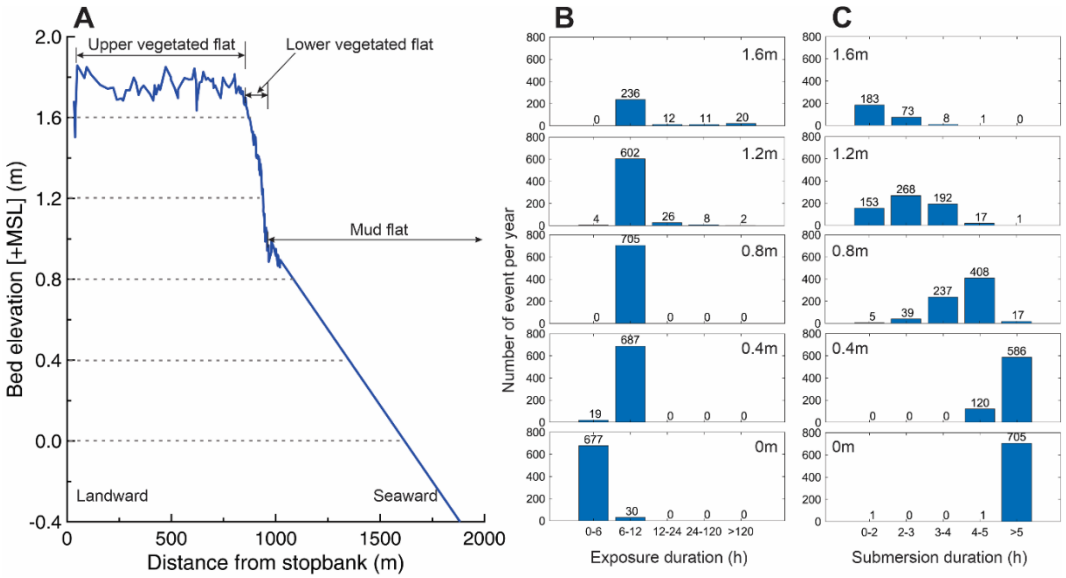

Figure 3.2 A) A typical profile of the intertidal area in the Firth of Thames (Montgomery et al., 2019). Frequency of B) exposure duration and C) submersion duration at bed elevations of 0, 0.4, 0.8, 1.2 and 1.6 m on the intertidal flat (elevations marked with dashed lines on panel A).

3.3 Methods

3.3.1 Collection and preparation of sediments

Sediments were collected at low tide in spring (on 8 Oct 2018) and summer (on 18 Jan 2019 and 15 Feb 2019). The Oct 2018 and Jan 2019 samples were used for exposure experiments, and the Feb 2019 samples were used for re-submersion experiments (described in detail below). On each sampling date, sediments were collected from 24 - 30 randomly-selected positions in a 100 × 100 m plot (Figure 3.1C). At a single sampling position, a pair of Perspex tubes (10 cm dia, 40 cm high) were used to collect 10 cm deep cores of surficial sediments. The cores were sealed by bottom caps fitted before filled with a 10 cm column of artificial seawater, salinity of 28 (a comparable salinity to seawater on the intertidal flat (Nguyen et al., 2019)), then caps fitted to keep the cores more stable during transport. The effect of the 10 cm water column on sediment consolidation is negligible (Fiot and Gratiot, 2006). Four small push cores (2.5 cm dia, 2 cm depth) were sampled from the area surrounding the Perspex tubes (Figure 3.1D), then

thoroughly mixed in a sealed plastic jar. These push core samples were used to determine the in situ sediment water content, bulk density, grain size distribution, and organic content (OC), and were considered to have the same properties as the 10 cm dia sediment cores from each sampling position. For the in situ *Chl-a* content, four sub-samples of 0 - 0.5 cm depth surficial sediment were also collected surrounding these tubes (Figure 3.1D), and well mixed in a plastic bag. Six grab samples (0 - 1 cm depth, ~2 kg per-sample) were collected at random locations in the sampling plot to measure the Atterberg limits (plastic and liquid limits). Therefore, grab samples were not collected at every single sampling positions in the 100 × 100 m plot.

After arriving at the laboratory, the cores were carefully drained. Three cores were used for immediate water content tests (by extracting the 0 - 0.5 cm surface sediment layer) and were considered to reflect the water content of sediments in their submerged state prior to the exposure and re-submersion experiments. Samples for *Chl-a* content were kept in the dark and at -20 °C to suppress the metabolism of micro-organisms before measurements (Arar and Collins, 1997), while push core samples were kept at 4 °C prior to analysis.

Water content (%) was estimated from the amount of water lost after drying samples in an oven at 105 °C for 24 h (Cambell and Mulla, 1990). In this study, the relative water content of a sediment mass is defined as the ratio of the mass of water in the voids to the total mass of solids (Flemming and Delafontaine, 2000). We distinguished observed water content ($W_{Obs.}$ gained from laboratory measurements) from that predicted by modelled water content ($W_{Mod.}$) presented in more detail below. Samples for grain size analysis were immersed in 10 % H_2O_2 to eradicate organics and 5 % calgon solution was used to dispersed particles prior to running them on Malvern Mastersizer 2000 (Day, 1965). OC was estimated as the weight loss on ignition (450 °C) for 4 h (Matthiessen et al., 2005) and *Chl-a* content (μg g^{-1} dry weight sediment) was determined by the fluorometric method after extraction with acetone (Arar and Collins, 1997). We report our *Chl-a* content

measurements per g dry weight, although care needs to be taken interpreting these data because changes in the *Chl-a* content could be caused by changes in the mass of other components making up the sediment, e.g., Flemming and Delafontaine (2000), Perkins et al. (2003) and Tolhurst et al. (2005). The cone penetrometer method and thread-rolling method were used to test the liquid limit and plastic limit of sediments, respectively (BSI, 1990).

3.3.2 Design of experiments

Two experiments on exposure and one on re-submersion were designed to examine the effects of exposure period and subsequent immersion periods on the erodibility of intertidal muddy sediments. Exposure and re-submersion durations used in the experiments were based on the probability distribution calculated using tide level data from the Firth of Thames (Figure 3.2).

The exposure experiment

Sediment cores, after arrival at the laboratory, were drained (by a siphon, following Nguyen et al., (2019)) and exposed to air for 6 h, 1, 4 and 10 d (called "exposure period" from here on, Figure 3.3B). To avoid the effect of rainfall on exposed sediments, the cores were put under a roof in an open environment where the wind, sunlight and relative humidity of the atmosphere controlled the evaporation process of sediments. For each exposure period, six cores were used: three cores for sediment erosion measurements (see below) and three for surface (0 - 0.5 cm) *Chl-a* and $W_{Obs.}$ content measurements. Samples were extracted from each core using a spatula and analysed separately.

The re-submersion experiment

Here we examined the erosive behaviour of exposed sediments after subsequent re-submersion events. Specifically, we compared the effect of re-submersion immediately after exposure (exposure only), after one tidal cycle (1 re-submersion event) and two tidal cycles (2 re-submersion events) for sediment exposed to air

for 1, 4 and 10 d. For the single re-submersion event, cores were kept submerged for 4 h, whilst cores used for two re-submersion events were exposed to air for 6 h between immersion events. Erosion measurements were made on three replicates cores for each combination of exposure period and re-submersion event. As in the exposure experiment, three additional cores of 10 cm dia (collected around the same position as the erosion cores) were subjected to the same exposure treatment and analysed for $W_{Obs.}$ and *Chl-a* content (for $W_{Obs.}$ and *Chl-a* content tests on each core).

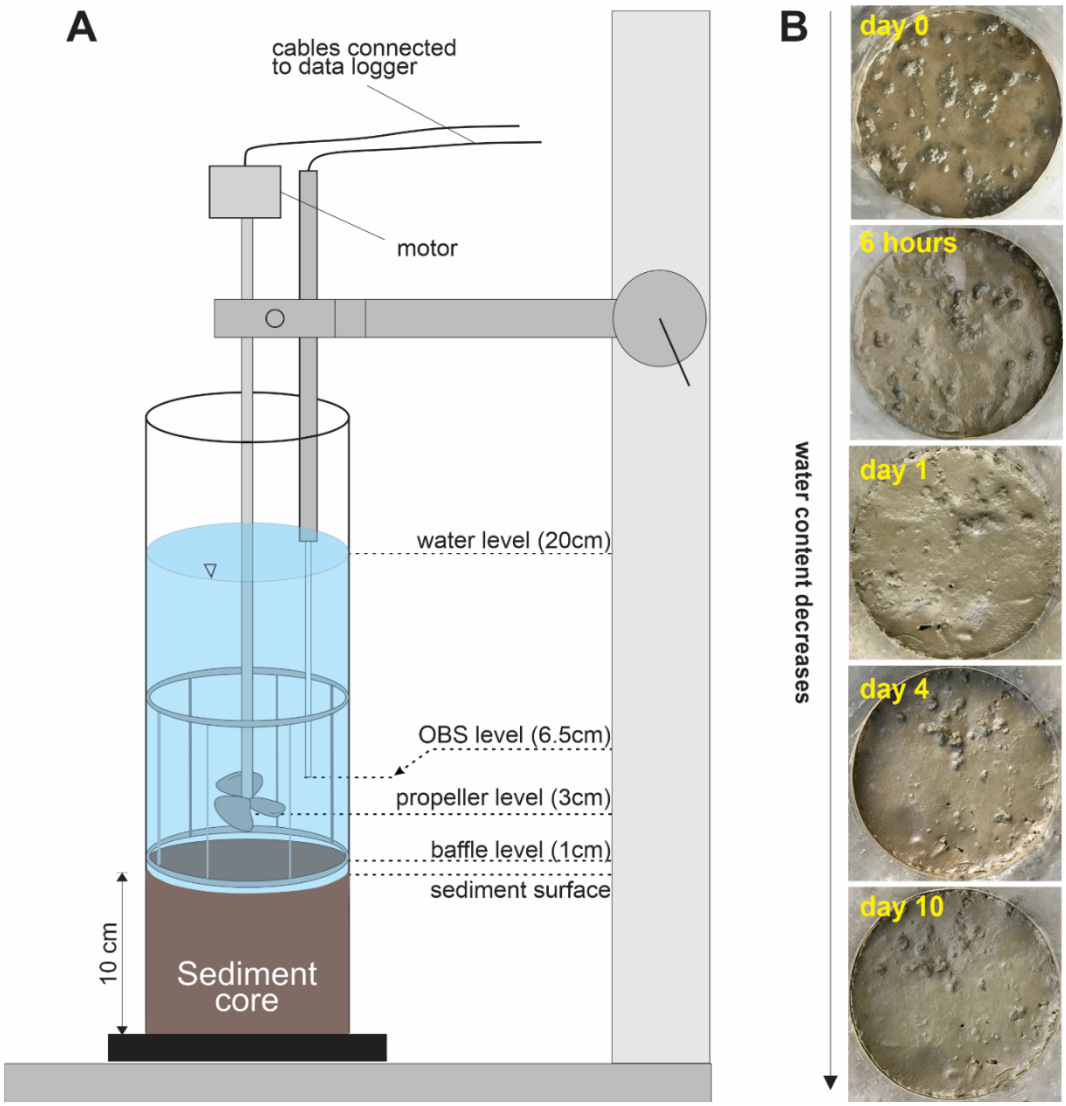

Figure 3.3 A) The set-up of the EROMES device (levels are measured from the sediment surface). B) Core surfaces immediately after draining (day 0) and after different periods of exposure. See text for further details.

Erosion measurements

In this research, the EROMES was used to measure sediment erosion properties (erosion threshold τ_{cr} and erosion rate *ER*, Figure 3.3A). The EROMES is a core based device and includes a propeller to create bed shear stress, a baffle ring to prevent circular flows (Doran, 1995), and an OBS (optical backscatter sensor) to measure the turbidity of the water column (in mA) every second (Andersen et al., 2007; Andersen et al., 2010; Schünemann and Kühl, 1991). The EROMES device creates turbulent fluctuations of varying intensity at the sediment surface (Widdows et al., 2007), which mimics those generated *in situ* by shallow wave and tidal currents (Andersen et al., 2007) that are responsible for sediment re-suspension and transport on tidal flats (reviewed by Green and Coco, 2014). The erosion thresholds and rates generated by the EROMES may not be directly transferrable to the field due to the small area of sediment on which measurements are made and the sequential, stepwise increase in bed shear stress generated by the propeller (see below). However, the device does provide a relative measure of sediment stability has been deployed extensively in both cohesive and non-cohesive sediments (e.g. Andersen et al., 2007; Andersen et al., 2010; Schünemann and Kühl, 1991). A known source of error with the EROMES device is the disturbance of surface sediment expected to occur during the collection and transport of samples from the site to laboratory and filling of the erosion device (Widdows, et al., 2007; Tolhurst et al., 2000). Sediment collection, filling of cores with water and transport is described in more detail in Nguyen et al. (2019). Briefly, we minimised disturbance by placing “bubble wrap” on the sediment surface when filling the cores and transporting the cores submerged to reduce potential for disturbance. The device measures a relatively small area and to reduce variability between replicates, we avoided collecting sediment disturbed by bioturbating macrofauna (that were not the focus of this study) that can alter sediment stability.

At the beginning of an EROMES run, a 20 cm artificial seawater column with a salinity of 28 was added to the Perspex core before the baffle ring, propeller and OBS were positioned at 1, 3 and 6.5 cm above the sediment surface, respectively (Figure 3.3A). Rotations of the propeller were converted to nominal bed shear stress based on the critical erosion shear stress of quartz sands (Andersen and Pejrup, 2002). The bed shear stress increased from 0.1 to 2.0 N m^{-2} in increments of 0.1 N m^{-2} (step), where each step lasts for 2 min. OBS readings are believed to be light sensitive therefore, five water samples (of at least 100 ml) were extracted from the water column for determination of suspended sediment concentration (by filtration). The volume of water removed was replaced immediately by the same volume of artificial seawater. Filter papers were dried at 105 °C for 10 h to determine the dry weight of sediment in the volume of the water sample. A separate calibration of OBS readings versus suspended sediment concentration was derived for each core (r^2 ranged from 0.96 to 0.98).

The erosion rate corresponding to each bed shear stress step was plotted, then an exponential curve fitted to the data was used to determine *ER* (g m^{-2} s^{-1}) and τ_{cr} (N m^{-2}) (Harris et al., 2016; Nguyen et al., 2019). In this study, τ_{cr} was defined as the bed shear stress required to generate an erosion rate of 0.1 g m^{-2} s^{-1}, and *ER* is the erosion rate of sediment caused by a given nominal bed shear stress of 0.5 N m^{-2} (Andersen et al., 2005; Harris et al., 2016; Nguyen et al., 2019).

3.3.3 Collection of meteorological data

A Hobo light and temperature logger was deployed to monitor light intensity and air temperature every minute during the core exposure period. The light intensity (lux) was converted to solar radiation (kW m^{-2}) (using a factor of 79×10^{-7} kW m^{-2} per lux at the wavelength of 555 nm - the middle of the visible-light spectrum corresponding to the frequency of 540 THz (Nouman et al., 2019). Other meteorological factors including wind speed and relative humidity were derived from the Moana weather station (operated by the University of Waikato, lat -37.925562°, long 175.369326°; about 15.7 km away from the laboratory). The data

were used in an evaporation model (detailed below) to estimate the evaporation rate of sediment cores during exposure.

3.3.4 Evaporation model

Meteorological conditions regulate the evaporation rate of sediments that in turn controls the water content (Fagherazzi et al., 2017). As a basis for our new sediment water content model, an evaporation model was used to evaluate the evaporation rate of water from sediments during the total exposure period of 10 d, forced by meteorological factors including air temperature, solar radiation, wind speed and air relative humidity. Results of the evaporation model were used to develop a water content model (that incorporates the effect of *Chl-a* content) that enables us to predict the water content of exposed sediments according to the exposure length.

Evaporation rate has been widely reported to exponentially decay during long-exposure periods related to water content dynamics (e.g. Brutsaert, 2014; Hang et al., 2016; Teuling et al., 2006). These studies showed that at lower water content, sediments have a lower evaporation rate compared with that at higher water content under the same meteorological conditions. Here we applied the results presented in Teuling et al., (2006) to include the decay of evaporation rate for exposed cores:

$$E_t = E_{0(t)} \exp\left(-\frac{d-d_0}{\beta}\right) \qquad (1)$$

where E_t is evaporation rate at time step t (30-min time steps), $E_{0(t)}$ is the evaporation rate at time step t when the effect of long-exposure was not taken into account, (d - d_0) is length of exposure in d, d_0 is the first day of the exposure period and β is the time scale regulating the temporal evolution of evaporation (β = 29.674 after Brutsaert (2014)). Therefore, when applied the Eq. (1), E_t was calculated according to the day of exposure the time step t belonged to.

Penman's equation was used to calculate $E_{0(t)}$ of sediments as (Dingman, 1994)

$$E_{0(t)} = \frac{s(T_a)(K+L) + \gamma K_E \rho \lambda_v v_a e_{sat}(T_a)(1-W_a)}{\rho \lambda_v (s(T_a)+\gamma)} \qquad (2)$$

where $s(T_a)$ is the slope of saturation vapour pressure curve, $e_{sat}(T_a)$ is the vapour pressure of the air at saturation, K is solar radiation, L is net longwave radiation, γ is the psychometric constant, K_E is a coefficient of the efficiency of vertical water vapour transport, ρ is density of water, λ_v is the latent heat of vaporization, v_a is wind speed, and W_a is relative humidity of air. K_E was calculated as (Dingman, 1994)

$$K_E = \frac{D_{WV}}{D_M} \frac{0.622\rho_a}{P\rho} \frac{1}{6.25\left[\ln\left(\frac{z_m - z_d}{z_0}\right)\right]^2} \qquad (3)$$

where D_{wv} and D_M are the diffusivities of water vapour and momentum, respectively, ρ_a is the density of air, P is the atmospheric pressure, z_m is the height at which wind speed is measured, z_d is the "zero-plane displacement", and z_0 is the roughness height of the sediment surface. In addition,

$$s(T_a) = \frac{25083}{(T_a + 237.3)^2} \exp\left(\frac{17.3T_a}{T_a + 237.3}\right), \qquad (4)$$

$$e_{sat}(T_a) = 6.11 \exp\left(\frac{17.3T_a}{T_a + 237.3}\right), \qquad (5)$$

$$L = L_{at} - L_w \qquad (6)$$

where T_a is air temperature, L_{at} is incoming atmospheric radiation, and L_w is radiation emitted by the sediment surface (Abramowitz et al., 2012; Dingman, 1994)

$$L_{at} = (0.031e_a + 2.84T_a - 522.5) * 0.001 \qquad (7)$$

$$e_a = 6.11W_a \exp\left(\frac{17.3T_a}{T_a + 237.3}\right) \qquad (8)$$

$$L_w = \varepsilon_w \mathrm{O}'(T_a + 273.15)^4 \qquad (9)$$

where e_a is vapour pressure of the overlying air, ε_w is emissivity of water and O' is the Stefan-Boltzmann constant. Published constant values were used for the λ_v (2257 kJ kg^{-1}), γ (0.66 mbar C^{-1}), ρ_w (1000 kg m^{-3}), ε_w (5.67×10^{-11} kW m^{-2} K^{-4}), ρ_a (1.22 kg m^{-3}) and *P* (1013 mbar) (Dingman, 1994; Fagherazzi et al., 2017).

3.3.5 Statistical analysis

We tested whether the sediment properties varied as a function of collection date (springtime (Oct 2018) and summertime (Jan and Feb 2019) n = 20 samples on each date) using a one-way ANOVA. To test whether the mean meteorological conditions differed between exposure periods and experiments conducted in October and January (season), we used t-test analysis. During the exposure experiments, the *Chl-a* content, $W_{Obs.}$, T_{cr} and *ER* changed with exposure period and season (tested with a two-way ANOVA, n = 3 for each exposure period/season). To determine how these changes in $W_{Obs.}$ and *Chl-a* content were correlated with changes in T_{cr} and *ER,* we used single (to test for the individual effect) and multiple-linear (to test for the combined effect) regression analysis. We compared the seasonal effect on T_{cr} and *ER* (because the *Chl-a* content was significantly different between Oct 2018 and Jan 2019 sediments) by fitting separate regressions to each season. If there was a linear relationship, a homogeneity of slope test was used to compare slopes and if not significantly different, we then compared the intercepts. For the re-submersion experiments, we tested whether re-submersion frequency (0, 1 and 2 events) changed the *Chl-a* content, $W_{Obs.}$, T_{cr} and *ER* using one-way ANOVA (n = 3 on each treatment). The combined effect of $W_{Obs.}$ and meteorological factors (we used mean values for each exposure period of mean air temperature (T_{a_Mean}), mean solar radiation

(K_{Mean})) on *Chl-a* content was tested by comparing standardised regression coefficients, β* from a multiple regression analysis. In this study, the statistical analyses were conducted by the Statistica 13© package, and a statistical test was considered significant when the probability, $p < 0.05$.

3.4 Results

3.4.1 Initial sediment characteristics

At the time of collection, the in situ summertime (Jan and Feb 2019) *Chl-a* content of sediments was approximately 6.5 times higher than that of sediments collected in springtime (Oct 2018) (one-way ANOVA $p < 0.001$) (Table 3.1).

Table 3.1 In situ sediment properties at the time cores were collected for use in laboratory experiments. Data represent the mean ± 1 standard deviation (n=20 except for the plastic and liquid limit parameters where n=6).

Properties	Oct 2018	Jan 2019	Feb 2019
	Exposure experiment		Re-submersion experiment
Wet bulk density (g cm^{-3})	1.36 ± 0.08	1.44 ± 0.05	1.43 ± 0.07
Dry bulk density (g cm^{-3})	0.32 ± 0.03	0.34 ± 0.06	0.33 ± 0.04
Median grain size (D_{50}, μm)	6.34 ± 1.72	6.94 ± 1.59	6.14 ± 0.85
Clay content (%)	38 ± 6	34 ± 5	35 ± 4
Silt content (%)	55 ± 4	63 ± 5	61 ± 5
Sand content (%)	6.11+3.98	2.36 ± 0.89	2.74 ± 1.03
Chlorophyll-a (*Chl-a*, μg g^{-1})	10.8 ± 1.9	78 ± 13	65 ± 6
Organic content (OC, %)	10.3 ± 0.6	12.6 ± 0.5	13.1 ± 0.4
Plastic limit (PL, %)	49 ± 2	63 ± 1	60 ± 3
Liquid limit (LL, %)	119 ± 5	145 ± 5	149 ± 2
Plastic index (PI, %)	70 ± 4	82 ± 3	88 ± 2

In situ springtime sediments also had a lower organic content, plastic limit and liquid limit compared with the summertime sediments by factors of 1.25, 1.23 and 1.25, respectively ($p < 0.001$). However, other sediment properties such as wet bulk density, dry bulk density, median grain size (D_{50}), and the % clay, silt and sand content did not differ significantly between seasons (Table 3.1).

3.4.2 Meteorological conditions

Figure 3.4 shows the mean value of meteorological factors for each exposure period (time-series are presented in Appendix 1). Air temperature ($T_{a\text{-}Mean}$) for the Jan 2019 experiment always surpassed the Oct 2018 experiment for all exposure periods ($p < 0.001$ for all exposure periods, Figure 3.4A). Solar radiation (K_{Mean}) was only significantly different between 6 h and 4 d exposure periods ($p < 0.001$, Figure 3.4B). Relative humidity ($W_{a\text{-}Mean}$) was only significantly difference between 4 d and 10 d exposure periods ($p < 0.001$, Figure 3.4C). Meanwhile, wind speed ($\upsilon_{a\text{-}Mean}$) was substantially different between 6 h, 4 d and 10 d ($p < 0.001$, Figure 3.4D).

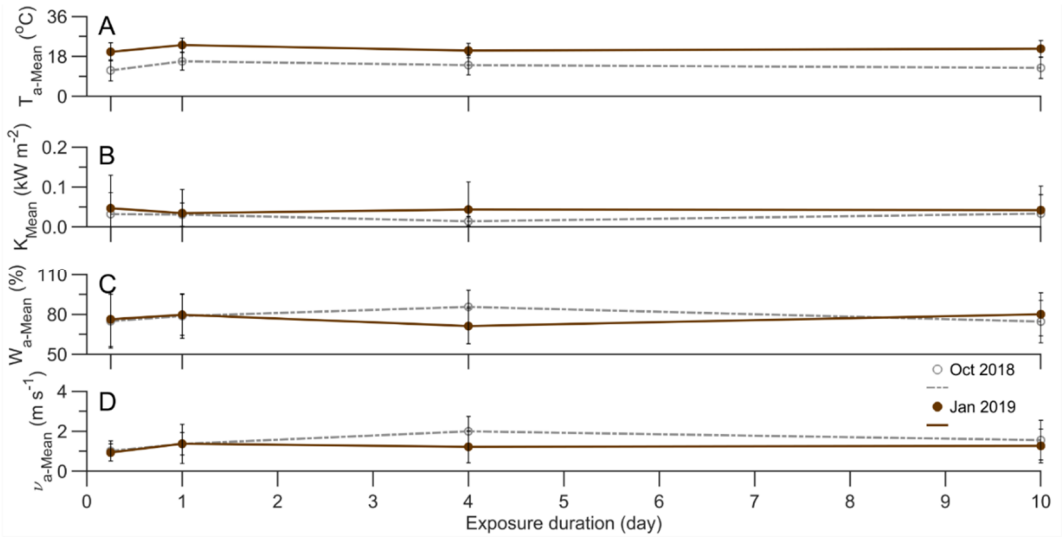

Figure 3.4 Average meteorological conditions for each exposure period. A) air temperature ($T_{a\text{-}Mean}$), B) solar radiation (K_{Mean}), C) relative humidity ($W_{a\text{-}Mean}$), and D) wind speed ($\upsilon_{a\text{-}Mean}$). Error bars correspond to ± 1 standard deviation.

3.4.3 Changes in sediment erodibility, Chlorophyll-a and water content during exposure

Results from the exposure experiment (Oct 2018 and Jan 2019 sampling dates) indicated that sediments were always more stable after aerial exposure (Figure 3.5A and 3.5B). Changes in τ_{cr} and *ER* showed similar patterns for both dates, and the erosion resistance of sediments sharply decreased (increased τ_{cr} and decreased *ER*) after the first day of exposure. Exposure for 10 d increased τ_{cr} by a factor of 4.4 in Oct 2018 and 1.7 in Jan 2019, respectively. With the increase in τ_{cr}, there was a corresponding decrease in *ER* over the exposure period by a factor of 21.5 in Oct 2018 and 11.6 in Jan 2019.

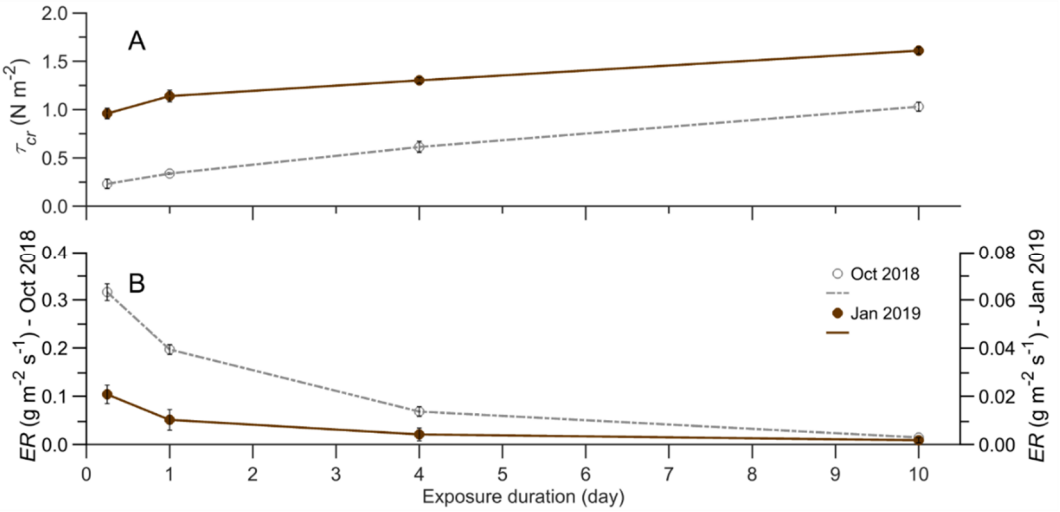

Figure 3.5 Seasonal changes in A) the erosion threshold (τ_{cr}) and B) the erosion rate (*ER*) of intertidal sediments as a function of aerial exposure period. Note that the Oct 2018 and Jan 2019 *ERs* are plotted on different scales. Data are the mean (n=3) ± 1 standard error.

Comparing across seasons, the summer sediment samples were more stable than the spring samples with τ_{cr} and *ER* of the Jan 2019 sediments were 1.6 – 4.2 times higher, and 8.2 – 19.2 times lower than those of the Oct 2018, respectively. Within the Oct 2018 sampling date, both τ_{cr} and *ER* were significantly different between exposure periods ($p < 0.001$), with the exception of τ_{cr} in the 6 h and 1 d exposure

period, which were not significantly different (p = 0.74). For the Jan 2019 experiment, T_{cr} increased with exposure duration but there was no significant difference found between *ER* for all exposure periods (*ER* values fluctuated within each exposure period within a range of 0.002 - 0.02 g m^{-2} s^{-1}).

Similar to the in situ sediments, there was significantly higher *Chl-a* content in sediments during the experiments for Jan 2019 compared with Oct 2018 sediments ($p < 0.001$, comparing each exposure period between the two sampling dates, Figure 3.6A). In Oct 2018 after 10 d of exposure, *Chl-a* content had increased by 3.9 times ($p < 0.001$). For the Jan 2019 samples, *Chl-a* content increased over the first 4 d of exposure (1.6 times higher than that on d 0, $p < 0.001$), then declined by 1.3 times ($p < 0.001$) over the next six days.

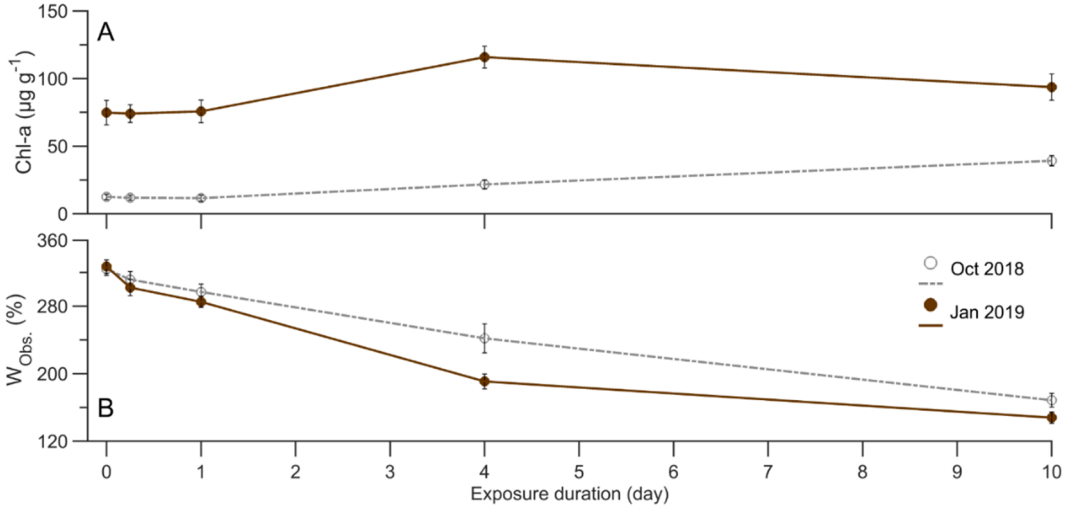

Figure 3.6 Season changes in sediment A) *Chl-a* content and B) observed water content ($W_{Obs.}$) as a function of aerial exposure period. Data are the mean (n=3) ± 1 standard error.

In general, $W_{Obs.}$ decreased over the exposure by a factor of 1.9 (Oct 2018, $p < 0.001$) and 2.2 (Jan 2019, $p < 0.001$) (compared d 10 with d 0, Figure 3.6B). The decrease in $W_{Obs.}$ was significant after 1 d of exposure for the Oct 2018 samples ($p < 0.001$), while it was significant after only 6 h of exposure for the Jan 2019 samples

($p < 0.001$). Comparing across two sampling dates, a significant difference only existed between 4 d and 10 d exposure periods ($p < 0.001$ for 4 d, $p < 0.05$ for 10 d).

3.4.4 Factors affecting the erodibility of sediments

The influence of $W_{Obs.}$ and *Chl-a* content on τ_{cr} and *ER* were significant individually (regression, $p < 0.001$) and in combination (multiple regression, $p < 0.001$). The $W_{Obs.}$ and *Chl-a* were negatively correlated (Pearson correlation of -0.38). A quadratic polynomial function best explained the relationship between *Chl-a* and τ_{cr} ($r^2 = 0.86$, $p < 0.001$), while the relationship between *Chl-a* and *ER* was best-described by an exponential function ($r^2 = 0.77$, $p < 0.001$) (Figure 3.7A and 3.7B). In contrast, $W_{Obs.}$ negatively affected erosion resistance with a linear fit to τ_{cr} ($r^2 = 0.52$, $p < 0.001$) and an exponential fit to *ER* data ($r^2 = 0.55$, $p < 0.001$) (Figure 3.7C and 3.7D). In addition to the general models fitting to pooled data of both dates to test for multiple models, separate lines were fitted to $W_{Obs.}$ data of individual date (Figure 3.7C and 3.7D) because changes in $W_{Obs.}$ of two sampling dates showed similar patterns (Figure 3.6B). This technique allowed us to test the seasonal effect on τ_{cr} and *ER* via $W_{Obs.}$ data using the homogeneity of slopes test. Homogeneity tests conducted on τ_{cr} and *ER* data for the two sampling dates showed identical slopes, and intercepts of τ_{cr} and *ER* lines of Jan 2019 samples were significantly higher and lower than those of the Oct 2018 lines respectively, implying that the seasonal impact on erosion properties is significant. Log-transformed *ER* values were used for multiple regression models (Eq. (10) and Eq. (11)) and the homogeneity of slope test. The best model incorporating both $W_{Obs.}$ and *Chl-a* was

$$\tau_{cr} = -0.0026W_{Obs.} - 0.00104(Chla)^2 + 0.0215(Chla) + 0.822 \quad (r^2 = 0.96,\ p < 0.001) \tag{10}$$

$$\ln(ER) = 0.011W_{Obs.} - 0.032(Chla) - 4.712 \quad (r^2 = 0.89,\ p < 0.001) \tag{11}$$

The combined, two-factor models explained 44 % and 34 % more variance of τ_{cr} and *ER* respectively than the simple single factor regression model on the pooled data (Figure 3.7C and 3.7D). Comparing standardized regression coefficients (β*) across the factors, *Chl-a* played a more important role in changes of τ_{cr} and *ER* compared with $W_{Obs.}$ (In Eq. (10), β* = -0.35, 1.75, -1.08 for $W_{Obs.}$, $(Chla)^2$, *Chla*, respectively; In Eq. (11), β* = 0.40, -0.68 for $W_{Obs.}$, *Chla*, respectively). The pooled regressions are much weaker for the relationship between W_{Obs} and τ_{cr} (Figure 3.7C, $r^2 = 0.52$) and *ER* (Figure 3.7D, $r^2 = 0.55$), indicating different responses in the different seasons.

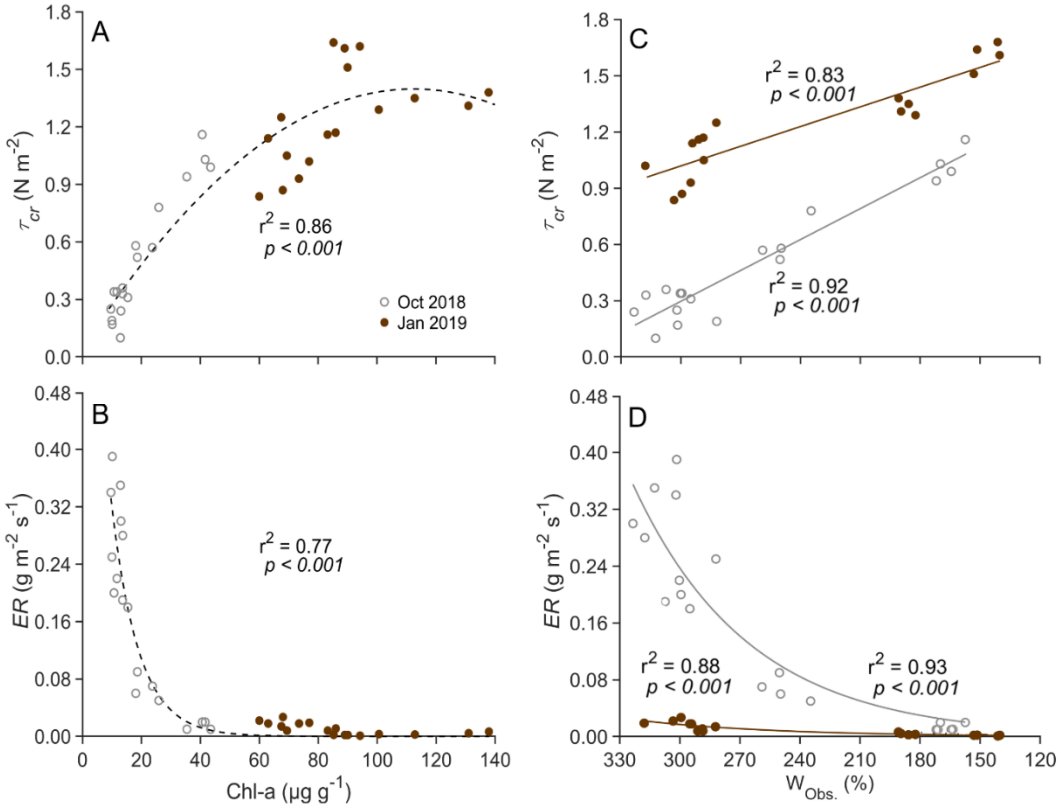

Figure 3.7 Relationships between sediment *Chl-a* content and A) erosion threshold (τ_{cr}) and B) erosion rate (*ER*), and observed water content ($W_{Obs.}$) and C) τ_{cr} and D) *ER*. Dash lines are fitted to data pooled across seasons (Oct 2018 and Jan 2019) whereas the grey (Oct 2018) and brown (Jan 2019) lines (panels C and D) are fitted separately.

3.4.5 Water content model

The regression results showed that water and *Chl-a* content are an essential driver of erosion characteristics so in the model developed here, both evaporation and measured *Chl-a* content were taken into account. The evaporation was calculated at each time step (E_t) using Eq. (1), where the time steps were equal to the sampling frequency of the meteorological data. Because observations of *Chl-a* content were only taken when erosion measurements were made, in order to provide *Chl-a* content at the same time intervals as the meteorological data, the *Chl-a* values were interpolated with a quadratic polynomial function (Figure 3.8A). E_t from the evaporation model (Figure 3.8B) was then used to develop a water content model (Eq. (12)), which was based on the principle that water content decreased with increased evaporation (as observed), and that the water content change was delayed by a time lag. The time lag would depend on the movement of water through the pore space between particles to reach the exposed surface. The coefficients in the model (including the time delay) were evaluated by fitting the model to data using the bootstrapping method (Figure 3.8C and 3.9)

$$W_{Mod.(t)} = W_{Obs.(0)} - 39.4 \times \sum \frac{1}{(Chla)_t} \times E_t \times exp\left(\frac{t}{1000}\right) \quad (12)$$

where $W_{Mod.(t)}$ is the water content at time *t* (30-min time steps), $W_{Obs.(0)}$ is the observed water content on day 0 of exposure, $(Chla)_t$ is the interpolated *Chl-a* content at time *t*.

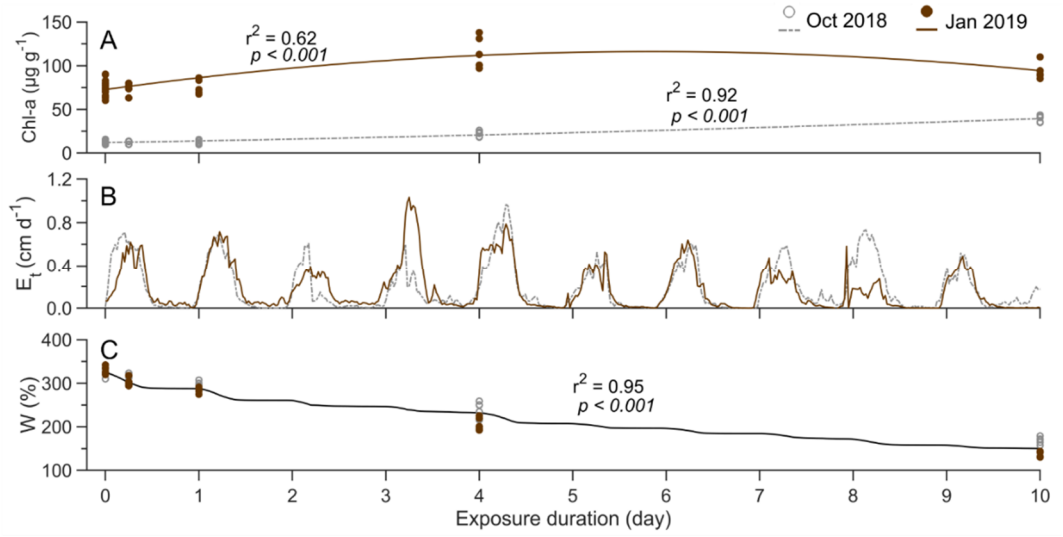

Figure 3.8 A) A quadratic polynomial function fitted to the observed sediment *Chl-a* content (circles) as a function of exposure period. B) Modelled temporal variation in evaporation rate (E_t), and C) modelled and observed sediment water content. See text for model details.

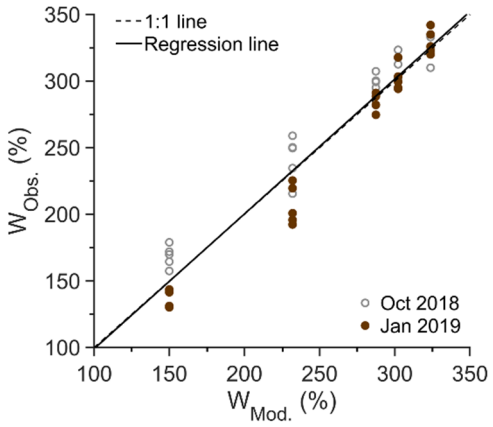

Figure 3.9 Relationship between modelled ($W_{Mod.}$) and observed sediment water content ($W_{Obs.}$). The regression line was fitted to data pooled across seasons (r^2 = *0.98, p < 0.001*).

3.4.6 The effect on erosion properties of re-submerged sediments

In general, erosion resistance did not show any substantial change when sediments were re-submerged (either after one or two re-submersion events) compared to sediments that were treated with exposure but not re-submerged (Figure 3.10A and 3.10B). This pattern was consistent across exposure durations

of 1 d (p = 0.68 for T_{cr}, p = 0.53 for *ER*), 4 d (p = 0.67 for T_{cr}, p = 0.80 for *ER*) and 10 d (p = 0.97 for T_{cr}, p = 0.99 for *ER*). Results of the re-submersion experiments showed that $W_{Obs.}$ and *Chl-a* content after one and two re-submersion events increased compared with the exposure-only, and the significant increase occurred for all exposure periods of 1 d ($p < 0.05$) (Figure 3.10C & 3.10D). For 4 d and 10 d, there was a significant difference between exposure-only and the two re-submersion events in $W_{Obs.}$ and *Chl-a* content ($p < 0.05$), except that *Chl-a* content at 10 d showed no difference between treatments (Figure 3.10D).

3.4.7 Factors affecting the growth of biofilms

Temperature ($T_{a\text{-}Mean}$), observed water content ($W_{Obs.}$), and solar radiation (K_{Mean}) significantly influenced the growth of biofilms both individually ($r^2 = 0.65$, $p < 0.001$; $r^2 = 0.45$, $p < 0.001$; $r^2 = 0.23$, $p < 0.001$ for $T_{a\text{-}Mean}$, K_{Mean} and $W_{Obs.}$, respectively; Figures 3.11A, 3.11B and 3.11C) and in combination at which the best multiple regression model included all three factors ($r^2 = 0.82$, $p < 0.001$). Comparing standardized regression coefficients (β*) across the factors, the growth of biofilms was more sensitive to the variation of $T_{a\text{-}Mean}$ (β* = 0.61) while $W_{Obs.}$ and K_{Mean} played less important roles (β* = -0.35 and 0.23, respectively). We excluded humidity ($W_{a\text{-}Mean}$) and wind speed ($\upsilon_{a\text{-}Mean}$) from the multiple regression because of non-significant relationship with *Chl-a* content (regression, $r^2 = 0.11$, $p = 0.07$; $r^2 = 0.06$, $p = 0.15$ for $W_{a\text{-}Mean}$ and $\upsilon_{a\text{-}Mean}$, respectively). Separate regressions were undertaken for Oct and Jan resulting in better model fits (higher r^2 and significance level) compared with the pooled data for both dates. Whilst *Chl-a* content in Oct and Jan both show an increase with $W_{Obs.}$, they are offset (Figure 3.11C). This presumably due to an interaction with other factors, such as greater $T_{a\text{-}Mean}$ and K_{Mean} in Jan (Figure 3.11A and 3.11B). There was no significant relationship between *Chl-a*/$W_{Obs.}$ and wind speed and humidity even when tested separately for Oct and Jan.

3.5 Discussion

Results indicate that long-exposure duration significantly decreased $W_{Obs.}$, which in turn increased erosion resistance of cohesive intertidal-flat sediments. Longer exposure durations resulted in higher τ_{cr} and lower *ER*, which could be predicted best by the combined effect of *Chl-a* content and $W_{Obs.}$ (Eq. (10) and Eq. (11)). Sediments deposited in the Firth of Thames are smectite clay-rich muds (Swales et al., 2019) that should show a reversible behaviour of swelling during re-submersion through processes of water infiltration (Yong and Warkentin, 1966). One would expect erosion resistance to decrease after immersion because of the increasing W_{Obs}. For example, Tolhurst et al. (2006a) indicated that sediments immersed for 30 min have significantly lower erosion thresholds than the emersed sediment. However, in our case, τ_{cr} and *ER* did not show significant differences between exposure-only, one and two re-submersion events (Figure 3.10A & 3.10B). This could be a consequence of increasing *Chl-a* content (either caused by growth or migration) where the strengthening effect of biofilms on erosion resistance might counteract the effect of increasing $W_{Obs.}$ (Figure 3.10C and 3.10D). In addition, our sediments were exposed for much longer durations (days versus 6 h exposure in Tolhurst et al. (2006a)), and so our water content might have been much lower prior to re-immersion. In a natural tidal flat, rain, poor drainage, and seeping ground water would preclude the drop in water content that we created in our experimental conditions. This finding could be a reason for the retention of the exposure effect on sediments after subsequent flooding cycles.

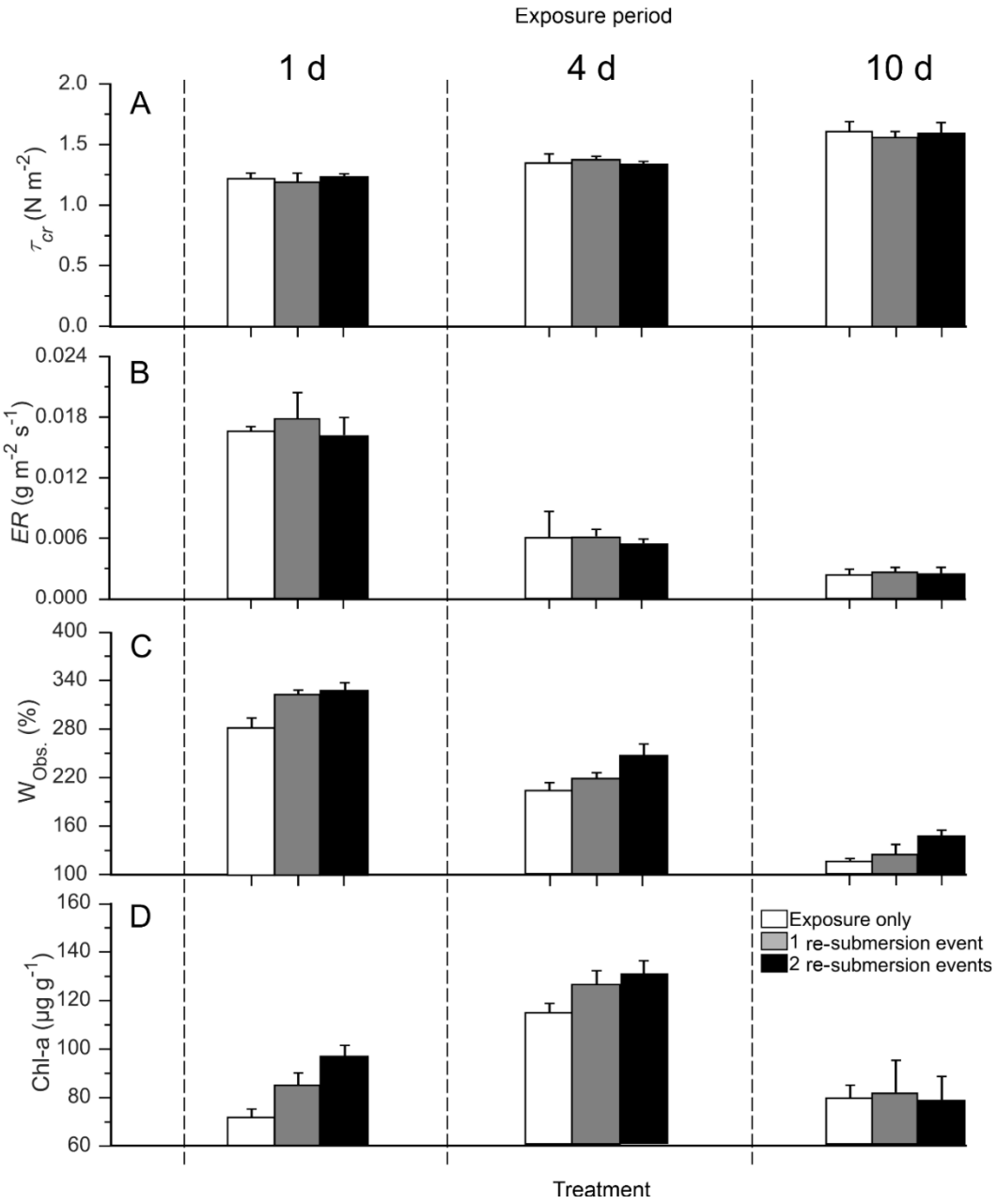

Figure 3.10 Effect of re-submersion (after 1, 4, and 10 d aerial exposure) on sediment A) erosion threshold (T_{cr}), B) erosion rate (*ER*), C) observed water content ($W_{Obs.}$), and D) *Chl-a* content. The data represent means (n=3) + 1 standard error.

Variations of T_{cr} and *ER* showed similar patterns over the exposure periods, but at different levels of stability with the Jan 2019 sediments being more stable than the Oct 2018 sediments (Figure 3.5A and 3.5B). It might be that comparable patterns of $W_{Obs.}$ reduction produced similar results in both sampling occasions (Figure 3.6B), and the *Chl-a* content really explained the variation between

seasons. *Chl-a* content was positively related to T_{cr} and negatively related to *ER*, which is similar to observations widely reported in the literature (e.g. Andersen, 2001; Austen et al., 1999; Sutherland et al., 1998). Our data showed that *Chl-a* content in Oct 2018 (cooler month) was much lower than that in Jan 2019 and Feb 2019 (hotter months) (Figure 3.6A), which was supported by previous studies (Migné et al., 2004; Nguyen et al., 2019; Staats et al., 2001). In addition, a positive correlation between the *Chl-a* content and OC in intertidal sediments has been reported in Riemann et al. (1989); therefore, the higher OC in the hotter months could be a result of the higher *Chl-a* content. The stabilising role of OC has also been widely recognised in the literature (e.g. Aberle et al., 2004; Gerbersdorf et al., 2007; Morgan, 2009; Righetti and Lucarelli, 2007). Organic materials increase inter-particle attraction (Winterwerp and Van Kesteren, 2004), and layers of fibrous organic materials are believed to protect erodible sediments underneath from erosion (Aberle et al., 2004). In other words, the higher *Chl-a* content and OC produced a compound stabilisation on sediments in the summertime.

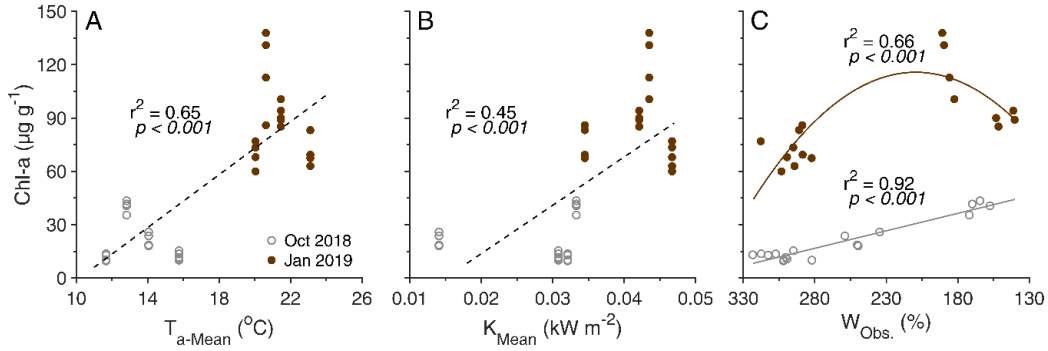

Figure 3.11 Relationship between sediment *Chl-a* content and A) mean air temperature ($T_{a\text{-}Mean}$), B) mean solar radiation (K_{Mean}) and C) observed water content ($W_{Obs.}$). $T_{a\text{-}Mean}$ and K_{Mean} are averaged values for the different aerial exposure periods (6 h – 10 d). Dash lines are fitted to data pooled across seasons (Oct 2018 and Jan 2019) whereas the grey (Oct 2018) and brown (Jan 2019) lines (panel C) fitted separately.

The presence of biofilms in sediments clogs pore spaces between particles, so decreases the effective porosity, which reduces the hydraulic conductivity of the sediment (Lianfang et al., 2009; Vandevivere and Baveye, 1992). Hence, as a consequence of the biofilm growth, the evaporation rate might be reduced, which would therefore affect water content. The influence of biofilm on the evaporation might affect our model results which indicated similar cumulative evaporation from d 8 of exposure for both sampling dates (Figure 3.12), however the $W_{Obs.}$ for the Jan 2019 sediments was still lower than that of the Oct 2018 sediments at d 10 (Figure 3.6B). In the conventional sense of the amount of water lost by evaporation, the water content of two dates should be similar from d 8 to d 10. The sharp increase in *Chl-a* in Oct 2018 and decrease in Jan 2019 from d 4 (Figure 3.6A) might lead to higher cumulative evaporation for the Jan 2019 and lower cumulative evaporation for the Oct 2018 samples compared with the predicted cumulative evaporation (Figure 3.12). Therefore, although altering meteorological conditions must be considered to more precisely predicting changes in the stability of intertidal flats in long subaerial periods (Fagherazzi et al., 2017), it is also necessary to consider the effect of biofilms on the evaporation of water from sediments.

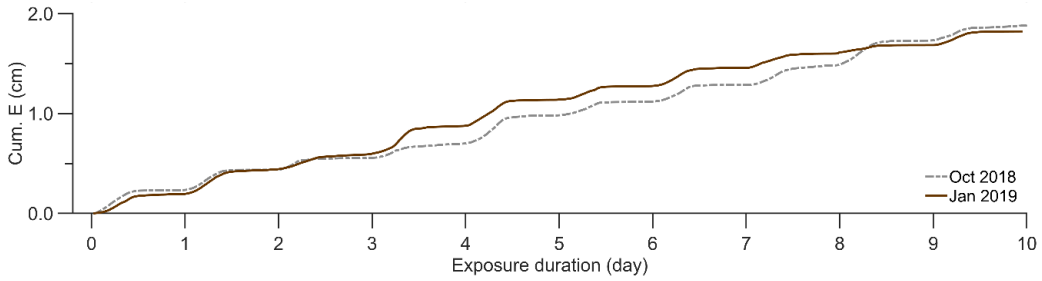

Figure 3.12 Predicted cumulative evaporation (*Cum.E*) of water as a function of aerial exposure period. Evaporation (*E, cm*) at time step t was determined by multiplying evaporation rate (E_t, *cm* d^{-1}) at t by the length of exposure between steps (30 min, equal to meteorological data sampling frequency). Cumulative evaporation for a given exposure period was the sum of evaporation for that period.

Our findings showed that the $W_{Obs.}$ with air temperature and solar radiation significantly contributed to explaining the growth of biofilms (Figure 3.11). Analyses on the effect of factors on the growth of biofilms indicated that $T_{a\text{-}Mean}$ was the driving factor while $W_{Obs.}$ and K_{Mean} showed smaller influence. Grant (1986) reported that the growth of biofilms was more sensitive to air temperature than solar radiation. Research results were also consistent with a previous study where the growth of biofilms increased with the increase in air temperature over wide ranges from 2.8 – 35.5°C in Migné et al. (2004) and 5 – 25°C in Blanchard et al. (1996). We could not find any studies on the relationship between water content and the growth of biofilms. Nutrient deficiency might be a reason for *Chl-a* decay of Jan 2019 samples after d 4 (Figure 3.6A) because there was no nutrient supplementation during exposure for the growth of biofilms as would occur in the field. Growth reduction due to nutrient limitation has been reported in Davoult et al. (2009). The Oct 2018 sediments (with lower *Chl-a* content), would have fewer living microphytobenthos and so consume less nutrient resulting in no nutrient deficiency preventing the dynamic growth of the micro-organisms. On the contrary, the lack of nutrients might be a consequence of the higher nutrient consumption of microphytobenthos inhabiting on the surficial layer of the Jan 2019 sediments.

The state alteration of clays caused by the decrease in $W_{Obs.}$ might lead to unchanged erosion resistance of the 10 d exposure period. After 10 d of exposure, the $W_{Obs.}$ of exposure-only cores ($W_{Obs.}$ = 113 %) had decreased far below the liquid limit of the sediment (LL = 149 %, Table 3.1), therefore altering to plastic state from the liquid state (as $W_{Obs.}$ was higher than the liquid limit). Although $W_{Obs.}$ increased after one and two events of rewetting, it was still lower than the liquid limit ($W_{Obs.}$ = 147 % after two re-submersion events) and so remained in its plastic behaviour regime. Grim (1962) indicated that repeated wetting and moderate drying frequently tend to increase the plastic properties of clay minerals in cohesive sediments. The increasing plastic properties, therefore, might confound

the effect of higher $W_{Obs.}$ on erosion properties, which results in non-significant changes in erosion properties of the 10 d exposed samples.

Past work has shown that erosion resistance is negatively related to water content and positively related to bulk density (e.g. Bale et al., 2007; Winterwerp and Van Kesteren, 2004). For cohesive sediments, the evaporation process during exposure reduces water content, which is conducive to lower void ratio and denser sediment with higher bulk density (Stark et al., 2005). Winterwerp and Van Kesteren (2004) applied a ratio between $W_{Obs.}$ and plastic index ($W_{Obs.}$/PI, [-]; PI = LL - PL) to assess the shear strength. Sediments with higher shear strength will have higher erosion threshold (Watts et al., 2003). Our results showed approximately a two-fold decrease in this ratio over the exposure period (Table 3.2), which is consistent with the previous study that reported the higher ratio was associated with higher erodibility (Winterwerp and Van Kesteren, 2004).

Table 3.2 Changes in the ratio $W_{Obs.}$/PI as function of exposure period. $W_{Obs.}$ is observed water content and PI is plastic index (PI = Liquid Limit (LL) – Plastic Limit (PL)). Data represent the mean (n=3) ± 1 standard deviation.

		Oct 2018	Jan 2019
Exposure duration	6 h	4.46 ± 0.23	3.67 ± 0.12
	1 d	4.12 ± 0.31	3.46 ± 0.08
	4 d	3.42 ± 0.24	2.32 ± 0.11
	10 d	2.38 ± 0.09	1.82 ± 0.08

Our model for water content of sediments explained a surprising amount of variability in observed water content, given its simplicity. However, the model did not have any ability to predict the timing delay caused by movement of water toward the surface in sediments, with this parameter evaluated by fitting our model to observations. The coefficient used in our model (39.4) was also

empirically fitted. The structure of our model incorporates the relevant trends, but we are clearly still missing important variables.

In the traditional sense of the Shields diagram, sediments collected in Oct 2018 and Jan 2019 (with quite similar median grain size, Table 3.1) should show the similar critical Shields parameters. In the Shields theory, critical Shields parameter ($\theta_{cr} = \tau_{cr}/(\rho_s - \rho)gD_{50}$), where ρ_s is the grain density of sediments, ρ is density of water, g is gravitational acceleration) is a function of dimensionless sediment size parameter ($D^* = D_{50}[g(\rho_s - \rho)/(\rho\upsilon^2)]^{1/3}$, where $\upsilon = 9.68\times10^{-7}$ m^2 s^{-1} at 20°C, is the kinematic viscosity). However, the estimation of cohesive-adhesive sediment incipient motion is far more complicated when cohesion/adhesion are taken into account (Grabowski et al., 2011; Righetti and Lucarelli, 2007). In this study, we considered the effects of water content and biofilms as drivers controlling cohesive/adhesive characteristics of sediments. Zhang and Yu (2017) researched the influence of yield stress which directly related to cohesion (inter-particle interaction) on various types of sediment with a wide range of median grain size (6 - 72 µm). Nguyen et al. (2019) also studied the effect of ambient temperature and *Chl-a* content on erosion resistance of intertidal sediments. Our data were consistent with these studies showing that critical Shields parameters varied widely for given particle sizes. Lower water content and higher *Chl-a* content resulted in more stable sediments. Although the Jan 2019 sediments have a larger median grain size compared with the Oct 2018 sediments, critical Shields parameters were higher for the former due to the stabilising effect of biofilms (Figure 3.13). The causes leading to higher θ_{cr} at similar D^* of our study compared with previous studies are due to differences in criterion to define incipient motion among studies and the level of sample disturbance, which was presented in more detail in (Nguyen et al. 2019).

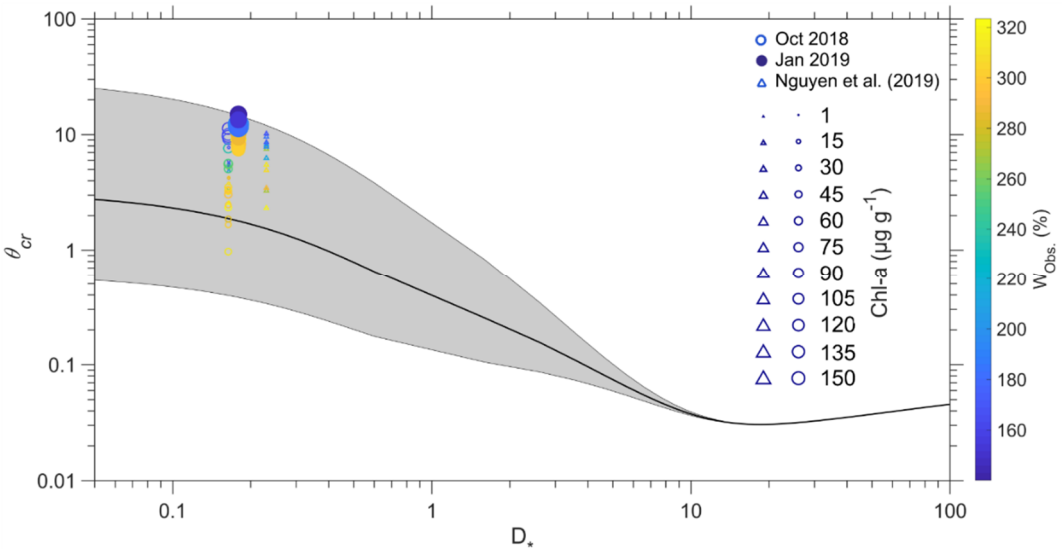

Figure 3.13 Comparison of results with previously published data on the variation of critical Shields parameter (θ_{cr}) with dimensionless grain size parameter (D^*). The shaded area shows the range of observed θ_{cr} (after Zhang and Yu, 2017). The colour legend shows the observed water content ($W_{Obs.}$), and the symbol size shows the sediment *Chl-a* content (note Oct 2018 and Jan 2019 share the same circle size scale).

Seasonal changes in meteorological conditions affect the water content via evaporation process, which consequently should affect erosion properties and sediment resuspension on intertidal mudflats. Over longer time scales such as associated with global warming, temperature changes might reduce potential erosion by promoting evaporation during the subaerial period, and thus contribute to intertidal stability. In meso-tidal zones where large intertidal areas exposed to air at low tide, the evaporation becomes particularly important (Fagherazzi, 2017; Mariotti and Fagherazzi, 2011).

In this study, we investigated the erosion behaviour of long-exposed cohesive sediments; however, longer periods of exposure might occur in nature due to bed elevation of intertidal flats and tidal level regimes. Moreover, our measurements were conducted at given durations of 6 h, 1, 4 and 10 d; therefore, more measurements between the durations might provide a better estimation of erosion resistance and controlling factors. Low tide rainfall was widely reported in

the literature to have substantial effects on the erodibility of surficial sediments on intertidal flats (Pilditch et al., 2008; Tolhurst et al., 2006b). Our study excluded the effect of rainfall that changes water content and also directly impacts sediment surfaces. Such an effect could easily be incorporated into our model. A difference in weather conditions between our experimental site and the data (air relative humidity and wind speed) derived from the Moana station (about 15.7 km far away) used for the evaporation model might have occurred, which could affect results of the water content model.

3.6 Conclusions

The main objective of this work was to examine the extent to which long-exposure affects erosion properties of cohesive sediments from intertidal mudflats. The results showed that sediments on intertidal areas became more stable when exposed to air, and the longer the exposure duration, the less erodible they were. T_{cr} could be 1.7 – 4.4 times higher, and *ER* could be 11.6 – 21.5 times lower after 10 d of exposure compared with 6 h exposure. Variations in erosion resistance could be predicted by changes in *Chl-a* and $W_{Obs.}$ during exposure. Although various studies have noted the effect of biofilms and water content on the stability of sediment, to our knowledge, this study is the first to evaluate the combined effect of the factors on the variation of T_{cr} and *ER.*

Results from the re-submersion experiments implied that the strengthening effect of exposure in the previous subaerial period on intertidal sediments remained in subsequent flooding cycles although the water content increased after re-submersion. The confounding effect of increasing *Chl-a* content in the surficial sediment could be a reason for that. Therefore, the results confirmed the necessity to consider the interplay of biofilms and water content to predicting erosion resistance of intertidal sediments.

Our water content model was developed to predict the variation of water content as a function of the evaporation rate and exposure duration. The growth of

biofilms is generally believed to prevent water evaporating from the pore space between particles, hence in this model, we show how measurements of the *Chl-a* content was taken into account to improve the capacity to predict the variation of $W_{Obs.}$ during exposure. Some additional work is needed to generalise this model.

The rising sea level potentially increases the erosion of sediments in low-lying areas; nevertheless, this threat might be eased as global warming will increase the air temperature during low tide exposure. Our findings showed that increased evaporation would result in enhanced erosion resistance during exposure, which might ultimately contribute to changing the intertidal morphology in the coming years.

Chapter 4

Modelling the effect of aerial temperature and exposure period on intertidal mudflat profiles

Nguyen, H.M., Bryan, K.R., Zeng Zhou, Pilditch, C. A. Modelling the effect of aerial temperature and exposure period on intertidal mudflat profiles. In preparation to submit to the journal of Geomorphology.

Contribution of authors

Chapter 4 presents the article entitled “Modeling the effect of aerial temperature and exposure period on intertidal mudflat profiles”, which is in preparation to be published in the journal of Geomorphology.

I was responsible for setting up model runs, data processing, data analysis and writing.

Zeng Zhou assisted with the code that combined integrated empirical models for erosion threshold and erosion rate of exposed sediments into the Delft3D modelling environment.

My supervisors Karin Bryan and Conrad Pilditch assisted with data analysis, reviewed drafts and advised on directions.

Abstract

This research demonstrates how the effect of exposure to air on intertidal flat profile development in cohesive coastal environments can be incorporated into applied numerical modelling. Semi-empirical relationships were used to include the sediment stabilizing effects of exposure on changes to the erosion threshold (T_{cr}; $N\ m^{-2}$) and erosion rate (ER; $g\ m^{-2}\ s^{-1}$) during low tide, which also take into account the effect of air temperature, T (°C) and exposure duration, D (h). The relationships were based on fundamental forms of the theoretical relationship between water content and evaporation rate, and were fitted to empirical data. Changes were incorporated into the Delft3D model, and scenarios monitored bed level profile development over an annual time scale with different T, sediment stabilizing biofilm biomass (using *Chl-a* content as a proxy), initial bed composition (mud/sand percentage), and spring and neap tides (regulating current velocity and exposure duration). Model results indicated that the stabilizing effect of exposure will lead to a more flat-topped shape of intertidal mudflats, implying that bed level changes caused by exposure occur lower on intertidal flats compared to runs with no exposure. Higher air temperatures had a greater effect on bed level change, with the maximum accretion of up to 0.039 m (77% higher) occurring in the case of 40 °C. Research findings will contribute to understanding of how intertidal flats evolve and is critical to predicting the resilience of these habitats to sea-level rise and warming temperatures.

Keywords: cohesive sediments, bed level change, numerical simulation, sediment stability, low-lying areas, Delftd3D, critical erosion threshold, erosion rate

4.1 Introduction

Understanding the evolution of coastal morphology is critical to planning how we adapt to sea-level rise (SLR). Some models suggest that low-lying areas will gain elevation to keep pace with rising sea-levels (e.g. Kirwan et al., 2016; van Maanen et al., 2013; Fagherazzi et al., 2006; Marani et al., 2007); conversely, other studies predict high sensitivity to the rate of SLR, and sediment supply and retention of sediment may not be insufficient (e.g. Fagherazzi et al., 2006; Marani et al., 2007). Consequences stretch beyond the simple loss of coastal land. Rising sea-levels can also change our exposure to ocean hazards such as waves and storm surges (and effectiveness of eco-defences), suspend new sediment from recently-inundated areas (Mi et al., 2020) and change coastal light regimes (Mangan et al., 2020), affecting primary productivity and ecosystem structure and function (e.g. Pratt et al., 2014).

Many studies have modelled the evolution of low-lying coastal land, both in mangrove-dominated tropical and subtropical areas, and in more temperate salt marshes. For example, Mariotti and Fagherazzi (2010) presented a numerical model for the coupled long-term evolution of salt marshes and intertidal flats, confirming that expansion or erosion of salt marshes is a function of SLR rate in combination with parameters such as sediment supply. A low rate of SLR induced marsh expansion while a high rate resulted in drowning of salt marshes. Even in cases where land keeps pace with sea-level rise, the size, shape and location of the intertidal areas will likely change (van Maanen et al., 2013).

One of the primary controls on how the coastal landscape functions (in terms of both ecological and socio-economic values) is the shape of the intertidal profile. Intertidal profiles can be concave or convex depending on such factors as relative intensity of wave and tidal forcing, sediment supply and grain size, and the local elevation of the flat relative to the mean sea level (Bearman et al., 2010). Tidal currents enhance convexity whereas waves favour concavity (Friedrichs et al., 1996; Pritchard and Hogg, 2003; Zhou et al., 2015). Sandier tidal flats, in turn, tend

to be associated with wave-dominated areas, and muddier flats are more common in tide-dominated areas (Yang et al., 2008; Zhou et al., 2015). Erosional flats tend to be more concave upward, meanwhile accretionary tidal flats are observed to become more convex upward (Dyer, 1998; Kirby, 2000; Le Hir et al., 2000; Mehta, 2002; Van Rijn, 1998), an effect which becomes more pronounced with increased tidal range (Friedrichs, 2011; Kirby, 2000).

Recent modelling exercises have focused on reproducing these subtle variations in the profile of intertidal flats. For example, an elegant analytical solution to predict equilibrium profiles of tidal flats for both wave and tide dominated environments was derived by assuming that equilibrium occurred when the spatial distribution of maximum bottom shear stress reached uniformity (Friedrichs et al., 1996; Zhou et al., 2016). Similar numerical models were developed using mass conservation and momentum balance to simulate mudflat profile changes (Roberts et al., 2000). Zhou et al. (2015) extended this work and developed a numerical model to investigate morphodynamics of intertidal flats, in particular examining the effect of sediment parametrization (i.e. the effect of initial bed sediment composition and sediment sources on the shape of intertidal flats). A larger mud concentration at the sea boundary promotes seaward advance and more convex-up intertidal flats (Liu et al., 2011; Pritchard et al., 2002; Pritchard and Hogg, 2003; Roberts et al., 2000; Zhou et al., 2015). A tidal flat with initially a larger percentage of mud tends to make the profile more convex up (Friedrichs, 2011; Kirby, 2000; Zhou et al., 2015), associated with the reduced erodibility of muddy sediment.

One of the effects that has not been well considered yet in profile models is the effect of atmospheric exposure on the properties of cohesive intertidal sediments. Recent work has shown that exposure to air during low tide can have pronounced effect on the erodibility of cohesive sediments (Fagherazzi et al., 2017; Nguyen et al., 2019; Nguyen et al., 2020), even more than grain size variations and bio-stabilisation by microphytobenthos (biofilms). Depending on the atmospheric

conditions during exposure and the duration, evaporation decreases the water content of sediments, which in turn increases erosion resistance (by increasing erosion threshold and decreasing erosion rate). These effects are in addition to the stabilizing effects of biofilm growth on sediment surface. Both evaporation and biofilms stabilise the sediment by strengthening bonds between particles and increasing the drag force required on the bed surface to cause erosion (Fagherazzi et al., 2017; Paterson, 1989; Tolhurst et al., 2006a; Underwood and Paterson, 2003; Widdows et al., 1998), with the strengthening effect remaining in subsequent flooding cycles (Fagherazzi et al., 2017; Nguyen et al., 2020). Laboratory measurements show an interaction between evaporation and biofilm growth that ultimately controls sediment erosion properties (Nguyen et al., 2020). For instance, after 10 days exposure critical erosion stress (T_{cr}) increased by 1.7 (low biofilm biomass) to 4.4 (high biofilm biomass) times and the erosion rate (*ER*) decreased by 11.6 to 21.5 times compared with compared with 6 h of exposure. Conversely exposure to rain during low tide destabilises sediments (Pilditch et al. 2008; Tolhurst et al. 2006b), by reducing bonding between particles.

This study aims to incorporate recent understanding on the changes to sediment properties that occur during short periods of exposure into numerical coastal profile modelling. Here, we hypothesize that the change in erodibility of sediments caused by exposure (including exposure temperature (*T* °C) and duration (*D* h)) as well as *Chl-a* content (a proxy of biofilm biomass) can change the way in which coastal profiles evolve. We used Delft3D to develop the numerical model, so that innovations added to the model can be made available through their open-source community. In addition, the effects of exposure temperature, *Chl-a* content, initial sediment bed composition (percentage of mud and sand) and spring and neap tidal cycles (effects current velocity and exposure period) on intertidal flat profile development were also investigated using the modifications to the bed transport sub-routines of Delft3D. The overarching aim of our work is to show how understanding exposure effects in sediment transport modelling could be critical

to predicting the resilience of intertidal zones into the future, when sea-level rise may exacerbate erosion in low-lying areas.

4.2 Methods

4.2.1 Modelling of erosion properties

The relationship between air temperature - *T* and exposure duration - *D* on the critical bed shear stress (τ_{cr}, $N\ m^{-2}$) and erosion rate *ER* ($g\ m^{-2}\ s^{-1}$) were expressed using semi-empirical models fitted to the data collected in Nguyen et al., (2019) (Exp. 1) and Nguyen et al., (2020) (Exp.2). The form of these models was based on the theoretical relationship between water content and evaporation rate, which depends on *T* and *D* (Nguyen et al., 2020). However, the coefficients were fitted empirically from experimental data because they depend on a number of complex and unknown effects such as the role of organic content in regulating moisture, the rate of vertical water movement through the sediment surface and the role of biofilms in binding the surface particles (bio-stabilization). τ_{cr} and *ER* were determined using a core based erosion device (EROMES) on sediment collected from a cohesive intertidal site at different times of the year and subjecting them to differing exposure periods (see Nguyen et al., (2019, 2020) for details).

In Exp.1, temperature was varied while holding the exposure duration constant at 6 h using treatments of sediments with high and low *Chl-a*, while in Exp.2 exposure duration was varied in two trials to represent typical summer and winter conditions. In Exp. 1. exposure temperature was controlled at 0, 8, 25 and 40°C to examine its effect on sediment erodibility. Exp. 2 exposed sediment cores to natural outdoor ambient conditions for 6 h, 1, 4 and 10 d with air temperature being logged every minute. Sediments used in both experiments were collected from intertidal mudflats in the Firth of Thames, New Zealand between 2017 and 2019 and collection times represented both winter and summer conditions. Overall, *Chl-a* content of winter samples were significantly lower than that of summer samples, while particle median grain size did not differ significantly

between seasons (Table 4.1). Note that these experiments were not specifically designed to parameterize this model and so a full range of combinations of *Chl-a*, temperature and exposure is not available.

Table 4.1 In situ sediment properties at the time cores were collected for use in laboratory experiments (data summarized from Nguyen et al., (2019) and Nguyen et al., (2020)).

Properties	Dec 2017	Mar 2018	Oct 2018	Jan 2019	Feb 2019
Wet bulk density (g cm^{-3})	-	-	1.36 ± 0.08	1.44 ± 0.05	1.43 ± 0.07
Dry bulk density (g cm^{-3})	-	-	0.32 ± 0.03	0.34 ± 0.06	0.33 ± 0.04
Median grain size (D_{50}, µm)	6.37 ± 1.05	8.90 ± 0.90	6.34 ± 1.72	6.94 ± 1.59	6.14 ± 0.85
Clay content (%)	37.8 ± 4.1	26.3 ± 2.8	37.6 ± 6.2	34.1 ± 5.2	34.8 ± 4.0
Silt content (%)	55.3 ± 5.3	63.4 ± 3.8	55.8 ± 4.1	62.8 ± 5.1	61.2 ± 5.0
Sand content (%)	6.9 ± 2.8	10.3 ± 3.1	6.6 + 3.98	3.1 ± 0.9	4.0 ± 1.0
Chlorophyll-a (*Chl-a*, µg g^{-1})	9.2 ± 2.7	21.6 ± 5.8	10.8 ± 1.9	78.0 ± 13.0	65.1 ± 6.2
Organic content (*OC*, %)	9.8 ± 0.3	10.1 ± 3.2	10.3 ± 0.6	12.6 ± 0.5	13.1 ± 0.4

- *Data represent the mean ± 1 standard deviation (n=20*)

While a linear model best fitted the relationship between T_{cr} and T and D (Figure 4.1A and 4.1C), an exponential model best described the relationship between ER and these two factors (Figure 4.1B and 4.1D). Both models needed to include an interaction term, so that at the moment of exposure, the T_{cr} and ER values were equal to the underwater values, regardless of exposure temperature. Nguyen et al. (2019, 2020) showed that the change in biofilm biomass on the intertidal flat was seasonal, with a higher *Chl-a* biomass in summer and lower in winter (Table 4.1). Data were therefore separated into high and low *Chl-a* content treatments to examine the effect of biofilm biomass on sediment erosion potential. In addition, pooled data from both the high and low *Chl-a* content were used to inform a general model. Our best fitted model resulted in the following equations for T_{cr} and ER:

$$ER = ER_{inn} \times e^{(a_1 T + a_2)D} \quad (1)$$

$$\tau_{cr} = \tau_{inn} + (b_1 T + b_2)D \quad (2)$$

Where τ_{inn} and ER_{inn} are erosion threshold and erosion rate of sediment when inundated, respectively and the a_1, a_2, b_1, b_2 are coefficients which were evaluated separately for high and low *Chl-a* content cases and the pooled data (see Table 4.2 for coefficient values).

Table 4.2 Coefficients model for erosion rate (Eq. 1: $ER = ER_{inn} \times e^{(a_1 T + a_2)D}$) and erosion threshold (Eq.2: $\tau_{cr} = \tau_{inn} + (b_1 T + b_2)D$) of sediment.

Chl-a cases	a_1	a_2	r^2	*F*	b_1	b_2	r^2	*F*
Pooled data	-0.0034	0.0173	0.23	2.2	0.0029	-0.02	0.57	8.5
Low *Chl-a* data	-0.0072	0.0451	0.92	31.0	0.0017	0.0101	0.81	10.8
High *Chl-a* data	-0.0077	0.0716	0.98	132.4	0.0032	-0.023	0.98	181.0

- *Pooled: mean Chl-a is 31.8, µg g^{-1}*
- *Low (Dec 2017&Mar 2918&Oct 2018): mean Chl-a is 15.0, µg g^{-1},*
- *High (Jan 2019&Feb 2019): mean Chl-a is 48.6, µg g^{-1}*

The strengthening effect of exposure on sediment stability is believed to remain over subsequent flooding cycles (Fagherazzi et al., 2017). Nguyen et al., (2020) demonstrated this by conducting re-submersion experiments on intertidal cohesive sediments after exposure periods of 1, 4 and 10 d. Their results showed that erosion resistance of exposed sediments showed no significance changes after one and two re-submersion events (each lasting for 4 h). However, to retain the potential that sediments recover to initial conditions (when re-inundated) after much shorter exposure times than covered in our experiments (for example, a single tidal cycle), we added recovery coefficients for T_{cr} and *ER* into the models, which allow sediment erosion properties to gradually return to submerged conditions when immersed. The more the erosion properties changed during exposure (e.g. higher *T* and longer *D*), the longer the recovery period (see below for details).

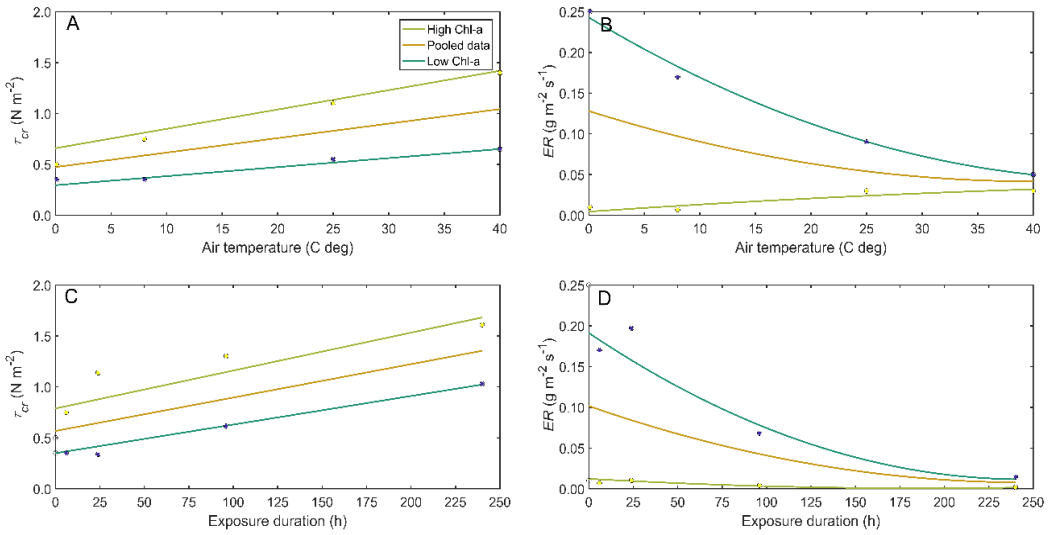

Figure 4.1 Empirical models for A & C) erosion threshold T_{cr} (N m^{-2}) and B & D) erosion rate ER (g m^{-2} s^{-1}), fitted to the experimental results of Nguyen et al. (2019, 2020).

4.2.2 Model setup

Following Roberts et al. (2000), the starting bed profile was linearly sloped from an elevation of 6 m (below Mean Sea Level, MSL) to 4 m above MSL over a distance of 10 km (i.e., slope is 0.1%, Figure 4.2A. This is a similar slope to the field site in Nguyen et al. (2019, 2020). The bed was covered with a 5 m sediment layer which was composed of sand and mud. The offshore tidal boundary was forced by the superposition of M_2 and S_2 constituents to simulate the spring-neap cycle. The spring tidal range was set as 3 m (the tidal range at the field site). The erosion threshold and erosion rate when the profile was inundated were set to 0.05 $N\ m^{-2}$ and 0.05 $g\ m^{-2}\ s^{-1}$ respectively, the values that were measured from erosion experiments on cores which were retained in a submerged state (sediment samples were submerged for 6 h prior to tests for erosion properties) from Nguyen et al. (2019, 2020).

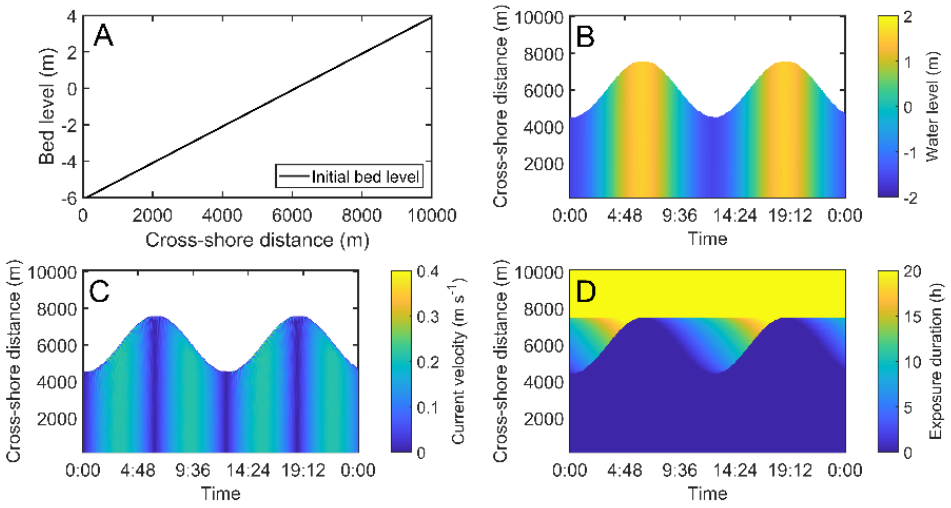

Figure 4.2 An example of model results (20 °C air temperature) showing A) initial bed level B) water level, C) current velocity and D) exposure duration.

Model scenarios were designed to explore the role of air temperature, spring and neap tides, biofilms, and bed sediment texture (percentage of sand/mud in the bed composition) on profile evolution (summarized in Table 4.3). Three model runs of 10, 20 and 40 °C were chosen to investigate the effect of air temperature, which covers a wide range of temperature and the extremes that occur at our field site. In other model runs that examine the influence of spring and neap tides, biofilms and sediment composition the air temperature was set at 20 °C. As a first attempt to understand the role of exposure on profile development, models were run for one year to simulate the initial influence on intertidal flats. Further work will explore the role of seasonality and precipitation on profile development.

Table 4.3 Parametrizations for the model setup

T (°C)	τ_{inn} (N m^{-2})	ER_{inn} (g m^{-2} s^{-1})	*Chl-a* content cases	Sand / Mud (%)	Tide constituents (m)
10	0.05	0.05	Pooled data	Mud only	M_2=1.5 S_2=0
20	0.05	0.05	Pooled data	Mud only	M_2=1.5 S_2=0
40	0.05	0.05	Pooled data	Mud only	M_2=1.5 S_2=0
20	0.05	0.05	Pooled data	Mud only	M_2=1.5 S_2=0
20	0.05	0.05	Pooled data	Mud only	M_2=1.5 S_2=0.45*
20	0.05	0.05	high Chl-a	Mud only	M_2=1.5 S_2=0
20	0.05	0.05	low Chl-a	Mud only	M_2=1.5 S_2=0
20	0.05	0.05	Pooled data	50/50	M_2=1.5 S_2=0
20	0.05	0.05	Pooled data	30/70	M_2=1.5 S_2=0
20	0.05	0.05	Pooled data	70/30	M_2=1.5 S_2=0

- *M_2 and S_2 are the principal lunar and solar semi-diurnal constituents, respectively.*
- *The "no exposure effect" case is set up with constant values of erosion threshold and erosion rate at 0.05 N m^{-2} and 0.05 g m^{-2} s^{-1}, bed composition of 100 % mud, and M_2 = 1.5 m, S_2 = 0 m.*
- **Spring-neap tide case.*

4.2.3 Formulae controlling sediment dynamics

In Delft3D, sand and mud fractions are considered individually. Therefore, physical process such as erosion and deposition are treated separately for each fraction. Sediment transport of cohesive fractions – mud is modeled using an advection equation

$$Q_{mud,e} - Q_{mud,d} = \frac{\partial (Ch)}{\partial t} + \frac{\partial (uCh)}{\partial x} \quad (3)$$

where $Q_{mud,e}$ and $Q_{mud,d}$ are erosion and deposition fluxes, respectively. C is depth averaged concentration (kg m^{-3}), h is water depth (m), u is depth averaged flow velocity (m s^{-1}), t is time (s), x is direction (m). These fluxes were modelled using the widely adopted Partheniades–Krone equations (Partheniades, 1965)

$$Q_{mud,e} = \begin{cases} ER\left(\frac{\tau_{max}}{\tau_{cr}} - 1\right) & if\ \tau_{max} > \tau_{cr,e} \\ 0 & if\ \tau_{max} \leq \tau_{cr,e} \end{cases} \quad (4)$$

$$Q_{mud,d} = \begin{cases} W_s C\left(1 - \frac{\tau_{max}}{\tau_{cr,d}}\right) & if\ \tau_{max} < \tau_{cr,d} \\ 0 & if\ \tau_{max} \geq \tau_{cr,d} \end{cases} \quad (5)$$

where *ER* is the erosion rate (g m^{-2} s^{-1}, described as the erosion parameter - M_e in Partheniades (1965)), τ_{cr} and $\tau_{cr,d}$ are the bed shear stress for the erosion threshold and deposition of the mud component, respectively (N m^{-2}). τ_{max} is the maximum bed shear stress (N m^{-2}) and W_s is the settling velocity (m s^{-1}). $\tau_{cr,d}$ is set at very large value of 1000 N m^{-2} as default (Winterwerp, 2007), which means that sediments always deposit when conditions are below the erosion threshold.

In traditional Delft3D modeling studies of sediment dynamics and bed level change, *ER* and τ_{cr} (in Equation 4) are typically set as constants and do not change with exposure. In this research, we have extended Equation 4 by embedding the formulations of *ER* and τ_{cr} described by Equation 1 and 2 into Delft3D. The air temperature to which the intertidal sediments are exposed was set as a constant value along with the empirical coefficients in Table 4.2. The duration of exposure is introduced as a new model variable, which depends on the bed level on the tidal flat, and is determined by whether the bed level is above or below the water level at each hydrodynamic time step. Also included is a new variable which determines the time over which the sediment returns to pre-exposure conditions after re-inundation. This was assumed to be a linear function (given that we have no experimental data on which to base a relationship), so that τ_{cr} decreases and *ER* increases with time (both rates set in the input file).

$$ER(t) = ER_{inn} + Rev_{ER} * t, \quad (6)$$

$$\tau_{cr}(t) = \tau_{inn} - Rev_{Tau} * t, \quad (7)$$

where $ER(t)$ (g m^{-2} s^{-1}) and $\tau_{cr}(t)$ are erosion rate and erosion threshold of submerged sediments at a given time *t* (minute), Rev_{ER} and Rev_{Tau} are arbitrarily-

set recovery coefficients of erosion rate and erosion threshold, respectively. The recovery coefficients are set at a constant value for each model run and vary exposure air temperatures.

Figure 4.2B, 4.2C and 4.2D present an example of a model setup in which the exposure duration at different levels on the intertidal flat was computed in the Delft3D sediment transport modules using the water level and bed elevation, and the current velocity during flood and ebb tides associated with each water level were calculated in the basic Delft3D hydrodynamic drivers. Two sets of runs were completed for each scenario: one with low time resolution over a whole year to track morphological change, and a shorter run at a higher time resolution to create detailed figures of the suspended sediment flux and currents for interpretation.

4.3 Results

4.3.1 Effect of air temperature on bed level change

In order to examine the effect of T on τ_{cr} and ER (Figure 4.3) and their ultimate control on bed level, models were run with T set to 10, 20 and 40 °C while tidal ranges (tide constituents of M_2 = 1.5 m and S_2 = 0 m) were held constant. In model runs with no exposure effect (i.e. in which the exposure effects on sediment stability during low tide was neglected), τ_{cr} and ER were unchanged during tidal cycles and were equal to inundated values (Figure 4.3A and 4.3B). In this case, there is a strong increase in suspended sediment concentration as the flooding tide moves over the intertidal region, which is not matched by a peak in ebbing suspended sediment concentration (Figure 4.3C). In comparison, when the effect of exposure is taken into account, model results indicated that intertidal sediments were stabilized during exposure with higher values of τ_{cr} and lower values of ER with the rate of increase/decrease dependent on T. Maximum values of τ_{cr} increased from 0.05 to 0.15, 0.5, 1.6 $N\ m^{-2}$, while maximum values of ER decreased from 0.05 to 0.035, 0.02, 0.01 $g\ m^{-2}\ s^{-1}$ in accordance with T of 10, 20, 40 °C. In these scenarios, the ebb and flood tide suspended sediment

concentrations are more similar in magnitude; when the bed is more stable, less sediment is eroded during the incoming tide. The flooding currents only start eroding sediments in the intertidal after the stabilization effect has worn off. As we employed a recovery factor for the values of T_{cr} and *ER*, the recovery of these values in the subsequence flooding cycles will depend on how much change the values gained during the exposure periods (Figure 4.3D, 4.3E, 4.3G, 4.3H, 4.3J and 4.3K). Consequently, T_{cr} and *ER* took longest time to return to inundated values for the case of 40 °C (Figure 4.3K-in which case the erosion threshold never returns to the submerged value), whereas these values recovered more quickly for the cases of 10°C and 20°C (returning to the submerged values before the ebbing tide drains from the intertidal region). The model simulates the amount of water lost by evaporation during exposure and the higher temperature caused more water to evaporate.

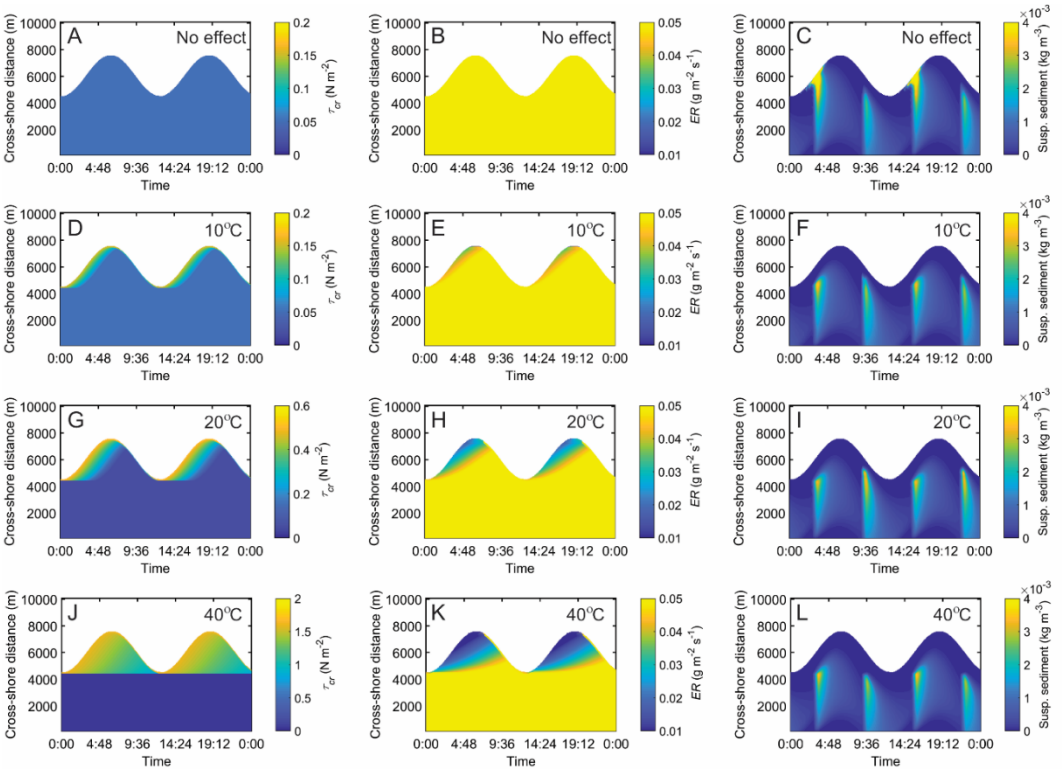

Figure 4.3 Effect of air temperature on T_{cr} (A, D, G, J), ER (B, E, H, K) and suspended sediment concentration (C, F, I, L). Note figures show variations over two tidal cycles and the colour scale has different ranges for the left column panels.

In general, net erosion occurred in the sub-tidal zone area while accretion occurred in the intertidal zone in all cases (Figure 4.4A). With no exposure effect, the change in bed level was evenly-distributed across the intertidal zone, except for minor erosion within the zone from 5100 m to 5500 m in the cross-shore (Figure 4.4A). The positive change of bed level was more evident within the upper part of the intertidal (5500 m-7000 m) and erosion mostly occurred in sub-tidal zone (Figure 4.4A). The pattern of bed level change could be explained by the cross-shore distribution of sediment flux (Figure 4.4B); the flood peak in the sediment flux occurs at a higher tidal stage than the ebbing flux, causing a flux shoreward of sediment in the intertidal area. In fact, there is only a flooding sediment flux on the upper intertidal (the ebb-flux is non-existent), and the flood tide sediment flux always surpasses that of the ebb tide in the intertidal. In the no exposure effect scenario, the imbalance between flood and ebb sediment flux would eventually cause the profile to flatten in the intertidal region (a convex profile development).

When the effect of air temperature is considered in the model, accretion of sediment on intertidal flat tended to focus on the lower intertidal, in comparison to the 'no effect case' (Figure 4.4A). On the lower flat, a bed level increase of from 0.02 (T = 10 °C) to 0.039 m (T = 40 °C) occurred compared to less than 0.01 m for the no exposure effect case. In contrast, on the higher intertidal, sediment accretion of 0.022 m occurred for no effect case compared with less than 0.01 m for cases when the temperature exposure effect was included. Higher T resulted in more sediment accumulation on the intertidal flat as a consequence of increased net sediment erosion in the sub-tidal zone. The currents are approximately the same in all the scenarios, so the difference in net sub-tidal erosion is likely because the sediment is more effectively trapped in the intertidal zone and not available to be transported seaward by the sub-tidal ebb currents (Figure 4.4B, green line at 4000m). (Whereas in the no-exposure effect case, sub-tidal erosion by the flooding tide is partially compensated by accretion by the ebbing tide). Within the intertidal, there was a transition from the upper to the

lower intertidal (seaward) of the accumulation zone between the 10 °C case and the cases with higher air temperature (20 °C and 40 °C), which would cause the intertidal profile to become flatter and the lower edge of the intertidal to become steeper. At higher elevations, the difference in sediment flux between the ebb-tide and flood-tide becomes more evident, for example from 5500 m shoreward there were only flood-directional sediment fluxes. The higher elevations on the intertidal flats are progressively exposed for increasing times, which means that the sediments there become increasingly more stable with temperature, and there is no source of sediment provided to the ebbing currents to carry seaward—therefore as temperature increases, more and more sediment accumulates on the lower intertidal. In summary, the larger the stabilizing effect (e.g. 40 °C), the larger the effect on the bed level.

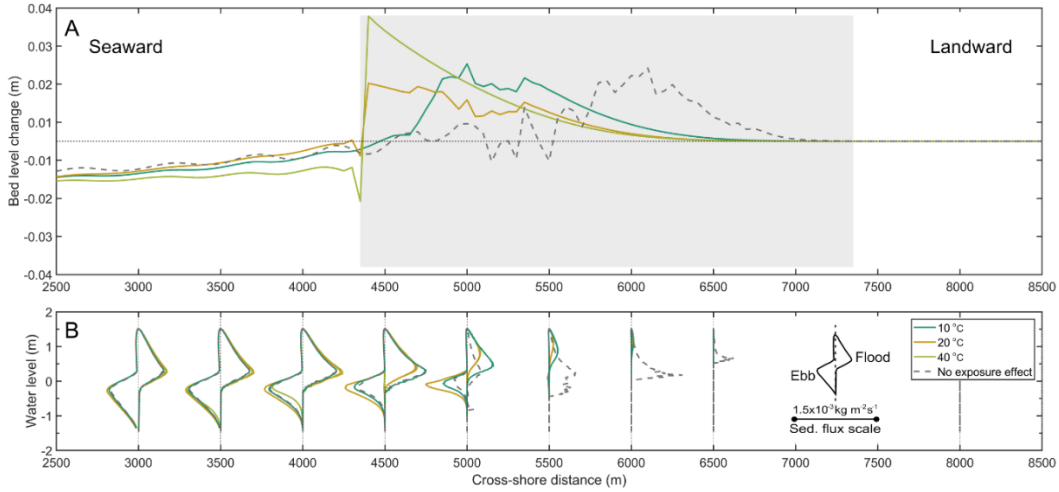

Figure 4.4 Effect of air temperature on bed level changes over one year, modelled using tide constituents M_2 = 1.5, S_2 = 0 (shaded area represents the inter-tidal area), using the pooled data *Chl-a* model, bed sediment composition mud only, ER_{inn} = 0.05 g m^{-2} s^{-1}, and T_{inn} = 0.05 N m^{-2}. The sediment flux scale is the same for each vertical sediment flux profile plot (scale bar plotted at the right side).

4.3.2 Effect of biofilm on bed level change

In order to examine the effect of biofilm stabilization, models were set up for low and high *Chl-a* content with the same temperature, bed composition and tidal conditions. Note that the low and high *Chl-a* runs represent different erosion values measured in experiments taken in winter and summer which were accompanied by changes to *Chl-a*; however experiments were not set up to test *Chl-a* effects on erosion, and so we cannot conclusively prove that observed changes to erosion conditions were caused by *Chl-a*. Instead, these runs should be consider as a demonstration of the sensitivity of bed-level changes to seasonal differences in conditions. Parametrizations used in the model are presented in Table 4.3. We assume that the difference in *Chl-a* only effect the intertidal regions, the subtidal erosion characteristics remain constant between all runs (Table 4.3). In fact, in the low *Chl-a,* the intertidal conditions are less stable than the subtidal. Bed level changes were substantially different between low and high *Chl-a* content cases (Figure 4.5A). For both the pooled data and the high *Chl-a* model runs, sediment started accumulating from 4350 m (at the seaward extent of the intertidal) then accumulation gradually decreased over the intertidal flat, with maximum changes of 0.015 m and 0.005 m for the former and the latter, respectively. The pattern of bed level change for the low *Chl-a* cases was different to the others in that the accumulation had two maxima, one on the lower flat (4350 – 4700 m, maximum of 0.012 m) and one on the upper flat (5600 – 7000 m, maximum of 0.018 m), separated by an eroded zone (4700 – 5600 m, minimum of 0.015 m). The low *Chl-a* case had greater landward sediment flux relative to seaward sediment flux, which caused the significant change of the bed level (Figure 4.5B). The very different patterns at low *Chl-a* are likely due to intertidal conditions being less stable than subtidal. In general, just as with the high-temperature runs, when stabilization increases (high *Chl-a*), the supply of sediment from the intertidal regions is suppressed, meaning a reduction of the sediment scoured seaward by the ebbing current, and landward by the flooding current.

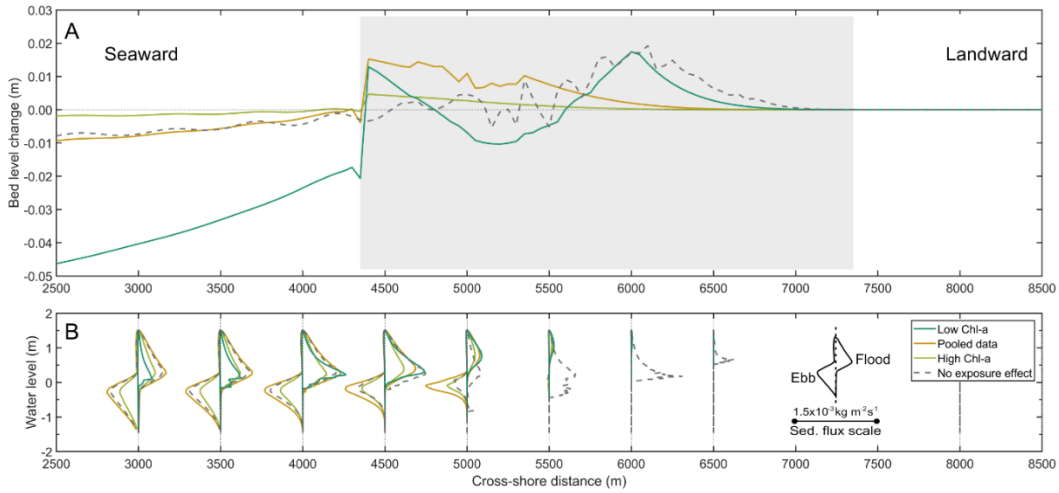

Figure 4.5 Effect of biofilm growth on bed level changes over one year, tidal constituents $M_2 = 1.5$, $S_2 = 0$ (shaded area represents the intertidal area), modelled with an air temperature 20 °C, bed sediment composition = mud only, $ER_{inn} = 0.05$ $g\ m^{-2}\ s^{-1}$, $T_{inn} = 0.05\ N\ m^{-2}$. The sediment flux scale is the same for each vertical sediment flux profile plot (scale bar plotted at the right side).

4.3.3 Effect of bed sediment composition on bed level change

Generally, changes to bed composition caused a similar pattern in bed level changes to the effect of changes in temperature and *Chl-a*, with an increase in the sediment accumulated in the region from 4350 to 7000 m over the intertidal flat (Figure 4.6A). After a year, transported sediment mostly accumulated in the zone of 4350 – 4600 m (+ 0.012 to 0.018 m), reduced in the zone of 4600 – 5200 m (+ 0.002 to 0.01m) and increased again from 5200 – 5500 m (+ 0.007 to 0.015 m) before a gradual decrease to no accumulation from 5500 – 7000 m. Bed composition with higher percentage of mud showed greater net erosion in the subtidal zone, and greater net accumulation in the intertidal. This is likely mainly because a greater fraction of the bed is affected by the differences in stabilization (the stabilization effect is only applied to the mud fraction in the model, and has no effect on the sand). It would also be in part caused by the spatial distribution of stabilisation effect (as in Figure 4.4), were when more sediment is trapped on the intertidal, the tide ebbing off the intertidal is deprived of sediment, and so

causing a decrease of accumulation in the subtidal. Greater sediment fluxes explained the higher level of bed level change for the cases with higher percent of mud fraction (Figure 4.6B). For example, 100 % mud always showed the greatest sediment fluxes while with 30 % mud/70 % sand had the lowest sediment fluxes over the cross-shore section (Figure 4.6B).

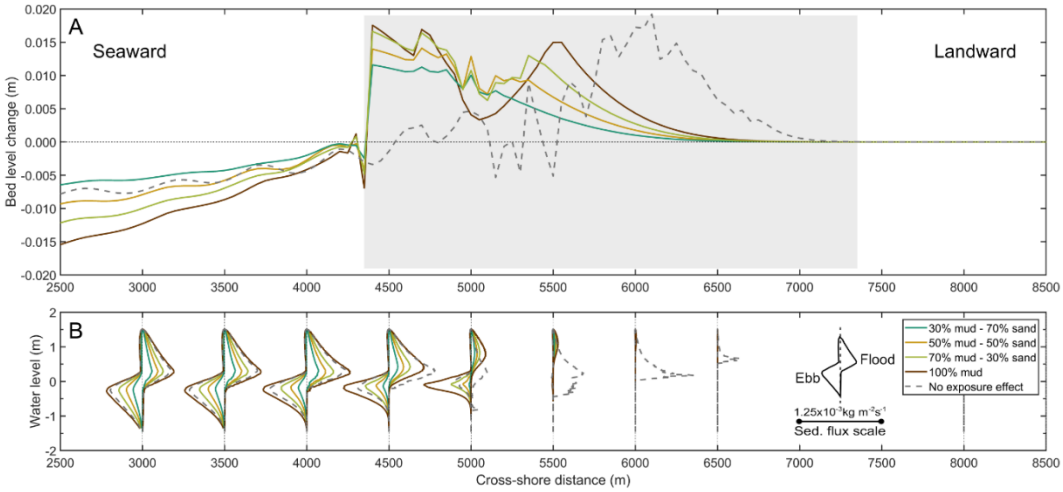

Figure 4.6 Effect of bed composition on bed level changes over one year, tidal constituents M_2 = 1.5, S_2 = 0 (shaded area represents the inter tidal area), air temperature 20 °C, pooled data *Chl-a* model, $ER_{inn} = 0.05\ g\ m^{-2}\ s^{-1}$, $T_{inn} = 0.05\ N\ m^{-2}$. Note that the exposure effect applied to the mud fraction only. The sediment flux scale is the same for each vertical sediment flux profile plot (scale bar plotted at the right side).

4.3.4 Effect of spring – neap tide on bed level change

To examine the effect of changes in the tidal range in combination with the exposure effect on bed level change, a model that included spring-neap variations (with a wider tidal range - M_2 = 1.5 m, S_2 = 0.45 m) and a model with normal tidal range (M_2 = 1.5 m, S_2 = 0 m) were set up at the same temperature (20 °C; Figure 4.7). This meant that areas on the high intertidal could remain exposed for up to 14 days. The results indicated that a wider (spring) tidal range led to the accumulation zone moving seaward (green line) compared to the normal tide

(yellow line) and with no exposure effect (black dashed line). The spring-neap tide case eroded more sediment in the sub-tidal zone seaward of 3900 m. For this case, bed level increased by 0.02 m in the zone of 3900 – 4000 m then decreased over the higher parts of the intertidal flat from 4000 – 7000 m. With a normal tide, sediment eroded in sub-tidal zone, accumulated on the lower tidal flat of up to 0.015 m then gradually decreased to 7000 m on the flat. Sediment fluxes in the spring – neap tide case always surpassed the normal tide case both with and without the exposure effect (associated with the stronger tidal currents occurring with spring tides); the asymmetry was also more flood-dominant in the spring-tide case, which resulted in wider range of bed level changes.

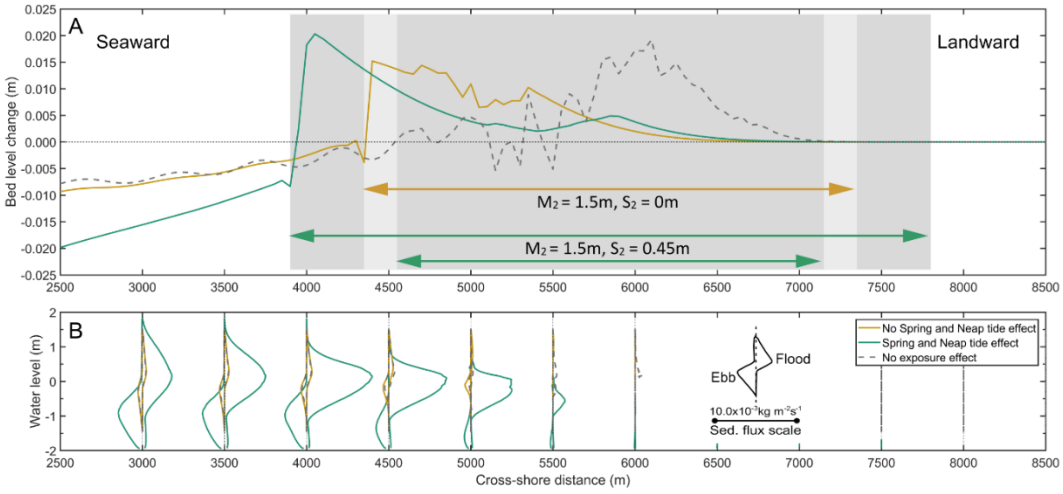

Figure 4.7 Effect of tide level on bed level changes over one year, air temperature 20 °C, pooled data *Chl-a* model, ER_{inn} = 0.05 g m^{-2} s^{-1}, T_{inn} = 0.05 N m^{-2}. Shaded areas represent inter tidal areas (green arrows represent spring and neap tides, golden arrow represents the intertidal tidal area for the case of no spring and neap tide effect). The sediment flux scale is the same for each vertical sediment flux profile plot (scale bar plotted at the right side).

4.4 Discussion

This paper sought to model differences that exposure of sediment to evaporation at low tide could potentially have on intertidal mudflat development, with the effect of *ChI-a* content, bed composition and tidal ranges being included in models. Areal exposure causes the surface sediment to loose moisture and the particles to bind more effectively together, increasing the critical erosion threshold and reducing the erosion rate. Both these parameters are a fundamental control to how sediment is eroded and accreted in cohesive environments. Our modelling results indicated that adding in the effect of exposure generally causes more accretion on the lower intertidal flats at sites with tidal currents that were sufficient to mobilize sediment. Consequently, the tendency to accrete means that convex tidal flats would be created in all cases if the models were run over a much longer timescale. Our results are consistent with previous studies that showed the interrelation between accumulation of sediment on intertidal flats and convexity of the profile (Dyer, 1998; Kirby, 2000; Le Hir et al., 2000; Mehta, 2002; Van Rijn, 1998). When the effect of exposure was taken into account, the formation of convex tidal flats occurred by building upward on the lower intertidal, whereas in previous studies, the convexity builds seaward as sediment accumulates on the landward fringe (Kirby, 2000).

The seaward shift of the accretion zone occurs because of the increase in stabilisation of the intertidal sediments. The sediment used to build the intertidal zone either comes from the outer boundary, or is eroded from the subtidal and lower intertidal regions. The flooding tide brings the sediment shoreward, where it settles out gradually throughout the intertidal. The following ebbing tide gathers momentum as it drains off the intertidal, resuspending the sediment on the lower intertidal, and so without any exposure effect, the sediment prefers to settle out on the higher intertidal. However, when the exposure effect is added, the suspension on the lower intertidal is dramatically reduced (compare Figure 4.3C and F), so there is less sediment available to supply the upper intertidal, and more

retained on the lower intertidal. Retaining sediment on the intertidal also means that there is less sediment transported into the subtidal, and net erosion occurs in the subtidal. The higher the temperature, the more pronounced this effect was. The extreme scenario of 40°C caused substantially higher tidal flat accumulation (0.039 m by the end of model simulation compared with 0.022 m build-up of sediments in the no exposure effect tidal flats, corresponding to 77% higher). However, 40 °C is an extreme case, and accretion rates for exposure treatments were generally similar to no exposure treatments, but were distributed quite differently, accumulating on the lower intertidal. Sediments with higher mud content built up bed elevation more which is consistent with previous studies in which profiles with greater mud fractions causing more transport to the upper tidal flat (Zhou et al., 2015; Kirby, 2000; Friedrichs; 2011). The exposure effect was applied to the mud fraction only, therefore, the higher mud percentage the more pronounced this effect was. Interestingly, there was often a bimodal distribution of accumulation (e.g. Figure 4.5, low *Chl-a* and Figure 4.6, 100% mud). Accumulation and accretion is a product of small changes in the balance of ebbing and flooding sediment fluxes, which change across the profile. There is a point on the mid-intertidal where sediment fluxes switch locally to ebb-dominant from a pattern that is generally flood-dominant across the intertidal.

Our model results show that the effect of increasing intertidal stabilization is likely to create a more convex profile (or a more flat-topped intertidal profile). Although such profiles are common in cohesive environments (Knight et al., 2009; Lovelock et al., 2010; Vo-Luong and Massel, 2008), it is difficult to isolate how much of the profile shape is caused by processes that occur only in the intertidal. One exception is the stabilization effect of some vegetation (e.g. mangroves and saltmarsh), which can only grow in the intertidal due to physiological restrictions. Bryan et al. (2017) explained that mangrove vegetation initially increases the currents and flood dominance just landward of the fringe of mangroves (due to tidal wave shoaling), transporting the sediment into forests. Once the sediment enters the forest, the stabilization effect of mangroves on intertidal flats can occur

in both direct and indirect ways. For instance, dense vegetation attenuates these currents (Bryan et al., 2017) while mangrove roots are believed to increase the consolidation processes by dewatering of sediments that in turn stabilizes the sediments against erosion (Roskoden et al., 2019). Consequently, both effects will cause gradual accretion just inshore of the fringe. The accumulation, over time, results in the increase in slope seaward of mangroves and flatten the slope inside the mangroves, resulting in flat-topped profiles characteristic of mangrove dominated mangrove sites (Bryan et al., (2017) summarise a range of examples from other studies). The effect of our stabilization on profile development is similar. Although note that the stabilizing effect of vegetation included in conventional Delft3D models (and in Bryan et al., 2017) is only a hydrodynamic one, caused by increased drag and reduced currents, which may not be the most important way that the vegetation acts on profile evolution.

Low-tide rainfall can have substantial effects on the erodibility of surficial sediments on intertidal flats (Pilditch et al., 2008; Tolhurst et al., 2006b). Our study excluded the effect of rainfall and consequent changes to water content and direct impacts on sediment surfaces. Such an effect could easily be incorporated into our model in a future version. As discussed earlier, the stabilizing effect of exposure and vegetation on intertidal mudflats are somewhat similar and the resulting accretion patterns would tend to result in flat-topped profiles. However, the stabilization effect of exposure only happens if it does not rain, whereas mangrove stabilization occurs perpetually. The temperature and duration are essentially a proxy for water content in the sediment, and ideally water content should be directly modelled. It would be possible to incorporate rain in a water content model, or to use a time series of water content loss rate as an input file. In addition, the effect of consolidation on bed level change is not included in this research. Zhou et al. (2016) introduced a self-weight consolidation model that incorporated influences of consolidation in simulations by gradually reducing the bed level and decreasing the bed erodibility (i.e., increasing the critical bed shear stress), which led to long-term morphodynamic effects on the intertidal mudflat.

Our model was developed to predict the effect of air temperature and exposure on the evolution of bed profile based on experimental results on sediments collected from the intertidal mudflat in the Firth of Thames. The samples have specific properties characterized by the grainsize, the inundated water content, the *Chl-a* content (as a proxy of biofilm biomass) and the organic content that will all play a role in controlling the erosional behavior of sediments, ultimately making the empirical fitting coefficients site-specific. Water content reduction and biofilm growth are believed to increase the erosion resistance (Amos et al., 2004; Black et al., 2002; Chen et al., 2017; Nguyen et al., 2019; Nguyen et al., 2020; Van Ledden et al., 2004). Nevertheless, the interaction between factors is complicated, for example, the reduction of water content might slow down the biofilm growth (Nguyen et al., 2020), meanwhile, a high *Chl-a* content on sediment surfaces might prevent evaporation (Lianfang et al., 2009; Vandevivere and Baveye, 1992).

We did not transitioned the change in stabilization smoothly into the subtidal in our simple model development, and indeed, some of our formulations (e.g. low-*Chl-a*) caused an increase in stabilization seaward. More work is needed to parameterize these transitions realistically. In addition, one would expect exposed erosion resistance should recover to inundated conditions after submergence as water content is replenished within the sediments (Tolhurst et al., 2006a). In contrast, Nguyen et al., (2020) showed no significant change to erodibility of re-submerged and exposed sediments, which was explained by combining the effect of long- term exposure and biofilm growth. In this research, we included coefficients of recovery that allow erosion resistance decrease during immersion (increases *ER* and decreases T_{cr}). However, we do not have experimental results to inform the selection of coefficients for the recovery rate of sediments. Nevertheless, including the processes gives an indication of the importance of this term as air temperature and exposure time varied. Generally, all our models are entirely parameterized with the empirical data, and additional work is needed to generalize the model to other sites. Nevertheless, although our

models are site-specific, the results are generally applicable to cohesive intertidal settings.

4.5 Conclusions

This study examined how exposure changes intertidal profile evolution over a short (annual) time scale (a morphological scale factor of 10 was used to shorten running time of models). The stabilizing effect of exposure is likely to be, to some extent, similar to vegetation on intertidal flats on the evolution of tidal profile, although the mechanism for causing sediment dewatering is different. Our results imply that muddy, highly stabilized intertidal areas evolve toward flat-topped (convex) profiles more quickly when stabilization is included in the evolution.

Our models also investigated the influence of different factors such as air temperature, *Chl-a* content, bed sediment composition and spring-neap tides on the changes of bed level, all of which contribute to stabilization in different ways. Although, some of the assumptions in our models are inevitably made (the lack of precipitation, the constant exposure temperatures), the key message is consistent. Subtle differences in exposure control the convexity of the profile that evolves, and so the way in which new coastal land will build in the future to protect the coast. Ultimately, these model experiments highlight the complexities that might play a role in shaping our coast with predicted changes to storm-surge climates (which change our inundation regimes) accompanied by rising temperatures.

Chapter 5

Modelling the effect of temperature and exposure on intertidal channel networks in cohesive coastal environments

Nguyen, H.M., Bryan, K.R., Zeng Zhou, Pilditch, C. A. In preparation to submit to the journal of Geomorphology. Modelling the effect of temperature and exposure on intertidal channel networks in cohesive coastal environments.

Contribution of authors

Chapter 5 presents the article entitled “Modelling the effect of temperature and exposure on intertidal channel networks in cohesive coastal environments”, which is in preparation to published in the journal of Geomorphology.

I was responsible for setting up model runs, data processing, data analysis and writing.

Zeng Zhou assisted with the code that combined integrated empirical models for erosion threshold and erosion rate of exposed sediments into the Delft3D modelling environment.

My supervisors Karin Bryan and Conrad Pilditch assisted with data analysis, reviewed drafts and advised on directions.

Abstract

Tidal channel networks regulate landscapes of intertidal zones, and are the channels to exchange water, nutrient, sediment and biota between land and ocean. The development of tidal networks is vital to the evolution of salt marshes and intertidal zones. This study aimed to investigate the effect of exposure on the development of tidal channel networks in short-term. Empirical models that simulate changes in erosion threshold (T_{cr}; N m^{-2}) and erosion rate (ER; g m^{-2} s^{-1})) of sediment on intertidal flat during low tide under the effect of exposure (taken into account air temperature, T (°C) and exposure duration, D (h)) was integrated into Delft3D models to investigate the development of tidal channels. Model results showed that exposure substantially enhances the development of tidal networks in both density and depth compared with the modelled cases without exposure effect. When exposure sediments at channel banks were stabilized and unlikely to be eroded and built up, while sediment in channels with shorter exposure duration was likely to be eroded. The two processes exacerbate the development of channel networks on intertidal flats. Our findings, therefore, significantly contribute to predicting the development of tidal channel networks, which will help to understanding the resilience of tidal flats and salt marshes in future when sea-level rise.

Keywords: Exposed sediment, intertidal zones, profile evolution, numerical modelling, sediment stability, low-lying areas

5.1 Introduction

Intertidal zones, including tidal flats and salt marshes are important and yet among the most vulnerable ecosystems on Earth (Coco et al., 2013; Kirwan and Megonigal, 2013; Zhang et al., 2016). Intertidal zone landscapes are characterized by tidal channels with their branched networks (Vandenbruwaene et al., 2013). Tidal channel networks are the main paths for exchanging of water, nutrients, sediments and biota between lands and oceans (Fagherazzi et al., 1999; Zedler and Kercher, 2005; Zhou et al., 2014). Hence, tidal channel networks play a crucial role in evolution of intertidal flats and salt marshes.

Simulation models have been extensively explored medium and long-term evolution of tidal channel networks (e.g. Belliard et al., 2015; D'Alpaos et al., 2005; Dastgheib et al., 2008; Lanzoni and D'Alpaos, 2015; Van Oyen et al., 2014). These models solve the coupled equations describing hydrodynamics, sediment transport, biological activities and morphological change, covering various spatial and temporal scales. Also, a wide range of environments such as salt marshes, intertidal flat and mangrove have been modelled in previous studies (Belliard et al., 2015; Zhang et al., 2016, van Maanen et al., 2015). Such models show that channels are initiated when a topographic perturbation concentrates the flow in hollows, causes the bed shear stress to be higher, which then causes a positive feedback which further erodes the hollows into channels. Another possibility that flow is diverted away from higher regions, causing accretion, which also causes a positive feedback. Both erosional and depositional processes can act at different stages within the ontogeny of tidal networks: channel origination stems from bottom incision in regions where initial local depressions occur, while channel development mostly results from differential deposition (Belliard et al., 2015).

Many factors are believed to affect the channel network formation and evolution such as vegetation, tidal prism, initial perturbation or anthropogenic reclamation and de-reclamation (e.g. Belliard et al., 2015; Chen et al., 2020; Kearney and Fagherazzi, 2016; Temmerman et al., 2012; Vandenbruwaene et al., 2013). For

example, previous studies have shown that vegetation might enhance the channel formation (e.g. Bouma et al., 2007; Schwarz et al., 2014; Temmerman et al., 2007) by removing energy from higher elevations and enhancing deposition. Zhang et al., (2018) indicated that over short and medium time scales, larger initial perturbations trigger wider channels and vice versa. In other research, land reclamation is believed to have different effects on tidal network development, especially it totally terminated tidal network evolution in the project areas (Chen et al., 2020). Van Maanen et al. (2015) indicated that the presence of mangrove was found to enhance the initiation and branching of tidal channels. It is because of vegetation-induced increase in erosion threshold and also extra flow resistance in mangrove forests results in erosion of sediment within vegetated areas caused by flow concentration.

The formation and development of channel systems on intertidal zones are widely recognized to interplay with the morphologic and ecological evolution of the surrounding intertidal platform (e.g. D'Alpaos et al., 2007; Kirwan and Murray, 2007; Temmerman et al., 2007). Most studies assume that the tidal network development is caused by erosional processes; therefore, focus has been on external forcing triggering channel erosion such as current flows or sea level rise (e.g. D'Alpaos et al., 2007; Perillo and Iribarne, 2003a; Perillo et al., 2003b; Perillo et al., 1996; van Maanen et al., 2013). Conversely, few studies have shown examples of the formation of tidal channels through depositional processes (Hood and Group, 2006; Hood and Group, 2010; Redfield, 1972).

Deeply incised tidal drainage channels have been observed in cohesive environments. Figure 5.1A shows unpublished observations from the Firth of Thames (Aotearoa New Zealand), where mangroves have expanded into such channels and stabilized them. These features were 0.39 m wide and 0.14 m deep with wavelength 1.3 m (n = 70, author's unpublished observations). Similar features have been reported previously (described as 'ridge-runnels') such as in the Severn Estuary shown in Figure 5.1B, Baie de Marennes-OleHron (France)

(Bassoullet et al., 2000; Carling et al., 2009; O'Brien et al., 2000). Although generally attributed to tidal currents, the specifics of how they form is not conclusive, some authors arguing vortices in the tidal flow and other forms of unstable flow.

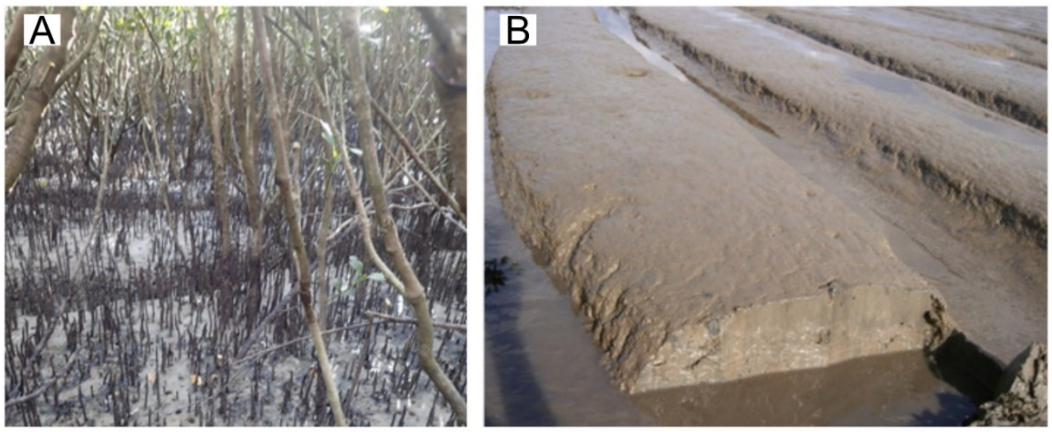

Figure 5.1 Examples of patterns forming in cohesive environments. A) Firth of Thames, Aotearoa New Zealand. B) Cohesive ridge-runnel feature from the Severn Estuary (photo from Carling et al., 2009).

Erosion properties of cohesive intertidal sediments are affected by many factors such as air water content, biofilm biomass or air temperature to which the sediments on intertidal flats are exposed to during low tides (Black et al., 2002; Grabowski et al., 2011; Nguyen et al., 2019; Nguyen et al., 2020), which in turn regulate the erosional processes on tidal zones. This study aimed to explore the influence of exposure (the influence of air temperature and duration of exposure) on the formation and development of channel patterns on an intertidal mudflat. We address the hypothesis, that differential exposure rates on topography with random elevation perturbations may play a role in the development of channel patterns in cohesive environments. We use a version of Delft3D in which differential exposure effects have been added to investigate this hypothesis. Our findings contribute to understanding the origin and evolution of tidal channel networks, which might ultimately contribute to understanding how low-lying coastal morphology might change during sea level rise which will drive changes to exposure rates.

5.2 Methods

5.2.1 Modelling of erosion properties

Semi-empirical models fitted to the data collected in Nguyen et al., (2019), Nguyen et al., (2020) that express the relationship between air temperature -*T* and exposure duration – *D* and the critical bed shear stress (τ_{cr}, N m^{-2}) and erosion rate *ER* (g m^{-2} s^{-1}) were incorporated into the Delft3D modelling environment. Nevertheless, the models rely on some empirical constants that are fitted with experimental data, which are needed to parameterize the effect of moisture transferring down through the water matrix and the effect of organic content and micro-phytobenthos (which use water to fuel physiological processes). Data for empirical parameterization were provided by running the EROMES erosion device on cores collected from a cohesive intertidal field setting (see cited papers Nguyen et al., (2019 & 2020) for more detail).

The fitting data sets consistent of two experiments. One in which temperature was varied while holding the exposure duration constant at 6 h using treatments of sediments with high and low *Chl-a*, and varying temperature between 0 and 40 °C. In the other experiment, exposure duration was varied in two trials to represent typical summer and winter conditions over 6 h, 1, 4 and 10 d, with cores left outside and in situ air temperature being logged every minute. Sediment properties of sediments used in both experiments were collected from intertidal mudflats in the Firth of Thames, New Zealand between 2017 and 2019.

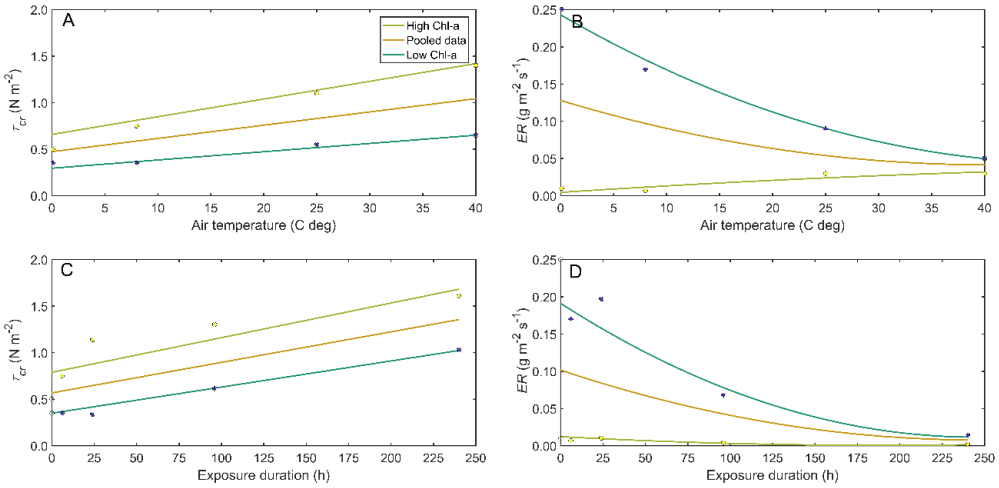

Figure 5.2 Empirical models for A & C) erosion threshold T_{cr} (N m^{-2}) and B & D) erosion rate *ER* (g m^{-2} s^{-1}), (Nguyen et al., in Prep.)

The relationship between T_{cr} and air temperature and exposure duration (Figure 5.2A and 5.2C) was best predicted with a linear relationship. Conversely erosion rate ER was best fit with an exponential model (Figure 5.2B and 5.2D).

$$ER = ER_{inn} \times e^{(a_1 T + a_2)D} \quad (1)$$

$$\tau_{cr} = \tau_{inn} + (b_1 T + b_2)D \quad (2)$$

Where T_{inn} and ER_{inn} are erosion threshold and erosion rate of sediment when inundated, respectively. *T* is air temperature (°C), *D* is exposure duration (h). a_1, a_2, b_1, b_2 are coefficients which were evaluated separately for high, low *Chl-a* content cases (for high *Chl-a* content case, data were extracted from experiments conducted in hot months of Mar 2019, Jan and Feb 2020, Table 5.1) and pooled data (coefficients are presented in Table 5.2). Consistent with observations by Fagherazzi et al., (2017), we added recovery coefficients for T_{cr} and *ER* into the models that allow sediment erosion properties to gradually return to submerged conditions when immersed. The more the erosion properties changed during exposure (e.g. higher *T* and longer *D*), the longer time is needed for recovery.

Table 5.1 In situ sediment properties at the time cores were collected for use in laboratory experiments (Nguyen et al., in Prep.)

Properties	Dec 2017	Mar 2018	Oct 2018	Jan 2019	Feb 2019
Wet bulk density (g cm^{-3})	-	-	1.36 ± 0.08	1.44 ± 0.05	1.43 ± 0.07
Dry bulk density (g cm^{-3})	-	-	0.32 ± 0.03	0.34 ± 0.06	0.33 ± 0.04
Median grain size (D_{50}, μm)	6.37 ± 1.05	8.90 ± 0.90	6.34 ± 1.72	6.94 ± 1.59	6.14 ± 0.85
Clay content (%)	37.8 ± 4.1	26.3 ± 2.8	37.6 ± 6.2	34.1 ± 5.2	34.8 ± 4.0
Silt content (%)	55.3 ± 5.3	63.4 ± 3.8	55.8 ± 4.1	62.8 ± 5.1	61.2 ± 5.0
Sand content (%)	6.9 ± 2.8	10.3 ± 3.1	6.6 + 3.98	3.1 ± 0.9	4.0 ± 1.0
Chlorophyll-a (*Chl-a*, μg g^{-1})	9.2 ± 2.7	21.6* ± 5.8	10.8 ± 1.9	78.0* ± 13.0	65.1* ± 6.2
Organic content (*OC*, %)	9.8 ± 0.3	10.1 ± 3.2	10.3 ± 0.6	12.6 ± 0.5	13.1 ± 0.4

Data represent the mean ± 1 standard deviation (n=20)
* Sediment collected in hot months with higher Chl-a content

5.2.2 Model setup

A model setup was based on the intertidal mud flat in the Firth of Thames, New Zealand (Figure 5.3A), where the sediments samples were collected for the erosion experiments used to parameterize the exposure terms in the model. The model geometry was characterized by a tidal flat consisting of a platform and an initial gentle slope of 0.4% to match observations at the site (Swales et al., 2015) (Figure 5.3B). The simulation domain was a rectangle (0.5 km × 4 km) and the spatial grid resolution is 20 m × 20 m (Figure 5.3C). The water depth at the seaside boundary was 4 m. The bed was covered with a 5 m thick sediment layer which was composed of mud (grain size < 63 μm). Random variations in the initial bathymetry (of the same size for all runs) were added to stimulate the development of morphology. The offshore tidal boundary was forced by the superposition of M_2 and S_2 constituents to simulate the spring-neap cycle. The spring tidal range was set as 3.8 m to match conditions at the site. Erosion threshold and erosion rate when the profile was inundated were set at 0.05 N m^{-2} and 0.05 g m^{-2} s^{-1} respectively, the values that were measured from erosion experiments on cores which were retained in a submerged state (sediment

samples were submerged for 6 hours prior to tests for erosion properties) from Nguyen et al. (2019, 2020).

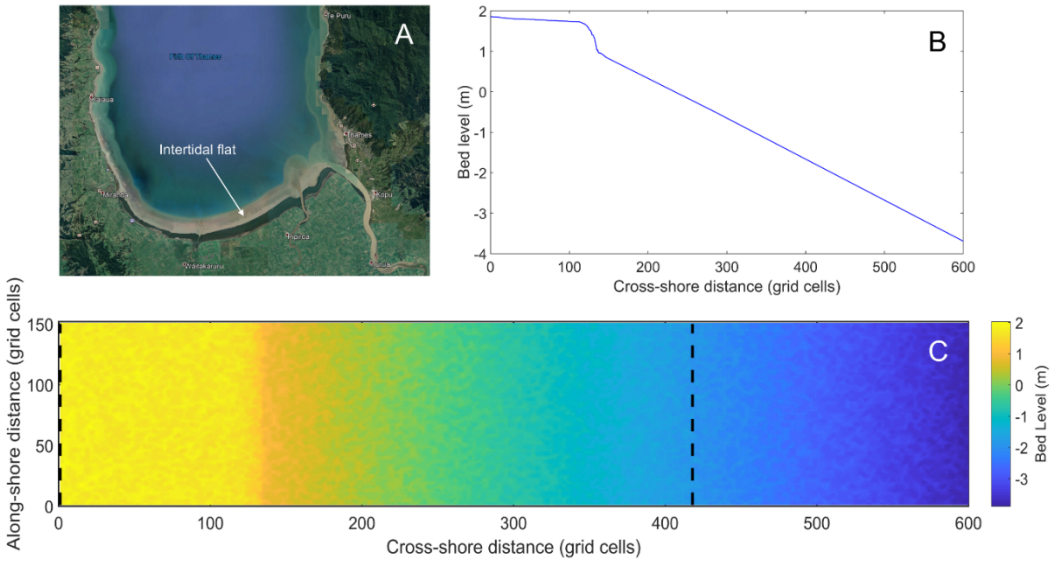

Figure 5.3 (A) Location of the mudflat in the Firth of Thames, New Zealand (Image courtesy of Google Earth, imagery date 18 April 2021). (B) A typical profile of the intertidal mudflat in the study area (Montgomery et al., 2019). (C) A 2D model setup of the initial profile. The intertidal area is terminated within dashed lines.

Model scenarios were designed to explore the role of air temperature on development of channel network on intertidal mud flat. Two model runs of 10 and 20°C were chosen to investigate the effect of air temperature, which covers a range of temperature that occur at our field site in the Firth of Thames. The model runs are hereafter referred to as “small effect” and “larger effect” cases. The model results were then compared with a model run without exposure effect (referred to as the “no effect” case from now on). This research aims to investigate the effect of temperature and exposure on the evolution of tidal-channel networks, therefore models were run for short term (800 model timesteps, each step was setup 1min) to simulate the initial influence on the intertidal flat morphology. In order to reduce the computational time, a morphological accelerating factor was set at 400, which linearly scale-up the development of channel networks.

5.2.3 Formulae controlling sediment dynamics

In Delft3D, sand and mud fractions are considered individually. Therefore, physical process such as erosion and deposition are treated separately for each fraction. Sediment transport of the cohesive fractions (the mud) is modelled using an advection equation

$$Q_{mud,e} - Q_{mud,d} = \frac{\partial(Ch)}{\partial t} + \frac{\partial(uCh)}{\partial x} \quad (3)$$

where $Q_{mud,e}$ *and* $Q_{mud,d}$ are erosion and deposition fluxes, respectively. *C* is depth averaged concentration (kg m^{-3}), *h* is water depth (m), *u* is depth averaged flow velocity (m s^{-1}), *t* is time (s), x is direction (m). These fluxes were modelled using the Partheniades–Krone equations (Partheniades, 1965)

$$Q_{mud,e} = \begin{cases} ER\left(\frac{\tau_{max}}{\tau_{cr}} - 1\right) & if\ \tau_{max} > \tau_{cr,e} \\ 0 & if\ \tau_{max} \leq \tau_{cr,e} \end{cases} \quad (4)$$

$$Q_{mud,d} = \begin{cases} W_s C\left(1 - \frac{\tau_{max}}{\tau_{cr,d}}\right) & if\ \tau_{max} < \tau_{cr,d} \\ 0 & if\ \tau_{max} \geq \tau_{cr,d} \end{cases} \quad (5)$$

where *ER* is erosion rate (g m^{-2} s^{-1}, described as erosion parameter - M_e in Partheniades (1965)), τ_{cr} and $\tau_{cr,d}$ are erosion threshold for erosion and deposition of mud component, respectively (N m^{-2}). τ_{max} is maximum bed shear stress (N m^{-2}). W_s is the settling velocity (m s^{-1}), $\tau_{cr,d}$ is set at very large value of 1000 N m^{-2} as default (Winterwerp, 2007) to ensure that sediments always deposit when conditions are below the critical erosion threshold.

Normally, *ER* and τ_{cr} (in Equation 4) are considered to be constant and do not change with exposure. In this research, we have extended the formulations used in Delft3D (Equation 4) to include the changes to *ER* and τ_{cr} caused by exposure (see summary in Nguyen et al. (in prep). The air temperature to which the intertidal sediments are exposed was set as a constant value in one of the input

files, along with the empirical coefficients in Table 5.2. The duration of exposure is tracked within the model, and depends on whether the bed level is above or below the water level at each time step. The time over which the sediment takes to return to pre-exposure conditions after re-inundation is also tracked, assuming a linear function.

Table 5.2 Coefficients model for erosion rate (Eq. 1: $ER = ER_{inn} \times e^{(a_1 T + a_2)D}$) and erosion threshold (Eq.2: $\tau_{cr} = \tau_{inn} + (b_1 T + b_2)D$) of sediment.

Chl-a cases	a_1	a_2	r^2	*F*	b_1	b_2	r^2	*F*
Pooled data	-0.0034	0.0173	0.23	2.2	0.0029	-0.02	0.57	8.5
Low *Chl-a* data	-0.0072	0.0451	0.92	31.0	0.0017	0.0101	0.81	10.8
High *Chl-a* data	-0.0077	0.0716	0.98	132.4	0.0032	-0.023	0.98	181.0

- Pooled: mean Chl-a is 31.8, µg g^{-1}
- Low (Dec 2017&Mar 2918&Oct 2018): mean Chl-a is 15.0, µg g^{-1},
- High (Jan 2019&Feb 2019): mean Chl-a is 48.6, µg g^{-1}

5.3 Results

Figure 5.4 compares patterns of the channel network over the tidal flat at the end of model run period (at timestep 800) between no-effect, small and larger effect cases. Model results indicated that the development of channels is greatest for the case of small effect, with the development of more channels that are deeper and wider (Figure 5.4B). There is very little difference between the no-effect and large effect cases and channels are poorly developed (Figures 5.4A and 5.4C). Figure 5.4B shows that the tidal-channel network is to be denser in terms of number of channels within the middle part of the tidal flat (from grid cells 120 to 300) compared to the upper part (from grid cells 0 to 100) and lower part (from grid cells 300 to 410).

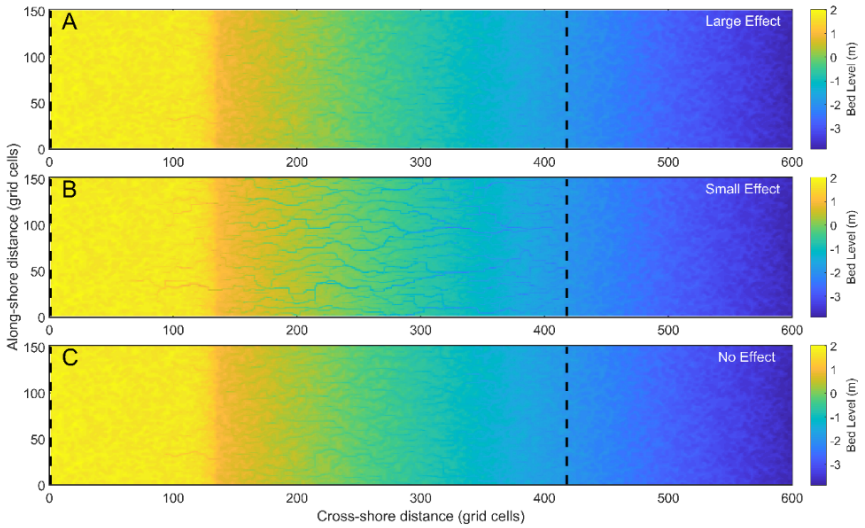

Figure 5.4 Development of intertidal channel networks after 800 model timesteps under different levels of exposure effect. The intertidal area is delineated by the dashed lines. A: Large effect; B: Small effect; C: No effect.

Figure 5.5 shows how the mean depth at each cross-shore location changes with time. In general, the middle tidal flat zone shows more changes compared to the other parts of the flat for all cases, and the case of small effect has the greatest change. Figure 5.5 is along-shore averaged and so does not show how the tidal channels develop.

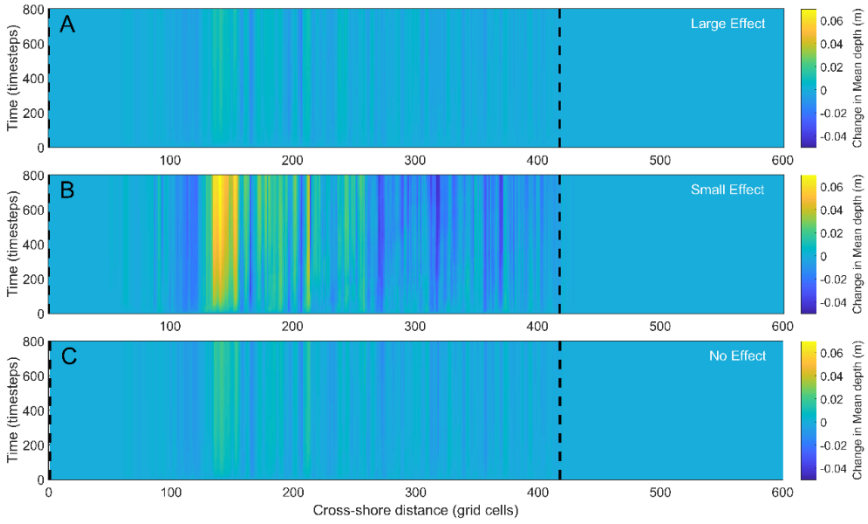

Figure 5.5 Change in mean depth over the intertidal flat under different level of exposure effect. The intertidal area is delineated within dashed lines. A: Large effect; B: Small effect; C: No effect.

The development of the alongshore variance through time shows that the variability associated with strong channel development (the small effect case) is greatest in the middle of the intertidal. The small effect case again showed the most changes within three cases (Figure 5.6B). The change in variance is slightly higher for the no effect case compared to the large effect case (Figures 5.6A and 5. 6C).

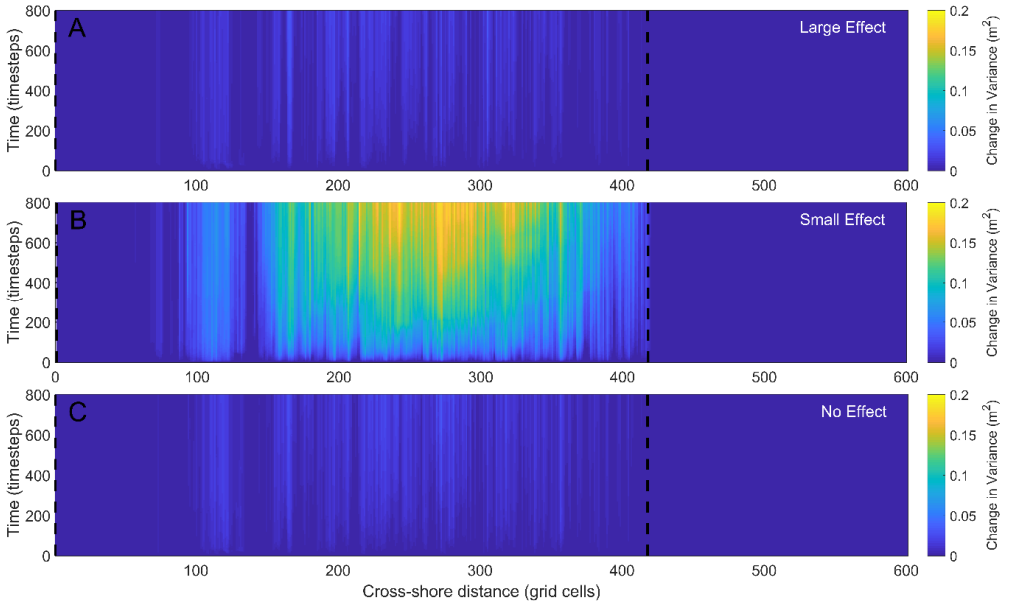

Figure 5.6 Change in variance with time over the intertidal flat under different levels of exposure effect. The intertidal area is delineated with dashed lines. A: Large effect; B: Small effect; C: No effect.

To compare the development of the channels measured by changes to the alongshore variances, the alongshore-averages of variance are shown in Figure 5.7. The variance increased sharply within the first 100 timesteps as the model adjusted to the initial conditions, then displayed a gradually increasing trend (Figure 5.7A). Although all runs showed a similar pattern with time, the no effect and large effect cases changes were much smaller. The variance of larger effect case was smaller than that of no effect case during the first 100 timesteps, then it surpassed the latter one for the remain period of the model run (Figure 5.7B). By the end of the model run, small effect case shows a variance magnitude of about two times higher than that of no effect and larger effect cases.

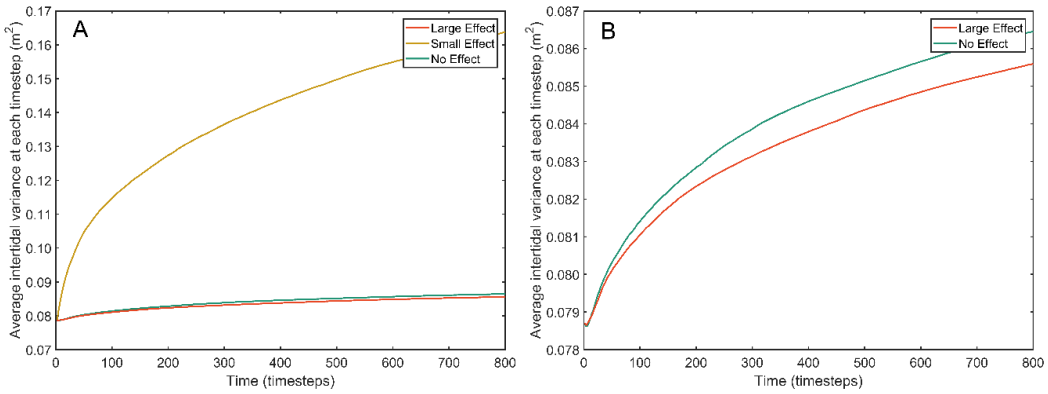

Figure 5.7 Comparison of the evolution of intertidal variance with the 3 different exposure effects (Panel B is a high-resolution version of panel A).

To further explore the differences in the channel characteristics, the depth of channels at halfway down the intertidal flat (at grid cell 200 in the cross-shore) are shown in Figure 5.8. In general, the small effect case has deeper channels compared to the channels of no effect and large effect cases. In contrast, the bank of each channel of small effect case is always higher than that of the other cases. For all cases, the bank level increased while the depth of channels decreased during timesteps, implying that sediment was relocated over the intertidal flat from channels onto channel banks. Overall, the location of channels is similar for all cases, however, the deepest channel for each case is not always at the same location on the along-shore section. All runs were started with the same bathymetry, so the initial imprint of the randomly-placed undulations probably ensures that channels develop at the same locations.

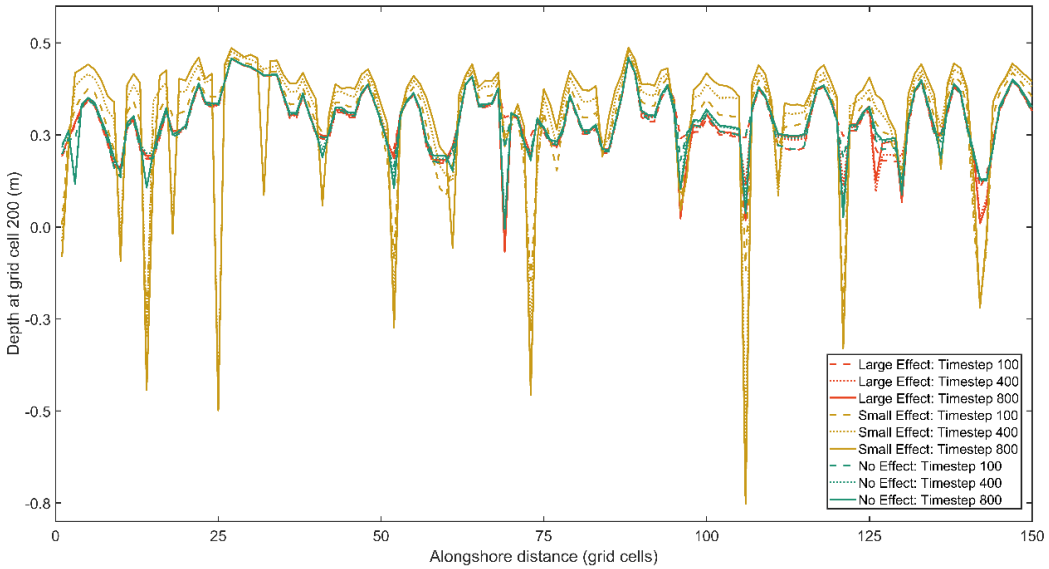

Figure 5.8 Comparison of changes in depth of tidal channels at the middle of intertidal flat (at grid cell 200 in the cross-shore) between different level of exposure effect at timesteps of 100, 400 and 800.

It is clear in Figure 5.8, that some of the channels are preferentially deepened to create more and less dominant channels. As certain channels deepen, they become favoured conduits of water (causing them to erode more), depriving lesser channels of water (causing them to erode less). Figure 5.9 shows how the number of channels changes through time, and how some channels become dominant at the expense of others (at cell 200 in the along-shore). Thirteen channels develop in the small effect case, which is significantly higher than that of the other cases with 2 and 5 channels for large effect and no effect cases, respectively. The depth of tidal channels ranged between 0.2m to 1.0m for small effect, 02m to 0.6m for no effect, and 0.2m to 0.4m for large effect.

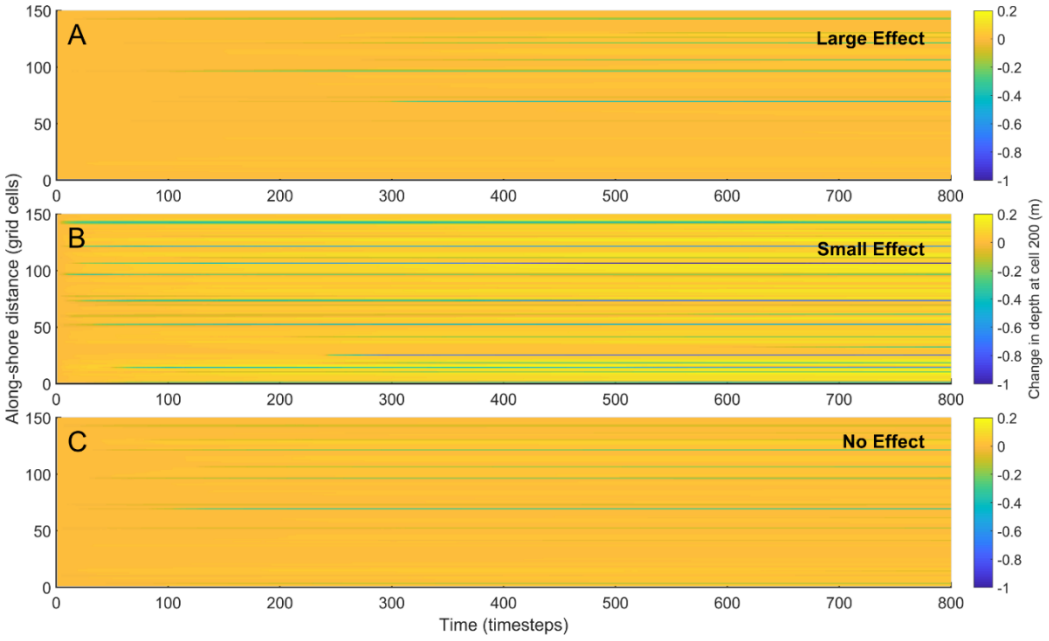

Figure 5.9 Development of channels at the middle of the intertidal flat (at grid cell 200 cross-shore distance) under different level of exposure effect.

To summarize the geomorphic evolution of the channels, we extracted the depth of each channel at a location in the intertidal (cell 200). These depths were ranked and plotted on Figure 5.10. Each of the rankings show that there is a characteristic distribution of channels, with a few very small insignificant ones (depth ~ 0.2m, which is similar to the initial perturbations), then a regime where the channel depth increases linearly with rank, and finally an upper region with 1-3 channels that are much deeper (0.35m+). As time develops, the number of channels that are in the linear regime extends, until the final case where the channels are most developed ('small effect' time step 800), the whole distribution is linear.

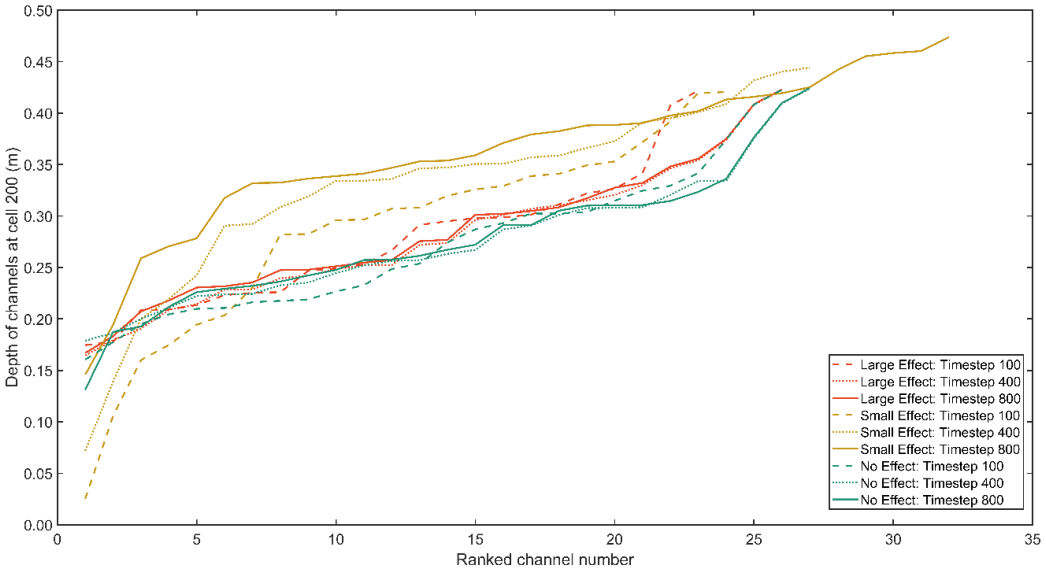

Figure 5.10 Differences between channel morphologies for the 3 effects. Channel morphology is quantified by the channels ranked according to depth allowing the change in the number of channels to be associated with scouring.

5.4 Discussion

Our model showed a dramatic difference between exposure effect and no exposure effect on the development of channel networks on an intertidal flat. The development relates to the spatial distribution of stabilizing effect of exposure on intertidal sediments, relative to the location of strongest tidal currents. The stabilizing effect increases landward, but the exposure to energy decreases landward. The channels develop at the maximum rate where these two trends cross.

Exposure effect is only effective in the regions of the profile which are exposed, therefore, in the lower parts of the intertidal flat or in the existing channels, the stabilizing effect on sediment was smaller because of shorter exposure duration. Consequently, the stabilizing effect of exposure on intertidal flat has a spatially variation in both vertical and horizontal directions. Our model results indicated that in the small effect case (which has a lower temperature), denser and deeper channel networks developed on the tidal flat compared to the case of no effect. However, it is interesting that the case of large effect had a smaller effect on the

development of the channel network compared to the no effect cases with smaller number of channel and shallower channels. In the large effect case (which was set with a temperature of 20 °C) the stabilizing effect was much stronger than the case of small effect; therefore, the erosion resistance of exposed sediments was much increased even under a short exposure duration, that it could not return to normal conditions during re-inundation. Nguyen et al. (2019) showed that large effect exposure might increase erosion threshold by 1.5 times, and decrease erosion rate of 2.0 times than small effect cases with only a short term of 6h exposure. Ultimately, strong stabilization actually suppresses pattern generation.

The stabilizing effect of exposure contributes to the development of the channels by increasing the difference between conditions in the channel compared to the banks. The development of the channels is therefore equally affected by build-up channel banks, because the channel banks are more stable and unlikely to erode. Within the 800 timesteps of our model runs, most of channels have developed and become stable. The vertical development of channels is likely limited by the bed shear stress generated by tidal flows. Further work is needed to understand whether the current arrangement has reached a stable equilibrium, or whether it is still reacting to initial conditions.

In this study, we assumed that the seasonal effect of biofilm on erodibility of sediment on intertidal flat is unchanged during model runs while the effect was widely recognized in the literature (e.g. Black et al., 2002; Nguyen et al., 2019; Nguyen et al., 2020). However, Chapter 4 examined the effect of biofilm on bed level change of intertidal flat by comparing model runs with low and high *Chl-a* content. Therefore, such an effect could be included into our model. Previous studies have reported a substantial effect of low-tide rainfall on the erodibility of surficial sediments on intertidal flats (Tolhurst et al., 2006b; Pilditch et al., 2008). Nevertheless, our study excluded the effect of rainfall that changes water content and sediment surface conditions. Future studies, therefore, should include these kinds of effect into more comprehensive model runs.

5.5 Conclusions

This study sought to examine the effect of exposure on development of tidal channel networks on intertidal mud flats in short term. Our findings implied that exposure caused a denser network with deeper tidal channels compared to no exposure effect. The effect of exposure on channel development are in both vertical and horizontal directions over the tidal flat. When exposure effect is taken onto account, the development of channels was accelerated by two processes of erosion in channels and accumulations on banks. Some other external factors such as low tide rainfall, mangrove or biofilm growth that affect erodibility of sediment on intertidal flat were excluded from our model. Therefore, a more complicated models that consider all the effect should be included in future studies into a more comprehensive model.

Chapter 6

General Conclusions

6.1 Review

In this PhD research project, I set out to expore the erosion behaviour of cohesive sediments on intertidal mudflats and how it changes when the sediments are exposed to air of varying temperature, over varying time periods. The overarching approach of this thesis is to support the idea that exposure causes evaporation which in turn decreases water content of sediment during exposure. To do so, two sets of expriments were conducted on sediment collected from an intertidal mudflat in the Firth of Thames, New Zealand, which comprised Chapters 2 and 3 of this thesis. The first experiment (Exp. 1) examined the effect of various air temperature (controlled at 0, 8, 25 and 40°C) on erodibility of exposed sediments over a duration of 6h. Meanwhile, the second experiment (Exp. 2) investigated the influence of different exposure durations (over 6 h, 1, 4 and 10 d) on erodibility of exposed sediments to outdoor ambient temperature that was logged every minute. In Exp. 1, air temperature was the only factor controlled evaporation of sediments, or in other words temperature controlled water content, whereas other weather-related factors apart from air temperature such as radiation, humidity, windspeed were also included in Exp. 2.

Seasonal changes associated with the time of year that sediments were collected meant that there were differences in the degree to which biofilms grew on the surface of the sediment (measured using *Chl-a* content as a proxy), and differences to grain size, organic content and densities. Small sediment cores (different than the larger cores used for erosion experiments) were collected in summer, autumn and spring. The Atterberg Limits (Plastic and Liquid Limits) were also investigated in Exp. 2. To test for changes in erosion characteristics, larger cores were collected and subjected to tests in the laboratory using the EROMES

test (erosion threshold, τ_{cr} *N m*$^{-2}$ and erosion rate, *ER g m*$^{-2}$ *s*$^{-1}$). Water content was also measured in these larger cores.

The main outcome of this thesis is to define the relationship between temperature and exposure duration and the erodibility of exposed sediments. In addition, the influence of the growth of biofilm during exposure which depended on weather factors and the behaviour of exposed sediments after re-wetting were also important findings of Exp. 2.

Experimental results from both sets of experiments were combined, and empirical models were fitted, where the optimal forms for the pooled data were:

$$ER = ER_{inn} \times e^{(a_1 T + a_2)D}$$

$$\tau_{cr} = \tau_{inn} + (b_1 T + b_2)D$$

Where τ_{inn} and ER_{inn} are erosion threshold and erosion rate of sediment when inundated, respectively. T is air temperature (°C), D is exposure duration (h). a_1, a_2, b_1, b_2 are coefficients.

The interaction term (between temperature and duration) was critical, because at the instant of exposure (zero duration), the erosion characteristics needed to match the submerged values.

The empirical equations were used in Chapters 4 and 5 of this thesis were incorperated into numerical coastal models in Delft3D environment. My collaborator at Hohai University, Prof Zeng Zhou, had the knowledge of the Delft3D Fortran code to added the needed functionality. Ultimately this required adding a new variable which stored the time since exposure/reinindation at each grid cell. The constants were added in an input file so that they could be changed without recompiling the code.

In Chapter 4, the effect of exposure on intertidal mudflat profiles in which air temperature, *Chl-a* content, tidal ranges and initial bed composition (mud/sand percentage) were taken into account. Chapter 5 also used the same models to explore the influence of exposure on the formation and development of tidal channel networks.

The four main chapters of this thesis are strongly connected to address the overarching research question whitin the study theme. Figure 6.1 below provides a map of how the research ideas connect and core findings of my research.

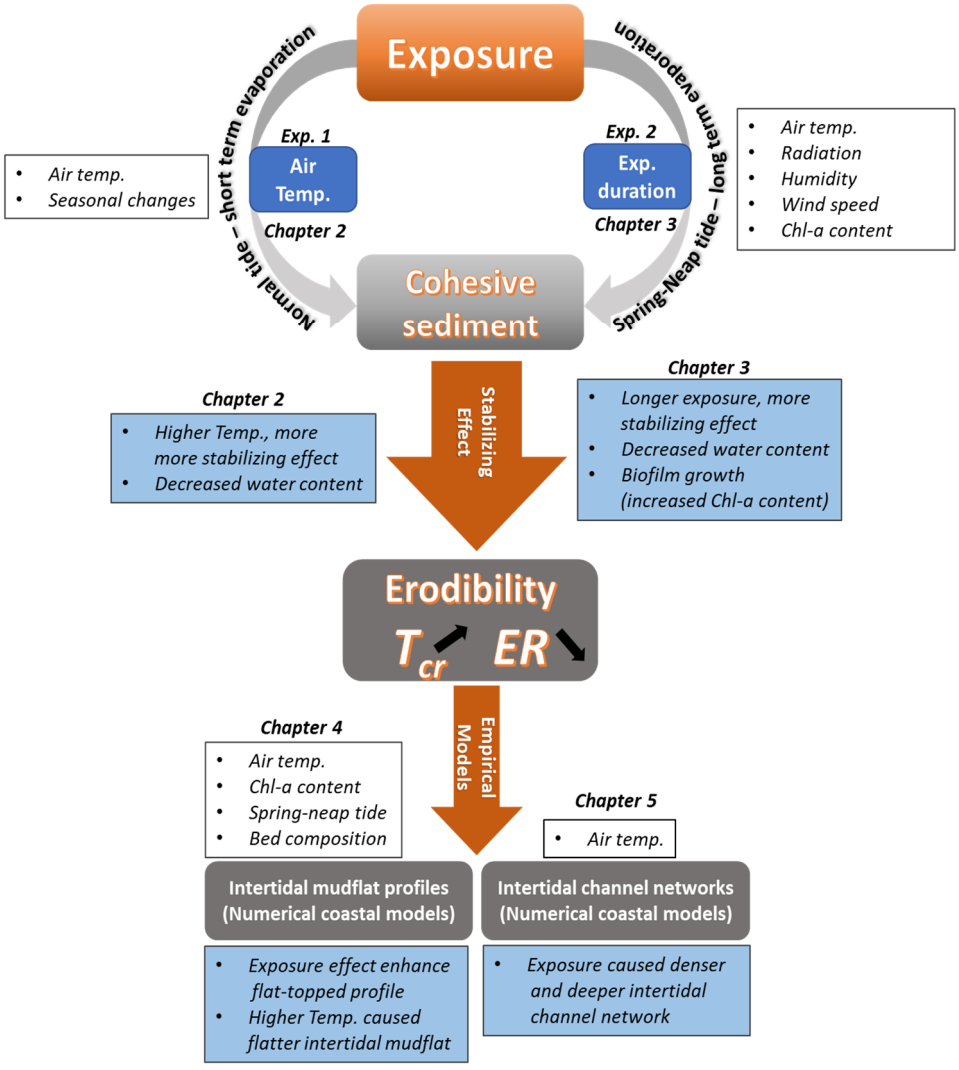

Figure 6.1 Schematic of research flow and key findings about the effect of exposure on erodibility of cohesive sediment and intertidal mudflat profiles and channel networks.

6.2 Key findings and implications of the research

One of the most important findings in this thesis is to conclude that exposure significantly stabilizes exposed sediments on intertidal mudflats. Results of Exp. 1 indicated that a higher ambient temperature led to lower water content of exposed sediment, which strengthens sediments against erosion in the subsequent flood periods. During 6h exposure, a wide range of temperatures (0 - 40°C) were conducive to a decrease in water content (ranging from 1.01 to 1.78 times). This corresponded to an increase in T_{cr} (by 1.2 to 2.2 times) and a decrease in *ER* (by 1.2 to 6.2 times). In addition, results from Exp. 2 showed that the longer the exposure duration of sediments, the less erodible they were. A long-term exposure of 10 d can cause an increase in T_{cr} by 1.7 to 4.4 times and a decrease in *ER* by 11.6 to 21.5 times compared with 6 h of exposure.

Experimental results indicated that biofilm significantly stabilised sediments even when they have larger median grain sizes that are expected to have lower critical shear stress in a traditional mean of the Shields diagram (in the cohesive range). Erodibility of intertidal sediments could be statistically predicted by changes in *Chl-a* content and water content during exposure. This thesis also introduced semi-empirical models that allow us to quantify variation levels of T_{cr} and *ER* using *Chl-a* content and water content as variables. Although the effect of biofilms and water content on the stability of sediment is widely recognized in the literature, to our knowledge, these models that first time combined the effect of both factors on erodibility.

Model results presented in Chapter 4 implied that the stabilizing effect of exposure caused muddy, highly stabilized intertidal areas to develop toward flat-topped profiles. Model results also showed that the exposure effect caused bed level changes at lower on intertidal flat compared to the case of no exposure effect. Higher temperatures have stronger impacts on evolution of intertidal flats, for example, the higher the temperatures the flatter the intertidal becomes and

the steeper the lower edge of the intertidal becomes. Moreover, it builds up the intertidal flats at higher rates.

Our findings in Chapter 5 implied that exposure caused a denser network of channels with deeper tidal channels compared to no exposure effect. The effect of exposure on channel development are in both vertical and horizontal directions over the tidal flat. When exposure effect is taken onto account, the development of channels was accelerated by two processes of erosion in channels and accumulations on channel banks.

Global warming is believed to have adverse effects on many different aspects of coastal areas. However, in term of increasing air temperature in the coming years, our findings on erosion properties of sediment indicated that substantial changes might occur during tidal cycles because of varying exposure conditions, which may ultimately contribute to changing the intertidal morphology as exposed sediment can be stabilised against erosion. Over longer time scales, temperature changes might reduce potential erosion by promoting evaporation during the subaerial period, and thus contribute to intertidal stability. The rising sea level potentially increases the erosion of sediments in low-lying areas; nevertheless, this threat might be eased as global warming will increase the air temperature during low tide exposure.

Seasonal changes in meteorological conditions affect the water content via evaporation process, which consequently should affect erosion properties and sediment resuspension on intertidal mudflats. In meso-tidal zones where large intertidal areas are exposed to air at low tide, the evaporation becomes particularly important. Our models introduced in this thesis could be a good approach to investigate morphological changes under the effect of these factors.

Our findings, therefore, significantly contribute to predicting the evolution of coastal morphology, particular the intertidal mudflat profile and the development

of tidal channel networks, which will help to understand the resilience of tidal flats and salt marshes in coming years when sea-level rise and global warming.

6.3 Limitations and suggestions for future research

The growth of biofilms is generally believed to prevent water evaporating from the pore space between particles. We show in Chapter 3, when measurements of the *Chl-a* content were taken into account, the capacity to predict the variation of water content during exposure was improved. Some additional work is needed to generalise this model. An evaporation rate was computed using equations from Dingman (1994). These equations should be confirmed by a much more extensive experimental base. More sophisticated measuring technology would also improve predictions. For example, evaporation rate (water content change) could be recorded using a weighing lysimeter while *Chl-a* content could be measured at greater frequency. To control unexpected effects of weather factors such as temperature, radiation, humidity and wind speed on evaporation, experiment design should consider an environment with a consistent weather conditions during the experiment.

In the numerical models used in this research (Chapters 4 & 5), I included coefficients of recovery that allow erosion resistance to decrease during the subsequent immersion (increases *ER* and decreases τ_{cr}). The linear form of this model, and the coefficients are not well tested because in the experiment 2, no recovery of sediments was detected (due to the confounding effect of biofilm growth). A series of experiments should be designed to address this issue. For example, sediment cores could be exposed to elevated temperature with various duration, then re-wetted following the procedure of the re-wetting experiment introduced in Chapter 3. Two sets of sediment cores could be used, one for testing erosion resistance of sediment after exposure and the other for after re-wetting. To investigate the recovery rate of sediments, re-wetting experiments should be conducted for 2, 4 and 6 h, followed by EROMES tests. Nevertheless, including the

rewetting process in the model based on limited data gives an indication of the potential importance of this term as air temperature and exposure time varied.

The numerical models were entirely parameterized with my empirical data from the Firth of Thames (New Zealand), and additional work is needed to generalize the model to other sites. I suggest that collection of sediment cores should be carried out on different intertidal flats (different median grain size and clay composition), and more seasonal samples should be collected.

Previous studies have reported a substantial effect of low-tide rainfall on the erodibility of surficial sediments on intertidal flats by changing water content, meanwhile mangroves have been widely recognised to have significant effect on dynamics of sediment on intertidal areas. Nevertheless, numerical models in this research excluded the effect of rainfall and mangroves. Future studies, therefore, should include these kinds of effects into more comprehensive model runs. Given that there are many models that investigated the effect of mangrove on coastal morphological evolution, it would be easily integrated into these models. Besides, to our knowledge there was no model undertaken to test the effect of low-tide rainfall on intertidal morphology yet. I suggest that a yearly probability function applied for low-tide rain events over intertidal flats could be used to modify the exposure parameterisation in numerical coastal models.

REFERENCES

Aberle, J., Nikora, V., & Walters, R. (2004). Effects of bed material properties on cohesive sediment erosion. *Marine Geology*, 207(1-4), 83-93. https://doi.org/10.1016/j.margeo.2004.03.012

Abramowitz, G., Pouyanné, L., & Ajami, H. (2012). On the information content of surface meteorology for downward atmospheric long-wave radiation synthesis. *Geophysical Research Letters*, 39(4). doi: https://doi.org/10.1029/2011GL050726

Amaryan, L. (1993). Soft soil properties and testing methods: AA Balkema, Rotterdam.

Amos, C., Bergamasco, A., Umgiesser, G., Cappucci, S., Cloutier, D., DeNat, L., . . . Cristante, S. (2004). The stability of tidal flats in Venice Lagoon—the results of in-situ measurements using two benthic, annular flumes. *Journal of Marine Systems*, 51(1-4), 211-241. doi:https://doi.org/10.1016/j.jmarsys.2004.05.013

Amos, C., Li, M., & Sutherland, T. (1998). The contribution of ballistic momentum flux to the erosion of cohesive beds by flowing water. *Journal of Coastal Research*, 564-569.

Amos, C. L., Droppo, I. G., Gomez, E. A., & Murphy, T. P. J. S. (2003). The stability of a remediated bed in Hamilton Harbour, Lake Ontario, Canada. *Sedimentology*, 50(1), 149-168.

Andersen, T. (2001). Seasonal variation in erodibility of two temperate, microtidal mudflats. Estuarine, *Coastal and Shelf Science*, 53(1), 1-12. doi:https://doi.org/10.1006/ecss.2001.0790

Andersen, T. J., Fredsoe, J., & Pejrup, M. (2007). In situ estimation of erosion and deposition thresholds by Acoustic Doppler Velocimeter (ADV). *Estuarine, Coastal and Shelf Science*, 75(3), 327-336.

Andersen, T. J., Lanuru, M., van Bernem, C., Pejrup, M., & Riethmueller, R. (2010). Erodibility of a mixed mudflat dominated by microphytobenthos and Cerastoderma edule, East Frisian Wadden Sea, Germany. *Estuarine, Coastal and Shelf Science*, 87(2), 197-206. doi:https://doi.org/10.1016/j.ecss.2009.10.014

Andersen, T. J., Lund-Hansen, L. C., Pejrup, M., Jensen, K. T., & Mouritsen, K. N. (2005). Biologically induced differences in erodibility and aggregation of subtidal and intertidal sediments: a possible cause for seasonal changes in sediment deposition. *Journal of Marine Systems*, 55(3-4), 123-138. doi:https://doi.org/10.1016/j.jmarsys.2004.09.004

Andersen, T. J., & Pejrup, M. (2002). Biological mediation of the settling velocity of bed material eroded from an intertidal mudflat, the Danish Wadden Sea. *Estuarine, Coastal and Shelf Science*, 54(4), 737-745. doi:https://doi.org/10.1006/ecss.2001.0856

Arar, E. J., & Collins, G. B. (1997). Method 445.0: In vitro determination of chlorophyll a and pheophytin a in marine and freshwater algae by fluorescence. *United States Environmental Protection Agency, Office of Research and Development, National Exposure Research Laboratory Cincinnati.*

Austen, I., Andersen, T. J., & Edelvang, K. (1999). The influence of benthic diatoms and invertebrates on the erodibility of an intertidal mudflat, the Danish Wadden Sea. *Estuarine, Coastal and Shelf Science*, 49(1), 99-111. doi:https://doi.org/10.1006/ecss.1998.0491

Bale, A., Stephens, J., & Harris, C. (2007). Critical erosion profiles in macro-tidal estuary sediments: Implications for the stability of intertidal mud and the slope of mud banks. *Continental Shelf Research*, 27(18), 2303-2312. doi:https://doi.org/10.1016/j.csr.2007.05.015

Bartzke, G., Bryan, K. R., Pilditch, C. A., & Huhn, K. J. (2013). On the stabilizing influence of silt on sand beds. *Journal of Sedimentary Research*, 83(8), 691-703.

Bartzke, G., Huhn, K., & Bryan, K. R. J. G.-M. L. (2017). A computational investigation of the interstitial flow induced by a variably thick blanket of very fine sand covering a coarse sand bed. Geo-Marine Letters, 37(5), 457-474.

Bassoullet, P., Le Hir, P., Gouleau, D., & Robert, S. (2000). Sediment transport over an intertidal mudflat: field investigations and estimation of fluxes within the “Baie de Marenngres-Oleron”(France). *Continental Shelf Research*, 20(12-13), 1635-1653.

Bearman, J. A., Friedrichs, C. T., Jaffe, B. E., & Foxgrover, A. C. (2010). Spatial trends in tidal flat shape and associated environmental parameters in South San Francisco Bay. *Coastal Research*, 26(2 (262)), 342-349.

Belliard, J. P., Toffolon, M., Carniello, L., & D'Alpaos, A. (2015). An ecogeomorphic model of tidal channel initiation and elaboration in progressive marsh accretional contexts. *Earth Surface*, 120(6), 1040-1064.

Black, K., Tolhurst, T., Paterson, D., & Hagerthey, S. (2002). Working with natural cohesive sediments. *Journal of Hydraulic Engineering*, 128(1), 2-8. doi:https://doi.org/10.1061/(ASCE)0733-9429(2002)128:1(2)

Blanchard, G., Guarini, J., Richard, P., Ph, G., & Mornet, F. (1996). Quantifying the short-term temperature effect on light-saturated photosynthesis of intertidal microphytobenthos. *Marine Ecology Progress Series*, 134, 309-313. doi:10.3354/meps134309

Borsje, B. W., de Vries, M. B., Hulscher, S. J., & de Boer, G. (2008). Modeling large-scale cohesive sediment transport affected by small-scale biological activity. *Estuaries, Coastal Shelf Science*, 78(3), 468-480.

Bouma, T., Van Belzen, J., Balke, T., Van Dalen, J., Klaassen, P., Hartog, A., . . . Temmerman, S. (2016). Short-term mudflat dynamics drive long-term cyclic salt marsh dynamics. *Limnology and Oceanography*, 61(6), 2261-2275. doi: https://doi.org/10.1002/lno.10374

Bouma, T., Van Duren, L., Temmerman, S., Claverie, T., Blanco-Garcia, A., Ysebaert, T., & Herman, P. (2007). Spatial flow and sedimentation patterns within patches of epibenthic structures: Combining field, flume and modelling experiments. *Continental Shelf Research*, 27(8), 1020-1045.

Brutsaert, W. (2014). Daily evaporation from drying soil: Universal parameterization with similarity. *Water Resources Research*, 50(4), 3206-3215. doi: https://doi.org/10.1002/2013WR014872

Bryan, K. R., Nardin, W., Mullarney, J. C., & Fagherazzi, S. (2017). The role of cross-shore tidal dynamics in controlling intertidal sediment exchange in mangroves in Cù Lao Dung, Vietnam. *Continental Shelf Research*, 147, 128-143. doi:https://doi.org/10.1016/j.csr.2017.06.014

BSI. (1990). BS 1377-2: 1990. British standard methods of test for soil for engineering purposes: Classification tests. In: BSI London, UK.

Cambell, G., & Mulla, D. (1990). Measurement of soil water content and potential. *Agronomy* (30), 127-142.

Carling, P., Williams, J., Croudace, I., & Amos, C. (2009). Formation of mud ridge and runnels in the intertidal zone of the Severn Estuary, UK. *Continental Shelf Research*, 29(16), 1913-1926.

Chappell, P. R. (2014). The climate and weather of Waikato: NIWA. https://www.niwa.co.nz/static/Waikato%20ClimateWEB.pdf.

Chen, L., Zhou, Z., Xu, F., Jimenez, M., Tao, J., & Zhang, C. (2020). Simulating the impacts of land reclamation and de-reclamation on the morphodynamics of tidal networks. *Anthropocene Coasts*, 3(1), 30-42.

Chen, X., Zhang, C., Zhou, Z., Gong, Z., Zhou, J., Tao, J., . . . Feng, Q. (2017). Stabilizing effects of bacterial biofilms: EPS penetration and redistribution of bed stability down the sediment profile. *Journal of Geophysical Research: Biogeosciences*, 122(12), 3113-3125. doi:https://doi.org/10.1016/S1001-0742(08)62336-0

Coco, G., Zhou, Z., Van Maanen, B., Olabarrieta, M., Tinoco, R., & Townend, I. (2013). Morphodynamics of tidal networks: advances and challenges. *Marine Geology*, 346, 1-16.

Collins M, Knutti R (2013) Long-term Climate Change: Projections, Commitments and Irreversibility. *In: Climate Change 2013: The Physical Science Basis. Contribution of Working Group I to the Fifth Assessment Report of the Intergovernmental Panel on Climate Change. Cambridge University Press, Cambridge, United Kingdom and New York*, NY, USA. http://www.climatechange2013.org/images/report/WG1AR5_Chapter12_FINAL.pdf.

Czurda, K., Ludwig, S., Schababerle, R., Hartge, K., & Stewart, B. (1995). Fabric changes in plastic clays by freezing and thawing. Soil structure: Its development and function. *Adv. in Soil Sci. Lewis Pub. Boca Raton*, FL, 71-91.

D'Alpaos, A., Lanzoni, S., Marani, M., Fagherazzi, S., & Rinaldo, A. (2005). Tidal network ontogeny: Channel initiation and early development. *Journal of Geophysical Research: Earth Surface*, 110(F2).

D'Alpaos, A., Lanzoni, S., Marani, M., & Rinaldo, A. (2007). Landscape evolution in tidal embayments: Modeling the interplay of erosion, sedimentation, and vegetation dynamics. *Journal of Geophysical Research: Earth Surface*, 112(F1).

Dagesse, D. F. (2013). Freezing cycle effects on water stability of soil aggregates. *Canadian Journal of Soil Science*, 93(4), 473-483.

Daly, C., Bryan, K. R., Roelvink, J., Klein, A., Hebbeln, D., & Winter, C. (2011). Morphodynamics of embayed beaches: the effect of wave conditions. *Journal of Coastal Research*, 1003-1007.

Dastgheib, A., Roelvink, J., & Wang, Z. (2008). Long-term process-based morphological modeling of the Marsdiep Tidal Basin. *Marine Geology*, 256(1-4), 90-100.

Davarzani, H., Smits, K., Tolene, R. M., & Illangasekare, T. (2014). Study of the effect of wind speed on evaporation from soil through integrated modeling of the atmospheric boundary layer and shallow subsurface. *Water Resources Research*, 50(1), 661-680.

Davoult, D., Migné, A., Créach, A., Gevaert, F., Hubas, C., Spilmont, N., & Boucher, G. (2009). Spatio-temporal variability of intertidal benthic primary production and respiration in the western part of the Mont Saint-Michel Bay (Western English Channel, France). *Hydrobiologia*, 620(1), 163-172. doi:https://doi.org/10.1007/s10750-008-9626-3

Day, P. R. (1965). Particle fractionation and particle-size analysis. *American Society of Agronomy, Soil Science Society of America*.

Decho, A. W. (1990). Microbial exopolymer secretions in ocean environments: their role (s) in food webs and marine processes. *Oceanogr. Mar. Biol. Annu. Rev*, 28(7), 73-153.

Dingman, S. L. (1994). Physical Hydrology Prentice Hall. Inc., New Jersey, 7458.

Doody, J. P. (2013). Coastal squeeze and managed realignment in southeast England, does it tell us anything about the future? *Ocean and Coastal management*, 79, 34-41.

Doran, P. M. (1995). Bioprocess engineering principles. *Elsevier*. London, UK

Dyer, K. (1998). The typology of intertidal mudflats. *Geological Society, London, Special Publications*, 139(1), 11-24.

Fagherazzi, S., Bortoluzzi, A., Dietrich, W. E., Adami, A., Lanzoni, S., Marani, M., & Rinaldo, A. (1999). Tidal networks: 1. Automatic network extraction and preliminary scaling features from digital terrain maps. *Water Resources Research*, 35(12), 3891-3904.

Fagherazzi, S., Carniello, L., D'Alpaos, L., & Defina, A. (2006). Critical bifurcation of shallow microtidal landforms in tidal flats and salt marshes. *Proceedings of the National Academy of Sciences*, 103(22), 8337-8341. doi:https://doi.org/10.1073/pnas.0508379103

Fagherazzi, S., Viggato, T., Vieillard, A., Mariotti, G., & Fulweiler, R. (2017). The effect of evaporation on the erodibility of mudflats in a mesotidal estuary. *Estuarine, Coastal and Shelf Science*, 194, 118-127. doi:https://doi.org/10.1016/j.ecss.2017.06.011

Fiot, J., & Gratiot, N. (2006). Structural effects of tidal exposures on mudflats along the French Guiana coast. *Marine Geology*, 228(1-4), 25-37. doi:https://doi.org/10.1016/j.margeo.2005.12.009

Fitzsimons, J. A., Hale, L., Hancock, B., & Beck, M. W. (2015). Developing a marine conservation program in temperate Australia: determining priorities for action. *Australian Journal of Maritime Ocean Affairs*, 7(1), 85-93.

Flemming, B., & Delafontaine, M. (2000). Mass physical properties of muddy intertidal sediments: some applications, misapplications and non-applications. *Continental Shelf Research*, 20(10-11), 1179-1197.

Foster, N. M., Hudson, M. D., Bray, S., & Nicholls, R. J. (2013). Intertidal mudflat and saltmarsh conservation and sustainable use in the UK: A review. *Journal of environmental management*, 126, 96-104.

Franz, G., Pinto, L., Ascione, I., Mateus, M., Fernandes, R., Leitão, P., & Neves, R. (2014). Modelling of cohesive sediment dynamics in tidal estuarine systems: Case study of Tagus estuary, Portugal. *Estuarine, coastal shelf science*, 151, 34-44.

Friedrichs, C. (2011). Tidal flat morphodynamics:asynthesis. *In: Eric Wolanski, E., McLusky, D.(Eds.), Treatise on Estuarine and Coastal Science, vol.3.Academic Press, Waltham*, 37–170. doi:http://dx.doi.org/10.1016/B978-0-12-374711-2.

Friedrichs, C., & Aubrey, D. (1996). Equilibrium Hyposometry of Intertidal. *Mixing in estuaries Coastal seas*, 50, 405-429.

Friend, P., Ciavola, P., Cappucci, S., & Santos, R. (2003). Bio-dependent bed parameters as a proxy tool for sediment stability in mixed habitat intertidal areas. *Continental Shelf Research*, 23(17-19), 1899-1917. doi:https://doi.org/10.1016/j.csr.2002.12.001

Fujino, K., Lewis, E., & Perkin, R. (1974). The freezing point of seawater at pressures up to 100 bars. *Journal of Geophysical research*, 79(12), 1792-1797.

Gerbersdorf, S. U., Jancke, T., & Westrich, B. (2007). Sediment Properties for Assessing the Erosion Risk of Contaminated Riverine Sites. An approach to evaluate sediment properties and their covariance patterns over depth in relation to erosion resistance. First investigations in natural sediments (11 pp). *Journal of Soils and Sediments*, 7(1), 25-35. doi:https://doi.org/10.1065/jss2006.11.190

Gillott, J. E. (2012). Clay in engineering geology (Vol. 41). *Elsevier*, Amsterdam.

Gilman, E. L., Ellison, J., Duke, N. C., & Field, C. (2008). Threats to mangroves from climate change and adaptation options: a review. *Aquatic botany*, 89(2), 237-250. doi:https://doi.org/10.1016/j.aquabot.2007.12.009

Grabowski, R. C., Droppo, I. G., & Wharton, G. (2011). Erodibility of cohesive sediment: the importance of sediment properties. *Earth-Science Reviews*, 105(3-4), 101-120. doi:https://doi.org/10.1016/j.earscirev.2011.01.008

Grant, J. (1986). Sensitivity of benthic community respiration and primary production to changes in temperature and light. *Marine Biology*, 90(2), 299-306. doi:https://doi.org/10.1007/BF00569142

Green, M. O., & Coco, G. (2014). Review of wave-driven sediment resuspension and transport in estuaries. *Reviews of Geophysics*, 52(1), 77-117.

Grim, R. E. (1962). Applied clay mineralogy. New York, US.

Han, J., & Zhou, Z. (2013). Dynamics of soil water evaporation during soil drying: laboratory experiment and numerical analysis. *The Scientific World Journal*, 2013. doi:http://dx.doi.org/10.1155/2013/240280

Hang, C., Nadeau, D. F., Jensen, D. D., Hoch, S. W., & Pardyjak, E. R. (2016). Playa soil moisture and evaporation dynamics during the MATERHORN field program. *Boundary-layer meteorology*, 159(3), 521-538. doi:https://doi.org/10.1007/s10546-015-0058-0

Harris, R. J., Pilditch, C. A., Greenfield, B. L., Moon, V., & Kröncke, I. (2016). The influence of benthic macrofauna on the erodibility of intertidal sediments with varying mud content in three New Zealand estuaries. *Estuaries and coasts*, 39(3), 815-828. doi:https://doi.org/10.1007/s12237-015-0036-2

Hewitt, J., Cummings, V., Ellis, J., Funnell, G., Norkko, A., Talley, T., & Thrush, S. (2003). The role of waves in the colonisation of terrestrial sediments deposited in the marine environment. *Journal of Experimental Marine Biology and Ecology*, 290(1), 19-47.

Hood, W. G. (2006). A conceptual model of depositional, rather than erosional, tidal channel development in the rapidly prograding Skagit River Delta (Washington, USA). *Earth Surface Processes Landforms: The Journal of the British Geomorphological Research Group*, 31(14), 1824-1838.

Hood, W. G. (2010). Tidal channel meander formation by depositional rather than erosional processes: examples from the prograding Skagit River Delta (Washington, USA). *Earth Surface Processes Landforms: The Journal of the British Geomorphological Research Group*, 35(3), 319-330.

Houwing, E.-J. (1999). Determination of the critical erosion threshold of cohesive sediments on intertidal mudflats along the Dutch Wadden Sea coast. *Estuarine, Coastal and Shelf Science*, 49(4), 545-555.

Hughes, A. L., Wilson, A. M., & Morris, J. T. (2012). Hydrologic variability in a salt marsh: Assessing the links between drought and acute marsh dieback. *Estuarine, Coastal Shelf Science*, 111, 95-106.

Hunt, S., Bryan, K. R., & Mullarney, J. C. (2015). The influence of wind and waves on the existence of stable intertidal morphology in meso-tidal estuaries. *Geomorphology*, 228, 158-174.

Jacobs, W., Le Hir, P., Van Kesteren, W., & Cann, P. (2011). Erosion threshold of sand–mud mixtures. *Continental Shelf Research*, 31(10), S14-S25. doi:https://doi.org/10.1016/j.csr.2010.05.012

Kearney, W. S., & Fagherazzi, S. (2016). Salt marsh vegetation promotes efficient tidal channel networks. *Nature communications*, 7(1), 1-7.

Kirby, R. (2000). Practical implications of tidal flat shape. *Continental Shelf Research*, 20(10-11), 1061-1077.

Kirwan, M. L., & Megonigal, J. P. (2013). Tidal wetland stability in the face of human impacts and sea-level rise. *Nature International journal of science*, 504(7478), 53. doi:https://doi.org/10.1038/nature12856

Kirwan, M. L., & Murray, A. B. (2007). A coupled geomorphic and ecological model of tidal marsh evolution. *Proceedings of the National Academy of Sciences*, 104(15), 6118-6122.

Kirwan, M. L., Temmerman, S., Skeehan, E. E., Guntenspergen, G. R., & Fagherazzi, S. (2016a). Overestimation of marsh vulnerability to sea level rise. *Nature Climate Change*, 6(3), 253-260. doi:https://doi.org/10.1038/nclimate2909

Kirwan, M. L., Walters, D. C., Reay, W. G., & Carr, J. A. (2016b). Sea level driven marsh expansion in a coupled model of marsh erosion and migration. *Geophysical Research Letters*, 43(9), 4366-4373.

Knight, J. M., Dale, P. E., Spencer, J., & Griffin, L. (2009). Exploring LiDAR data for mapping the micro-topography and tidal hydro-dynamics of mangrove systems: An example from southeast Queensland, Australia. *Estuarine, Coastal Shelf Science*, 85(4), 593-600. doi:https://doi.org/10.1016/j.ecss.2009.10.002

Kobayashi, T., & Miyagawa, K. (1992). A method for estimating the daily amount of evaporation from bare soils with dry surfaces. *Precipitation Scavenging and Atmosphere-Surface Exchange*, 2, 729-739.

Lanzoni, S., & D'Alpaos, A. (2015). On funneling of tidal channels. *Journal of Geophysical Research: Earth Surface*, 120(3), 433-452.

Le Hir, P., Roberts, W., Cazaillet, O., Christie, M., Bassoullet, P., & Bacher, C. (2000). Characterization of intertidal flat hydrodynamics. *Continental Shelf Research*, 20(12-13), 1433-1459.

Lehrsch, G., Sojka, R., & Jolley, P. (1993). Freezing effects on aggregate stability of soils amended with lime and gypsum. Catena Verlag, Germany.

Lianfang, Z., Wei, Z., & Wei, T. (2009). Clogging processes caused by biofilm growth and organic particle accumulation in lab-scale vertical flow constructed wetlands. *Journal of Environmental Sciences*, 21(6), 750-757. doi:https://doi.org/10.1016/S1001-0742(08)62336-0

Liu, X. J., Gao, S., & Wang, Y. P. (2011). Modeling profile shape evolution for accreting tidal flats composed of mud and sand: A case study of the central Jiangsu coast, China. *Continental Shelf Research*, 31(16), 1750-1760. doi:https://doi.org/10.1016/j.csr.2011.08.002

Lovelock, C. E., Sorrell, B. K., Hancock, N., Hua, Q., & Swales, A. (2010). Mangrove forest and soil development on a rapidly accreting shore in New Zealand.

Ecosystems, 13(3), 437-451. doi:https://doi.org/10.1007/s10021-010-9329-2

Mangan, S., Bryan, K. R., Thrush, S. F., Gladstone-Gallagher, R. V., Lohrer, A. M., & Pilditch, C. A. (2020). Shady business: the darkening of estuaries constrains benthic ecosystem function. *Marine Ecology Progress Series*, 647, 33-48.

Marani, M., D'Alpaos, A., Lanzoni, S., Carniello, L., & Rinaldo, A. (2007). Biologically-controlled multiple equilibria of tidal landforms and the fate of the Venice lagoon. *Geophysical Research Letters*, 34(11).

Mariotti, G., & Fagherazzi, S. (2010). A numerical model for the coupled long-term evolution of salt marshes and tidal flats. *Journal of Geophysical Research: Earth Surface*, 115(F1).

Mariotti, G., & Fagherazzi, S. (2011). Asymmetric fluxes of water and sediments in a mesotidal mudflat channel. *Continental Shelf Research*, 31(1), 23-36. doi:https://doi.org/10.1016/j.csr.2010.10.014

Matthiessen, M. K., Larney, F. J., Brent Selinger, L., & Olson, A. F. (2005). Influence of Loss-on-Ignition Temperature and Heating Time on Ash Content of Compost and Manure. *Communications in soil science and plant analysis,* 36(17-18), 2561-2573. doi:https://doi.org/10.1080/00103620500257242

McCarthy, J. J. (2001). Climate change 2001: impacts, adaptation, and vulnerability: contribution of Working Group II to the third assessment report of the Intergovernmental Panel on Climate Change: Cambridge University Press.

Mehta, A. J. (2002). Mudshore dynamics and controls. *In: Healy, T., Wang, Y., and Healy, J.A. (eds.), Muddy Coasts of the World: Processes, Deposits and Function*, 19–60.

Mi, H., Fichot, C. G., Bryan, K. R., Qiao, G., & Fagherazzi, S. (2020). Rapid shoreline flooding enhances water turbidity by sediment resuspension: An example

in a large Tibetan lake. *Earth Surface Processes Landforms*, 45(15), 3780-3790.

Migné, A., Spilmont, N., & Davoult, D. (2004). In situ measurements of benthic primary production during emersion: seasonal variations and annual production in the Bay of Somme (eastern English Channel, France). *Continental Shelf Research*, 24(13-14), 1437-1449. doi:https://doi.org/10.1016/j.csr.2004.06.002

Montgomery, J., Bryan, K., Horstman, E., & Mullarney, J. (2018). Attenuation of Tides and Surges by Mangroves: Contrasting Case Studies from New Zealand. *Water*, 10(9), 1119.

Montgomery, J. M., Bryan, K. R., Mullarney, J. C., & Horstman, E. M. (2019). Attenuation of storm surges by coastal mangroves. *Geophysical Research Letters*, 46(5), 2680-2689.

Morgan, R. P. C. (2009). Soil erosion and conservation: John Wiley & Sons.

Murphy, R., Tolhurst, T., Chapman, M., & Underwood, A. (2009). Seasonal distribution of chlorophyll on mudflats in New South Wales, Australia measured by field spectrometry and PAM fluorometry. *Estuarine, Coastal and Shelf Science*, 84(1), 108-118. doi:https://doi.org/10.1016/j.ecss.2009.06.003

Nemes, A., Rawls, W. J., & Pachepsky, Y. A. (2005). Influence of organic matter on the estimation of saturated hydraulic conductivity. *Soil Science Society of America Journal*, 69(4), 1330-1337.

Nguyen, H. M., Bryan, K. R., & Pilditch, C. A. (2020). The effect of long-term aerial exposure on intertidal mudflat erodibility. *Earth Surface Processes Landforms*, 45(14), 3623-3638. doi: https://doi.org/10.1002/esp.4990

Nguyen, H. M., Bryan, K. R., Pilditch, C. A., & Moon, V. G. (2019). Influence of ambient temperature on erosion properties of exposed cohesive sediment

from an intertidal mudflat. *Geo-Marine Letters*, 1-11. doi:https://doi.org/10.1007/s00367-019-00579-x

Nguyen, H.M., Bryan, Zhou, Z., K.R., Pilditch, in preparation. Modeling the effect of aerial temperature and exposure period on intertidal mudflat profiles.

Nguyen, H.M., Bryan, Zhou, Z., K.R., Pilditch, in preparation. Modelling the effect of temperature and exposure on intertidal channel networks in cohesive coastal environments.

Nouman, A. S., Chokhachian, A., Santucci, D., & Auer, T. (2019). Prototyping of Environmental Kit for Georeferenced Transient Outdoor Comfort Assessment. *ISPRS International Journal of Geo-Information*, 8(2), 76. doi: https://doi.org/10.3390/ijgi8020076

O'brien, D., Whitehouse, R., & Cramp, A. (2000). The cyclic development of a macrotidal mudflat on varying timescales. *Continental Shelf Research*, 20(12-13), 1593-1619.

Partheniades, E. (1965). Erosion and deposition of cohesive soils. *Journal of the Hydraulics Division*, 91(1), 105-139.

Paterson, D. M. (1989). Short-term changes in the erodibility of intertidal cohesive sediments related to the migratory behavior of epipelic diatoms. *Limnology and Oceanography*, 34(1), 223-234. doi:https://doi.org/10.4319/lo.1989.34.1.0223

Paterson, D. M., & Black, K. S. (2000). Temporal variability in the critical erosion threshold of saltmarsh and upper intertidal sediments. British Saltmarshes. *Forrest Text for the Linnean Society of London*. Ceredigion, UK, 51-63.

Perillo, G. M., & Iribarne, O. O. (2003a). New mechanisms studied for creek formation in tidal flats: from crabs to tidal channels. *Transactions American Geophysical Union*, 84(1), 1-5.

Perillo, G. M., & Iribarne, O. O. (2003b). Processes of tidal channel development in salt and freshwater marshes. *Earth Surface Processes Landforms: The Journal of the British Geomorphological Research Group*, 28(13), 1473-1482.

Perillo, G. M., Ripley, M. D., Piccolo, M. C., & Dyer, K. R. (1996). The formation of tidal creeks in a salt marsh: new evidence from the Loyola Bay salt marsh, Rio Gallegos Estuary, Argentina. *Mangroves Salt Marshes*, 1(1), 37-46.

Perkins, R. G., Honeywill, C., Consalvey, M., Austin, H. A., Tolhurst, T., & Paterson, D. M. (2003). Changes in microphytobenthic chlorophyll a and EPS resulting from sediment compaction due to de-watering: opposing patterns in concentration and content. *Continental Shelf Research*, 23(6), 575-586.

Pilditch, C. A., Widdows, J., Kuhn, N., Pope, N., & Brinsley, M. (2008). Effects of low tide rainfall on the erodibility of intertidal cohesive sediments. *Continental Shelf Research*, 28(14), 1854-1865. doi:https://doi.org/10.1016/j.csr.2008.05.001

Pratt, D. R., Lohrer, A. M., Pilditch, C. A., & Thrush, S. F. (2014). Changes in ecosystem function across sedimentary gradients in estuaries. *Ecosystems*, 17(1), 182-194.

Pritchard, D., & Hogg, A. J. (2003). Cross-shore sediment transport and the equilibrium morphology of mudflats under tidal currents. *Journal of Geophysical Research: Oceans*, 108(C10).

Pritchard, D., Hogg, A. J., & Roberts, W. (2002). Morphological modelling of intertidal mudflats: the role of cross-shore tidal currents. *Continental Shelf Research*, 22(11-13), 1887-1895. doi:https://doi.org/10.1016/S0278-4343(02)00044-4

Redfield, A. C. (1972). Development of a New England salt marsh. *Ecological monographs*, 42(2), 201-237.

Riemann, B., Simonsen, P., & Stensgaard, L. (1989). The carbon and chlorophyll content of phytoplankton from various nutrient regimes. *Journal of Plankton Research*, 11(5), 1037-1045. doi:https://doi.org/10.1093/plankt/11.5.1037

Righetti, M., & Lucarelli, C. (2007). May the Shields theory be extended to cohesive and adhesive benthic sediments? *Journal of Geophysical Research: Oceans*, 112(C5). doi: https://doi.org/10.1029/2006JC003669

Roberts, W., & Le Hir, P. (2000). Investigation using simple mathematical models of the effect of tidal currents and waves on the profile shape of intertidal mudflats. *Continental Shelf Research*, 20(10-11), 1079-1097.

Roskoden, R. R., Bryan, K. R., Schreiber, I., & Kopf, A. (2019). Rapid transition of sediment consolidation across an expanding mangrove fringe in the Firth of Thames New Zealand. *Geo-Marine Letters*, 1-14.

Schünemann, M., & Kühl, H. (1991). A device for erosion-measurements on naturally formed, muddy sediments: the EROMES-System. *Report of GKSS Research Centre*.

Schwarz, C., Ye, Q., van der Wal, D., Zhang, L., Bouma, T., Ysebaert, T., & Herman, P. (2014). Impacts of salt marsh plants on tidal channel initiation and inheritance. *Journal of Geophysical Research: Earth Surface*, 119(2), 385-400.

Snelgrove, P. V. (1999). Getting to the bottom of marine biodiversity: sedimentary habitats: ocean bottoms are the most widespread habitat on earth and support high biodiversity and key ecosystem services. *BioScience*, 49(2), 129-138.

Spanger-Siegfried, E., Fitzpatrick, M., & Dahl, K. (2014). Encroaching tides: How sea level rise and tidal flooding threaten US East and Gulf Coast communities over the next 30 years. *Retrieved from the University of Minnesota Digital Conservancy*, https://hdl.handle.net/11299/189228.

Staats, N., de Deckere, E. M., de Winder, B., & Stal, L. J. (2001). Spatial patterns of benthic diatoms, carbohydrates and mud on a tidal flat in the Ems-Dollard estuary. *Hydrobiologia*, 448(1-3), 107-115. doi:https://doi.org/10.1023/A:1017545204214

Stark, T. D., Choi, H., & Schroeder, P. R. (2005). Settlement of dredged and contaminated material placement areas. II: Primary consolidation, secondary compression, and desiccation of dredged fill input parameters. *Journal of Waterway, port, coastal, and ocean engineering*, 131(2), 52-61. doi:DOI: 10.1061/(ASCE)0733-950X(2005)131:2(52)

Sterling, E. J., & Hurley, M. M. (2008). Vietnam: a natural history: Yale University Press.

Sutherland, T., Amos, C., & Grant, J. (1998). The effect of buoyant biofilms on the erodibility of sublittoral sediments of a temperate microtidal estuary. *Limnology and Oceanography*, 43(2), 225-235. doi:https://doi.org/10.4319/lo.1998.43.2.0225

Swales, A., Bentley Sr, S. J., & Lovelock, C. E. (2015). Mangrove-forest evolution in a sediment-rich estuarine system: opportunists or agents of geomorphic change? *Earth Surface Processes and Landforms*, 40(12), 1672-1687. doi:https://doi.org/10.1002/esp.3759

Swales, A., Reeve, G., Cahoon, D., & Lovelock, C. (2019). Landscape Evolution of a Fluvial Sediment-Rich Avicennia marina Mangrove Forest: Insights from Seasonal and Inter-annual Surface-Elevation Dynamics. *Ecosystems*, 1-24. doi:https://doi.org/10.1007/s10021-018-0330-5

Temmerman, S., Bouma, T., Van de Koppel, J., Van der Wal, D., De Vries, M., & Herman, P. (2007). Vegetation causes channel erosion in a tidal landscape. *Geology*, 35(7), 631-634.

Temmerman, S., Moonen, P., Schoelynck, J., Govers, G., & Bouma, T. J. (2012). Impact of vegetation die-off on spatial flow patterns over a tidal marsh. *Geophysical Research Letters*, 39(3).

Teuling, A., Seneviratne, S. I., Williams, C., & Troch, P. A. (2006). Observed timescales of evapotranspiration response to soil moisture. *Geophysical Research Letters*, 33(23). doi:https://doi.org/10.1029/2006GL028178

Thrush, S. F., Hewitt, J. E., Norkko, A., Nicholls, P. E., Funnell, G. A., & Ellis, J. I. (2003). Habitat change in estuaries: predicting broad-scale responses of intertidal macrofauna to sediment mud content. *Marine Ecology Progress Series*, 263, 101-112.

Tolhurst, T., Defew, E., Perkins, R., Sharples, A., & Paterson, D. (2006a). The effects of tidally-driven temporal variation on measuring intertidal cohesive sediment erosion threshold. *Aquatic Ecology*, 40(4), 521-531. doi:DOI: 10.1007/s10452-005-9001-7

Tolhurst, T., Friend, P., Watts, C., Wakefield, R., Black, K., & Paterson, D. (2006b). The effects of rain on the erosion threshold of intertidal cohesive sediments. *Aquatic Ecology*, 40(4), 533-541. doi:DOI: 10.1007/s10452-004-8058-z

Tolhurst, T., Underwood, A., Perkins, R., & Chapman, M. (2005). Content versus concentration: Effects of units on measuring the biogeochemical properties of soft sediments. *Estuarine, coastal shelf science*, 63(4), 665-673.

Tolhurst, T. J., Riethmüller, R., & Paterson, D. M. (2000). In situ versus laboratory analysis of sediment stability from intertidal mudflats. *Continental Shelf Research*, 20(10-11), 1317-1334.

Underwood, G. J., & Paterson, D. M. (2003). The importance of extracellular carbohydrate productionby marine epipelic diatoms. *Advances in botanical research*, 40, 183-240. doi:https://doi.org/10.1016/S0065-2296(05)40005-1

Urumović, K., & Urumović Sr, K. (2016). The referential grain size and effective porosity in the Kozeny–Carman model. *Hydrology and Earth System Sciences*, 20(5), 1669-1680.

Van Ledden, M., Van Kesteren, W., & Winterwerp, J. (2004). A conceptual framework for the erosion behaviour of sand–mud mixtures. *Continental Shelf Research*, 24(1), 1-11. doi:https://doi.org/10.1016/j.csr.2003.09.002

van Maanen, B., Coco, G., & Bryan, K. R. (2015). On the ecogeomorphological feedbacks that control tidal channel network evolution in a sandy mangrove setting. *Proceedings of the Royal Society A: Mathematical, Physical Engineering Sciences,* 471(2180), 20150115.

van Maanen, B., Coco, G., Bryan, K. R., & Friedrichs, C. T. (2013). Modeling the morphodynamic response of tidal embayments to sea-level rise. *Ocean Dynamics*, 63(11-12), 1249-1262.

Van Oyen, T., Carniello, L., D'Alpaos, A., Temmerman, S., Troch, P., & Lanzoni, S. (2014). An approximate solution to the flow field on vegetated intertidal platforms: Applicability and limitations. *Journal of Geophysical Research: Earth Surface*, 119(8), 1682-1703.

Van Rijn, L. C. (1998). Principles of Coastal Morphology Aqua Publications. Amsterdam, The Netherlands.

Vandenbruwaene, W., Bouma, T. J., Meire, P., & Temmerman, S. (2013). Bio-geomorphic effects on tidal channel evolution: impact of vegetation establishment and tidal prism change. *Earth Surface Processes Landforms*, 38(2), 122-132.

Vandevivere, P., & Baveye, P. (1992). Effect of bacterial extracellular polymers on the saturated hydraulic conductivity of sand columns. *Appl. Environ. Microbiol*., 58(5), 1690-1698.

Vo-Luong, P., & Massel, S. (2008). Energy dissipation in non-uniform mangrove forests of arbitrary depth. *Journal of Marine Systems*, 74(1-2), 603-622. doi:https://doi.org/10.1016/j.jmarsys.2008.05.004

Volk, E., Iden, S. C., Furman, A., Durner, W., & Rosenzweig, R. (2016). Biofilm effect on soil hydraulic properties: Experimental investigation using soil-grown

real biofilm. *Water Resources Research*, 52(8), 5813-5828. doi: https://doi.org/10.1002/2016WR018866

Watts, C., Tolhurst, T., Black, K., & Whitmore, A. (2003). In situ measurements of erosion shear stress and geotechnical shear strength of the intertidal sediments of the experimental managed realignment scheme at Tollesbury, Essex, UK. *Estuarine, Coastal and Shelf Science*, 58(3), 611-620. doi:https://doi.org/10.1016/S0272-7714(03)00139-2

Widdows, J., Brinsley, M., Bowley, N., & Barrett, C. (1998). A benthic annular flume forin situmeasurement of suspension feeding/biodeposition rates and erosion potential of intertidal cohesive sediments. *Estuarine, Coastal and Shelf Science*, 46(1), 27-38. doi:https://doi.org/10.1006/ecss.1997.0259

Widdows, J., Brinsley, M., Salkeld, P., & Lucas, C. (2000). Influence of biota on spatial and temporal variation in sediment erodability and material flux on a tidal flat (Westerschelde, The Netherlands). *Marine Ecology Progress Series*, 194, 23-37. doi:DOI: 0.3354/meps194023

Widdows, J., Friend, P., Bale, A., Brinsley, M., Pope, N., & Thompson, C. (2007). Inter-comparison between five devices for determining erodability of intertidal sediments. *Continental Shelf Research*, 27(8), 1174-1189.

Winterwerp, J. (2007). On the sedimentation rate of cohesive sediment. *Proceedings in Marine Science*, 8, 209-226. doi:https://doi.org/10.1016/S1568-2692(07)80014-3

Winterwerp, J. C., & Van Kesteren, W. G. (2004). Introduction to the physics of cohesive sediment dynamics in the marine environment (Vol. 56): Elsevier.

Winterwerp, J. C., Zhou, Z., Battista, G., Van Kessel, T., Jagers, H., Van Maren, D. S., & Van Der Wegen, M. (2018). Efficient consolidation model for morphodynamic simulations in low-SPM environments. *Journal of Hydraulic Engineering*, 144(8), 04018055.

Xie, W., He, Q., Wang, X., Guo, L., & Zhang, K. (2018). Role of mudflat-creek sediment exchanges in intertidal sedimentary processes. *Journal of Hydrology*, 567, 351-360. doi:https://doi.org/10.1002/2017WR021066

Xu, D., Bai, Y., Ji, C., & Williams, J. (2015). Experimental study of the density influence on the incipient motion and erosion modes of muds in unidirectional flows: the case of Huangmaohai Estuary. *Ocean Dynamics*, 65(2), 187-201.

Yang, S., Li, H., Ysebaert, T., Bouma, T., Zhang, W., Wang, Y., . . . Ding, P. (2008). Spatial and temporal variations in sediment grain size in tidal wetlands, Yangtze Delta: On the role of physical and biotic controls. *Estuarine, Coastal Shelf Science*, 77(4), 657-671.

Yong, R. N., & Warkentin, B. P. (1966). Introduction to soil behaviour. The Macmillan Company, New York.

Zedler, J. B., & Kercher, S. (2005). Wetland resources: status, trends, ecosystem services, and restorability. *Annu. Rev. Environ. Resour*., 30, 39-74.

Zhang, M., & Yu, G. (2017). Critical conditions of incipient motion of cohesive sediments. *Water Resources Research*, 53(9), 7798-7815. doi:https://doi.org/10.1002/2017WR021066.

Zhang, Q., Gong, Z., Zhang, C., Townend, I., Jin, C., & Li, H. (2016). Velocity and sediment surge: what do we see at times of very shallow water on intertidal mudflats? *Continental Shelf Research*, 113, 10-20.

Zhang, Y., Zhou, Z., Geng, L., Coco, G., Tao, J., & Zhang, C. (2018). Simulating The Formation Of Tidal Channels Along An Open-Coast Tidal Flat: The Effects Of Initial Perturbation. *Coastal engineering*, 2.

Zhou, Z., Coco, G., Townend, I., Olabarrieta, M., Van Der Wegen, M., Gong, Z., . . . Gelfenbaum, G. (2017). Is “morphodynamic equilibrium” an oxymoron? *Earth-Science Reviews*, 165, 257-267.

Zhou, Z., Coco, G., van der Wegen, M., Gong, Z., Zhang, C., & Townend, I. (2015). Modeling sorting dynamics of cohesive and non-cohesive sediments on intertidal flats under the effect of tides and wind waves. *Continental Shelf Research*, 104, 76-91.

Zhou, Z., Stefanon, L., Olabarrieta, M., D'Alpaos, A., Carniello, L., & Coco, G. (2014). Analysis of the drainage density of experimental and modelled tidal networks. *Earth Surface Dynamics*, 2(1), 105-116.

Zhou, Z., van der Wegen, M., Jagers, B., & Coco, G. (2016a). Modelling the role of self-weight consolidation on the morphodynamics of accretional mudflats. *Environmental Modelling Software*, 76, 167-181.

Zhou, Z., Ye, Q., & Coco, G. (2016b). A one-dimensional biomorphodynamic model of tidal flats: sediment sorting, marsh distribution, and carbon accumulation under sea level rise. *Advances in Water Resources*, 93, 288-302.